A Comparative Study of Occupant Thermal Modeling

Amid Shakeri

A Thesis

in

The Department

of

Mechanical and Industrial Engineering

Presented in Partial Fulfillment of the Requirements
For the Degree of Masters of Applied Science (Mechanical Engineering) at
Concordia University
Montreal, Quebec, Canada

May 2006

® Amid Shakeri, 2006

Library and Archives Canada

Published Heritage Branch

395 Wellington Street
Ottawa ON K1A 0N4
Canada

Bibliothèque et Archives Canada

Direction du Patrimoine de l'édition

395, rue Wellington
Ottawa ON K1A 0N4
Canada

Your file Votre référence
ISBN: 0-494-14312-6
Our file Notre référence
ISBN: 0-494-14312-6

NOTICE:
The author has granted a non-exclusive license allowing Library and Archives Canada to reproduce, publish, archive, preserve, conserve, communicate to the public by telecommunication or on the Internet, loan, distribute and sell theses worldwide, for commercial or non-commercial purposes, in microform, paper, electronic and/or any other formats.

The author retains copyright ownership and moral rights in this thesis. Neither the thesis nor substantial extracts from it may be printed or otherwise reproduced without the author's permission.

AVIS:
L'auteur a accordé une licence non exclusive permettant à la Bibliothèque et Archives Canada de reproduire, publier, archiver, sauvegarder, conserver, transmettre au public par télécommunication ou par l'Internet, prêter, distribuer et vendre des thèses partout dans le monde, à des fins commerciales ou autres, sur support microforme, papier, électronique et/ou autres formats.

L'auteur conserve la propriété du droit d'auteur et des droits moraux qui protège cette thèse. Ni la thèse ni des extraits substantiels de celle-ci ne doivent être imprimés ou autrement reproduits sans son autorisation.

In compliance with the Canadian Privacy Act some supporting forms may have been removed from this thesis.

While these forms may be included in the document page count, their removal does not represent any loss of content from the thesis.

Conformément à la loi canadienne sur la protection de la vie privée, quelques formulaires secondaires ont été enlevés de cette thèse.

Bien que ces formulaires aient inclus dans la pagination, il n'y aura aucun contenu manquant.

Canada

ACKNOWLEDGMENTS

This project was primarily funded by Public Works and Government Services Canada (PWGSC). It support in this endeavor is immensely appreciated. Experimental data were provided by our collaborator Dr. Taghi Karimipanah from Sweden. Their contribution is as well appreciated and acknowledged.

I want to thank my supervisors Dr. Ali Dolatabadi and Dr. Fariborz Haghighat for all their support and insightful advice in this research. Finally, I would like to thank my parents and family members for their absolute support in the past two years.

The comments and advice of the members of defense committee, Dr. Tien Dai Bui, Dr. Marius Paraschivoiu and Dr. Kamran Siddiqui are as well greatly appreciated.

A Comparative Study of Occupant Thermal Modeling

Amid Shakeri

In North America, the ventilation system in indoor environments have been almost exclusively associated with the use of conventional ceiling air distribution systems, where the air is moved via ducts through ceiling diffusers. However, in the past years there has been a growing interest in the application of localized ventilation systems for which numerous studies have been conducted looking at different aspects such as enhanced thermal comfort, improved indoor air quality and lower energy consumption. It has also been determined that a typical localized ventilation system creates a non-uniform thermal environment, which might cause thermal discomfort due to excessive vertical temperature difference, draft, and asymmetric thermal conditions. As an alternative to the experimental measurments, the Computational Fluid Dynamics (CFD) methods have been used to predict the airflow field around the occupant. The correct prediction of the flow field is dependent upon the proper modeling of the occupant body since the actual shape of human body is complicated and its heat distribution is known to be non-uniform. However, past CFD studies on the subject were mainly performed by modeling the occupant as a block with uniform heat distribution, in order to simplify the problem and decrease the computational cost. In the present study, commercially available CFD software, Airpak from Fluent Inc., is used to simulate the occupant body by using a variety of modeling techniques in order to quantify the impact of occupant modeling assumptions on the bouyancy and inertia in induced flow fields.

TABLE OF CONTENTS

LIST OF TABLES

LIST OF FIGURES

NOMENCLATURE

c_p	Specific heat at constant pressure, (J/kg°C)
f_{cl}	Ratio of a person's surface area for clothed/naked, (n.d.)
g	Gravity, (m/s^2)
h_c	Convective heat transfer coefficient on surface, (W/m^2 °C)
I_{cl}	Thermal resistance of the clothing, (m^2°C/W)
k	Turbulence kinetic energy, (m^2/s^2)
k_p	Turbulence kinetic energy at the first grid point, (m^2/s^2)
q	Heat flux, (W/m^2)
u	Air velocity, (m/s)
u_o	Initial jet velocity, (m/s)
u_m	Centerline jet velocity at a distance x from the diffuser, (m/s)
u_{supply}	Supply air velocity from diffuser, (m/s)
u^*	Frictional velocity, (m/s)
v_{ar}	Relative air velocity, (m/s)
x	Point distance from the diffuser, (m)
y_p	Distance of the first grid node from the wall, (m)
y^+	Dimensionless distance from the wall, (n.d.)

A_0	Effective area of supply diffuser, (m^2)
A_{geom}	Geometric cross-section area of supply diffuser, (m^2)
$A_{surface}$	Surface area, (m^2)
C_μ	Constant, 0.09, (n.d.)
K_1	Velocity decay constant
L	Reference Length, (m)
M	Metabolic rate, (W/m^2)
P	Air pressure, (N/m^2)
P_v	Partial water vapor pressure, (Pa)
PD	Percentage of dissatisfied people due to draft
PMV	Predicted mean value
PPD	Predicted percentage dissatisfied
S_t	Source term, (W/m^3)
S_u	Source term, (N/m^3)
T_a	Air temperature, (°C)
T_{supply}	Supply air temperature from diffuser, (°C)
T_{cl}	Surface temperature of the clothing, (°C)
T_w	Inner surface temperature of the wall, (°C)
T_{mrt}	Mean radiant temperature, (°C)
W	External work, (W/m^2)

Greek Symbols

α	Under-relaxation factor
β	Thermal expansion coefficient of air, (K^{-1})
ε	Rate of dissipation of turbulence energy, (m^2/s^3)
λ_l	Laminar thermal conductivity, (W/m^oC)
λ_t	Turbulent conductivity, (W/m^oC)
μ	Laminar viscosity, (kg/m.s)
μ_t	Turbulent viscosity, (kg/m.s)
ν	Kinematics viscosity, (m^2/s)
ρ	Air density, (kg/m^3)
τ	Stress tensor
τ_w	Wall shear stress, ($kg/m.s^2$)
θ	Thermal diffusivity, ($W.m^2/J$)
ϕ	Relative Humidity

1.0 INTRODUCTION

In the industrial countries, most people spend a great deal of their time indoors and they often share the same working space, e.g. office, schools, public buildings etc. It is known that the occupant's comfort and productivity are influenced by the thermal quality of the indoor air. In a study that was carried out in the US, it was showed that about 800,000 to 1,200,000 commercial buildings with 30 to 70 million workers have health problems related to indoor environment (Wyon, 2004). Numerous health complaints such as Sick Building Syndrome (SBS) among employees in office buildings have occurred since 1970s (Brohus, 1997; Awbi, 1991). Dissatisfaction with the working environment could result in reduced productivity and economic loss. The cost on the health care has been estimated on the order of several billion dollars. Furthermore, the extensive use of electronic appliances and the increase in number of occupants per space have resulted in an increase of the contaminant and heat emission rate in the working space. Also, individual preferences for thermal conditions vary from hour to hour, day to day, and from person to person. Therefore, providing optimal thermal comfort to this heterogeneous population is not a straightforward approach and the conventional strategy of uniformly bathing a space in conditioned air may not be the best option (Heinemeier et al., 1990). This has lead to the development and implementation of newer systems aiming at more localized ventilation, better thermal comfort, greater indoor air quality and lower energy expense.

Since localized ventilation systems typically create highly asymmetric or non-isothermal environments around occupants (Bauman et al., 1993), with significant vertical

temperature gradients and highly non-uniform airflow regimes that are sometimes directed toward a segment of the body, their developments have made a detailed study of the occupant microclimate more urgent (Heinemeier et al., 1990). These newer localized ventilation systems create a microclimate within a macroclimate aiming to reduce energy consumption (Loomans, 1992). The microclimate is described as the region very near to the occupant, within approximately 1 m range.

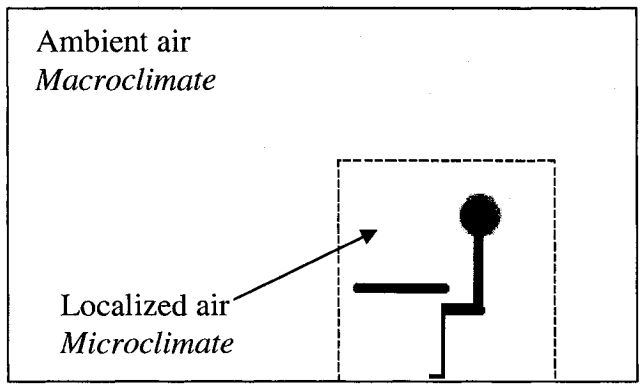

Figure 1.1: Occupant microclimate

It is known that the thermal sensation of the human body is a direct function of the local heat transfer characteristics of the body surface and the ambient environment. The complex interaction of air temperature, radiant temperature, air velocity, humidity, clothing and metabolic rate that makes up the thermal environment has large influence on the health, comfort and performance of the occupants (Bauman et al., 1993). The airflow field and temperature distribution near the occupant can be determined either by performing full-scale measurements or by simulation. Usually, human subjects or manikins are used to conduct various field studies using measurements. As an alternative to the full-scale measurement, Computational Fluid Dynamics (CFD) has been proven to be a strong tool for the task of predicting the airflow field with numerical methods. However, the accuracy of the predictions of the local airflow in the microclimate of the

occupant is highly dependent on the proper modeling of the occupant itself. The human body not only has a complicated physical shape, but also has complex thermo-physiological properties (Huizenga et al. 2004). The modeling of all these aspects is a formidable challenge and extremely hard to perform. Therefore, various simplifications have been made in order to decrease the level of complexity so that the computation may be performed with the available computer resources.

2.0 LITTERATURE REVIEW

2.1 Occupant Thermal Modeling

Nielsen (1974) was one of the first who used Computational Fluid Dynamics (CFD) methods for the simulation of indoor airflow. Later, Gan et al. (1994) used CFD methods to evaluate the thermal sensations of human body, after which occupant thermal modeling slowly became an important avenue of research by itself. As stated before, the actual human body has a complex thermo-physiological properties and non-uniform heat distribution (Huizenga et al. 2004). Therefore, past numerical studies, performed in ventilated enclosures, have used various simplification means to model the occupant. The modeling of the occupant can vary with respect to size, form (rectangular-coordinate or body-fitted), body heat emission and the turbulence model used, etc. (Nielsen et al., 2003). Brohus and Nielsen (1996) presented various CFD models of an occupant being constructed of rectangular geometry. They studied the effect of occupant model geometry on the prediction of the contaminant source in a ventilated room by proposing three models. The first model was a heated cuboid model, the second consisted of a block with two legs, and the last one consisted of two legs, the body and the head of the occupant. Brohus only considered the convective portion of body heat loss using a uniform heat flux. Much more sophisticated computational models were developed later on, considering moisture transport, respiratory effect, actual body temperature distribution and radiation (Murakami et al., 2000), but none of them were implemented as a standard model in the available Computational Fluid Dynamics (CFD) packages for large-scale modeling. This was partly due to the overwhelming computational cost of the occupant

model integration into a large-scale enclosure. Additionally, other factors such as inadequate description, uncertainties and disagreement between numerical and experimental work have also hindered the implementation of such complex occupant models into available CFD codes. As a result, past and present CFD studies that were performed on the subject of thermal comfort, ventilation effectiveness and indoor air quality in a realistic ventilated enclosure approached the issue of occupant modeling by simply assuming uniform heat distribution over the entire body and by using blocks as segments of the body. A commonly used method is shown in Figure 2.1a, where a single block is used to model the whole body. Another approach that gives a more realistic representation of the body is shown in Figure 2.1b, in which a multi-node configuration is used where each node 'block' represents a segment of the body.

Figure 2.1a

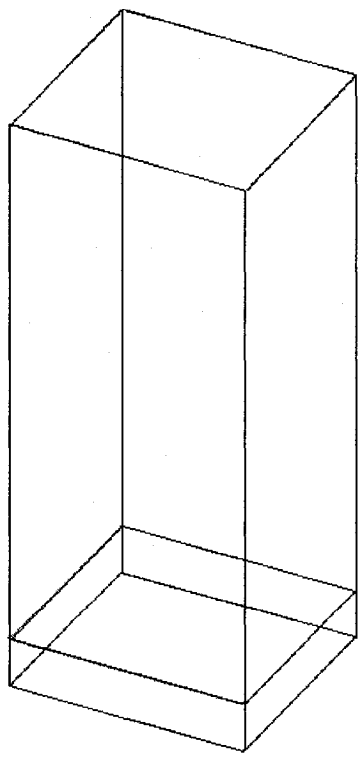

Figure 2.1b

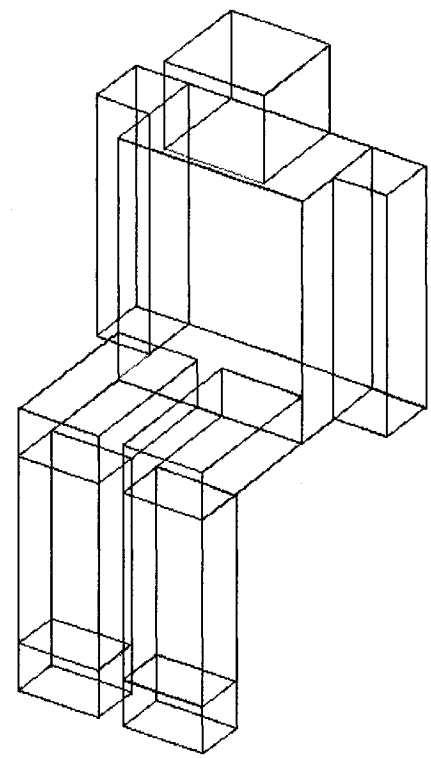

Figure 2.1: Illustrations of various occupant configurations used

Author	Occupant Model	Heat Distribution	Flow Domain	Ventilation System
Karimipanah, T. et al. (2000)	Single Block	Uniform	Large room	DV and impinging
Chiang, H. (2001)	Multi-node	Uniform	Small cavity	Personalized control
Xing, H. (2001)	Multi-node	Uniform	Small cavity	DV
Karimipanah, T. et al. (2002)	Single Block	Uniform	Large room	DV and impinging
Zhao, B. et al. (2003)	Single Block	Uniform	Large room	DV and mixing
Sekhar, SC et al. (2004)	Multi-node	Uniform	Large room	Linear and CAD
Karimipanah, T. et al. (2005)	Single Block	Uniform	Large room	Jet ventilation
Lin, Z. et al. (2005)	Single Block	Uniform	Large room	DV and mixing

Table 2.1: Previous studies using a variety of occupant configurations

Table 2.1 shows a number of CFD studies conducted in the past using a variety of occupant models. As observed, occupant model configurations with lower complexity levels (i.e. a single Block) are used for larger flow domains, while occupant model configurations with higher levels of complexity (i.e. Multi-node) are used for smaller flow domains. It is also observed that various occupant configurations are used irrespective of the type of flow field in the room, i.e. ventilation systems. Figure 2.2 depicts the flow domain of three such cases where simplified occupant configurations are used. Past and present research, evaluated occupant thermal comfort level by measuring several points around the body to get the whole-body thermal comfort equations (Fanger, 1970). The whole-body thermal comfort equation is function of the air velocity, air temperature, metabolic rate, clothing value, relative humidity and mean radiant temperature. Any significant change in any of these parameters influences the correct prediction of the overall thermal comfort (Fanger, 1970).

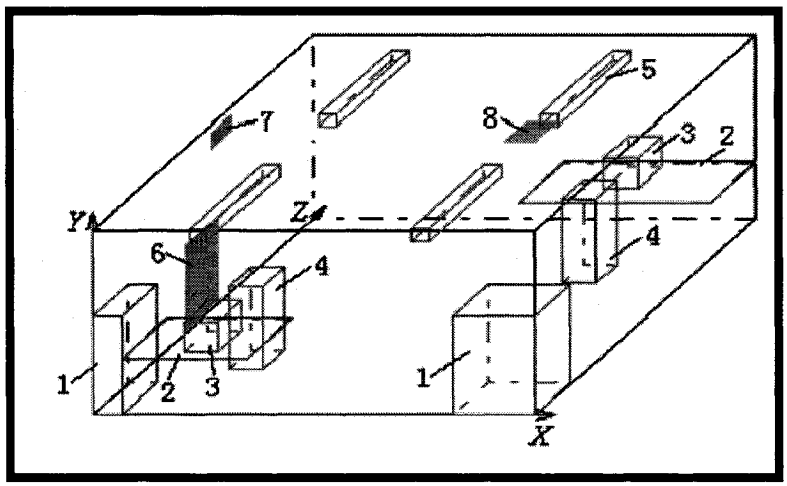

(a) Occupant model used by Zhao B. et al. (2003). (1-cabinet, 2-table, 3-computer, 4-occupant, 5-lamp, 6-displacement diffuser, 7-return grill and 8-ceiling diffuser). It is seen that the occupant is modeled using a single block as a heat source.

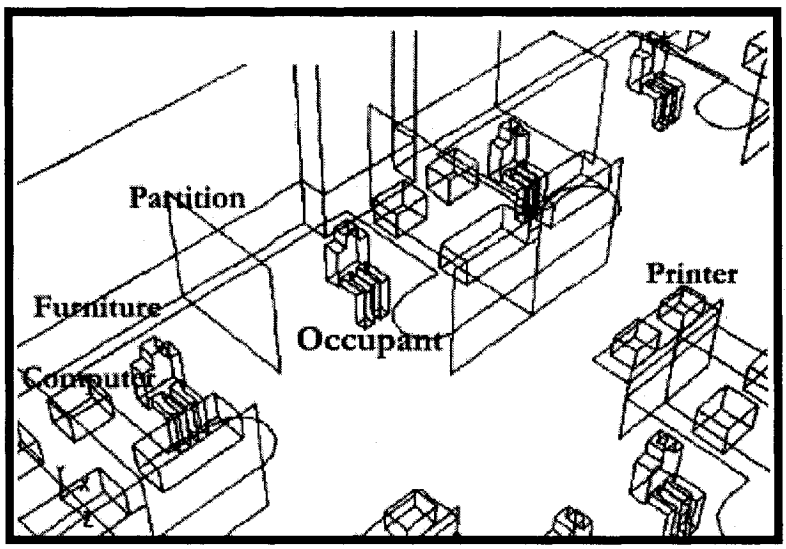

(b) Occupant model used by Sekhar, SC. et al. (2004). In this study a multi-node seated occupant model is built using several smaller size blocks.

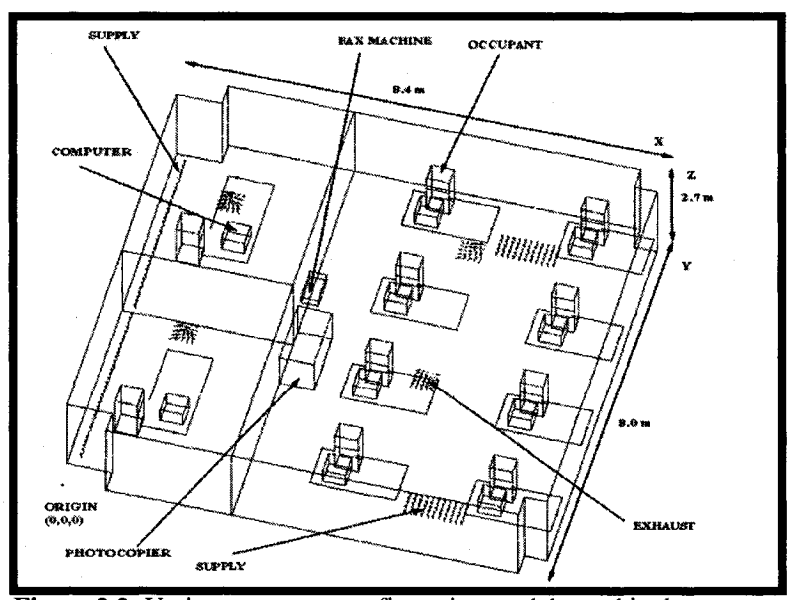

(c) Occupant model used by Lin, Z. et al. (2005). In this CFD study carried out in typical open-plan office, the occupants are modeled by using a single block as a heat source.

Figure 2.2: Various occupant configuration models used in the past

2.2 Detailed Computational Manikins

Advancements made in computer technology had helped push further the boundaries in order to develop new and more reliable occupant models. Murakami et al. (1997-99) developed a thermal model loosely based on the shape of the human body, by combining arms with the body and removing all facial details in order simplifying the geometry of their model. Murakami studied the coupling between convective heat transfer and the various flow fields, such as buoyancy and horizontally driven flow field. Murakami et al. (2000) further finalized a complete energy-balance human model by integrating their model with internal thermo-physiological regulation, moisture transport from sweating coupled with a CFD and radiation models. However, the occupant model used by Murakami was located in a small empty room, due to restriction in computing power.

Topp et al. (2002) studied mixed flow around a person in a wind tunnel exposed to a uniform horizontal flow field using two occupant models: a detailed occupant model and a simple occupant configuration made of three cuboids. It was concluded that the geometry of the occupant had indeed some influence on the local flow field near the body but almost no influence on the global flow field. Sørensen et al. (2003) further refined the detailed model used by Topp et al. (2002) in order to predict the radiative heat transfer characteristics for various body segments using non-uniform heat distribution. Sørensen et al. (2003) reported that the pelvic region of the body has the lowest value for the radiative heat transfer coefficient. Later, Nielsen, Murakami, Kato, Topp and Yang combined their work and presented two benchmark tests for evaluating CFD within the

microclimate of the occupant (Nielsen et al., 2003). Sideroff and Dang (2005) performed several studies on the benchmark tests (Nielsen et al., 2003) for the displacement and mixing ventilation systems. They studied computational aspects such as grid resolution, boundary conditions and turbulence model for a highly detailed occupant model. In summary, some of the models (Sørensen et al, 2002-03) were highly detailed in terms of shape, while others models (Murakami et al., 2000) were more realistic, accounted body thermo-physiology, considered latent heat, respiration and radiation. Additionally, Nielsen et al. (2003), Sideroff and Dang (2005) and Topp et al. (2002) have extensively studied the influence of the shape of the occupant configuration on the local flow field assuming uniform heat distribution. On the other hand, the study performed by Sørensen et al. (2003), Yigit (1998) and DeDear et al. (1997) did consider non-uniformity of heat distribution for the different body segments (see Table 2.2).

Author	Modeling Aspect	Computational Aspect
Brohus et al. (1996)	'Block' configuration	Standard k-ε Model
Kato et al. (1996)	Detailed model (uniform)	Launder-Sharma type Low-Reynolds Number k-ε Model
DeDear et al. (1997)	Detailed model (Non-uniform)	---
Murakami et al. (1997-98)	Detailed model (uniform)	Launder-Sharma type Low-Reynolds Number k-ε Model
Murakami et al. (2000)	Detailed model (Non-uniform)	Launder-Sharma type Low-Reynolds Number k-ε Model
Topp et al. (2002)	Detailed model (uniform)	Launder-Sharma type Low-Reynolds Number k-ε Model
Sørensen et al. (2002-03)	Detailed model (Non-uniform)	Launder-Sharma type Low-Reynolds Number k-ε Model
Sideroff et al. (2005)	Detailed model (uniform)	Launder-Sharma type Low-Reynolds Number k-ε Model

Table 2.2: Occupant models used for different application with various level of complexity

The studies shown in Table 2.2 performed their work in an empty room with only one highly detailed occupant model and without any other heat sources. None of the discussed detailed occupant configurations were integrated in any large-scale modeling of

offices or classrooms due to the very large computational requirement. The high computational cost is due to the fact that the Launder-Sharma type Low-Reynolds Number k-ε Model requires a very fine grid distribution at surface boundaries, making it inapplicable for large-scale CFD modeling. Finally the complicated shape of the occupant model itself requires a large number of cells: for example, Murakami et al. (2000) used 163,008 cells for the surface of the occupant model in a flow domain of 2.7 m by 2.2 m by 2.6 m (see Figure 2.3a). Sørensen et al. (2002) used approximately 500,000 cells alone for the surface of the occupant model in a flow domain of 2.95 m by 2.95 m by 2.4 m (see Figure 2.3b). Therefore, it is plausible that a typical volume grid for the entire flow domain could be in order of several millions for a small empty room: Sideroff and Dang (2005) report that for the case of detailed occupant model in a small empty room in order to achieve grid convergence with tetrahedral cells and using the Launder-Sharma type Low-Reynolds Number k-ε Model, a volume grid of 4.6×10^6 was required! Obviously due to limited computer resources, various uncertainties, lack of standards and the disagreements that exist, none of the discussed detailed models are being employed in any full-scale CFD simulations for large enclosure.

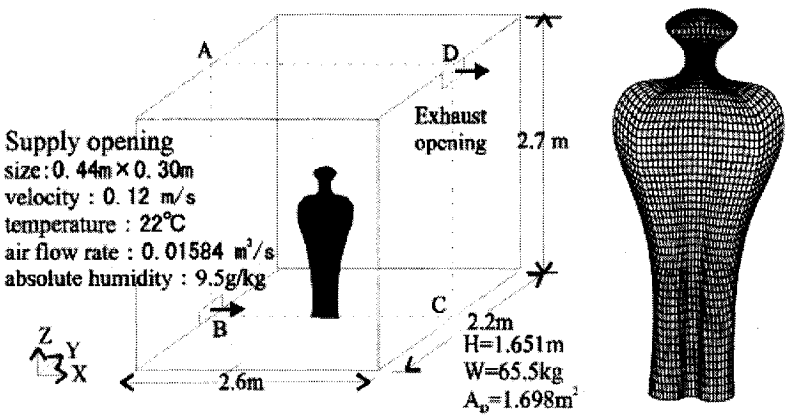

Figure 2.3a: Occupant model developed by Murakami S. et al. (1997).

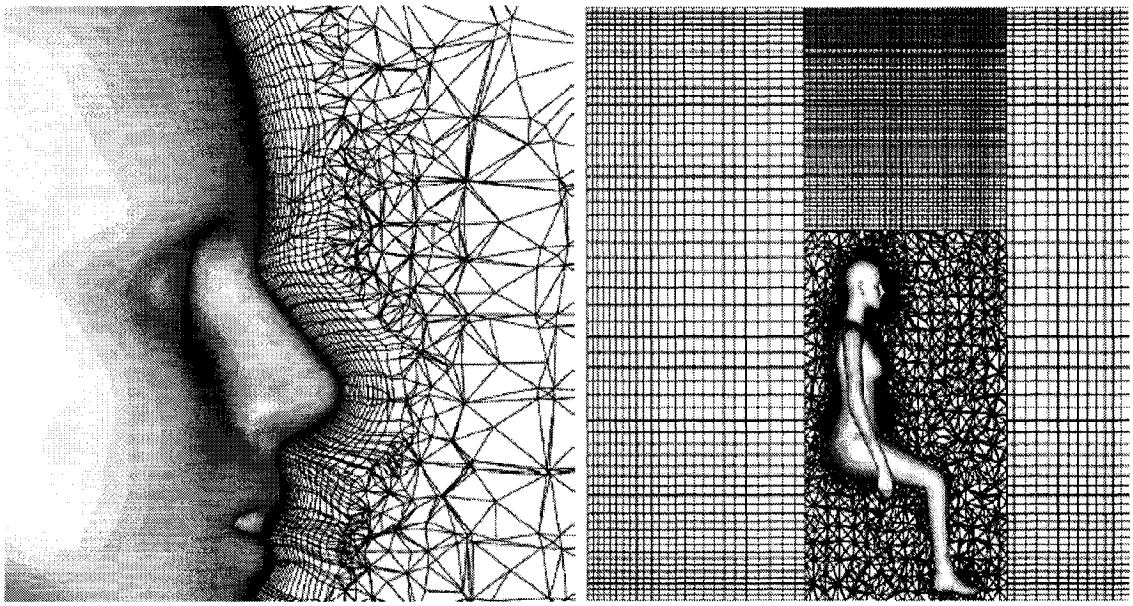

Figure 2.3b: Occupant model developed by Sørensen, DN. et al. (2003).

An occupant model influences the flow field and the local thermal distribution by posing as a physical obstacle to the flow and by its heat distribution. As seen in Table 2.1, for large-scale CFD modeling of ventilated enclosures different occupant configurations are used irrespective of the type of ventilation system. Therefore, it is very important to investigate the interaction of different occupant configurations with various Heating, Ventilation and Air-Conditioning (HVAC) systems, such as full-mixing air distribution, localized ventilation and buoyancy-driven displacement ventilation systems. Previous works by Nielsen et al. (2003) and Sideroff and Dang (2005) on the subject of mixing ventilation system assumed that the occupant is exposed to a uniform horizontal flow field as depicted in Figure 2.4. However, the uniform horizontal flow field is an assumption and is not the case in more realistic scenarios. Therefore, the influence of the occupant configuration and heat distribution must be quantified in a ventilated enclosure equipped with a full-mixing ceiling air distribution system.

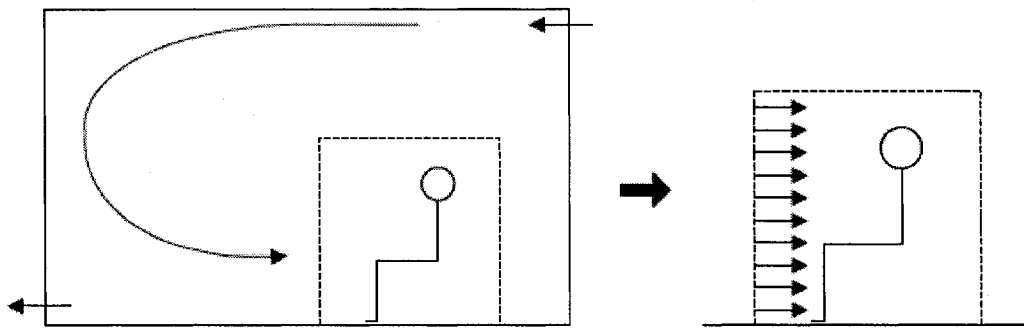

Figure 2.4: A person is exposed to a flow field in a mixing ventilated room that locally may be considered as a uniform flow (Nielsen, P. et al., 2003);
"Benchmark Tests for Computer Simulated Person" (2003), Aalborg University, Indoor Environmental Engineering

Furthermore, the effect of occupant configuration and its heat distribution for a room equipped with underfloor air distribution system was not addressed in previous research and thus must be studied. The effect of occupant configuration with uniform heat distribution for an empty room equipped with a displacement ventilation system with one occupant was addressed in previous work by Sørensen et al. (2002), Topp et al. (2002), Nielsen et al. (2003) and Sideroff and Dang (2005). However, this needs to be expanded to study in a large and realistic ventilated enclosure.

2.3 Objective of the Study

There has been a new surge of interest in the development of the localized ventilation systems in the industry, consequently focusing the study on the flow field within the occupant microclimate. Various aspects of occupant thermal modeling were covered: from the detailed occupant models (Sørensen, 2002; Murakami, 2000) conceived for the study of human body's thermo-regulatory system, to basic occupant modeling methods

that are being used for realistic large-scale CFD modeling of indoor environment. The problem of occupant modeling is complicated, first, by the lack of any standards for available CFD packages on the detailed modeling of the occupant body. Although Murakami et al. (2000) have been trying to bridge that gap by developing a complete energy-balance human model. Second, the limitation of today's computer resources is the governing parameter that imposes severe constraints on the proper CFD modeling of the occupant's body. Thus, various simplifications and assumptions are made in order to make a numerical study of an indoor environment feasible. Occupant model configurations are simplified by being presented as heated blocks and are assumed to have a uniform heat distribution over each of the body segments. It is the objective of this study to investigate the following points:

- To verify the assumption of uniform heat distribution for various flow fields
- To perform a study in order to quantify the kind of simplification can be made on the configuration of the occupant model without affecting the local flow field drastically
- To design an optimized occupant configuration to be applicable for full-scale CFD modeling of ventilated enclosure that is however simplified enough to be used with the available computational resources.

3.0 METHODOLOGY

3.1 Mathematical Model

All the variants of Computational Fluid Dynamics (CFD) methods are based on the governing equations for a fluid flow, which have been known for over 150 years. The fluid governing equations are derived from the laws of conservation of mass, momentum and energy.

3.1.1 Governing Equations

The conservation of mass ensures that the mass flow is conserved for a small volume of the flow as depicted in Equation 3.1. It makes the difference between ingoing and outgoing airflow zero.

$$\frac{\partial \rho}{\partial t} + \nabla . (\rho \vec{u}) = 0 \qquad (3.1)$$

where,

$\rho =$ Density of the fluid (kg/m^3)

$\vec{u} =$ Velocity of the fluid (m/s)

The airflow in indoor environment is generally assumed to be incompressible thus yielding the following formulation from Equation 3.1.

$$\nabla . (\vec{u}) = 0 \qquad (3.2)$$

The conservation of momentum is derived from the Newton's Second Law as shown in Equation 3.3. The right hand side shows the sum of all the forces, where the ∇p is the pressure gradient, τ is the stress tensor and is the function of μ, the molecular viscosity, ρg is the gravitational body force and finally S_u is designated to show other forces that might exist. Finally, the convective term on the left hand side expresses the net supply of momentum from surroundings fluid.

$$\frac{\partial}{\partial t}(\rho\vec{u}) + \nabla.(\rho\vec{u}\vec{u}) = -\nabla p + \nabla.(\tau) + \rho\,\vec{g} + S_u \tag{3.3}$$

where,

ρ = Density of the fluid (kg/m^3)

$\vec{u}$ = Velocity of the fluid (m/s)

τ = Stress tensor

P = Pressure (N/m^2)

$\vec{g}$ = Gravitational acceleration (m/s^2)

S_u = Source term (N/m^3)

The conservation of energy shown in Equation 3.4 is derived from the First Law of Thermodynamics. It describes the temperature distribution throughout a non-isothermal flow domain. The first term in the left-hand side is the rate of increase in internal energy with change in time, the second term in the left-hand side is the net heat convection into the fluid element. The right hand side is the heat diffusion by laminar thermal conductivity, λ_l, and by conductivity due to turbulence transport, λ_t. The laminar

thermal conductivity, λ_l, is a property of the fluid, while the turbulent conductivity, λ_t is the property of the flow. The last term on the right-hand side is the source term S_t, which represents heat sources.

$$\frac{\partial}{\partial t}(\rho c_p T) + \nabla . (\rho c_p \vec{u} T) = \nabla . [(\lambda_l + \lambda_t) \nabla T] + S_t \tag{3.4}$$

where,

ρ = Density of the fluid (kg/m^3)

c_p = Specific heat at constant pressure (J/kg^{o}C)

$\vec{u}$ = Velocity of the fluid (m/s)

T = Air temperature (^{o}C)

λ_l = Laminar thermal conductivity (W/m^{o}C)

λ_t = Turbulent conductivity (W/m^{o}C)

S_t = Source term (W/m^3)

Another important note is the Boussinesq approximation, which stated that the change in fluid density is negligible, i.e. incompressible flow, for all terms except for the buoyancy term in the momentum equation (Equation 3.3), because of the importance of the change in density that gives rise to buoyancy.

3.1.2 Turbulence Modeling

The correct prediction of the airflow pattern and the temperature distribution is very importance for detailed analysis of the performance of any HVAC system. Generally, the

air motion in a ventilated enclosure is incompressible, non-isothermal and turbulent in nature. The detailed modeling of the turbulence with today's limited computer technology through Direct Numerical Solution (DNS) or Large Eddy Simulation (LES) is impossible for building airflow problems (Schild, 1997). Therefore, for practical CFD prediction of the turbulent behavior in a flow field, the governing equations are decomposed into the mean and fluctuating components, since only the mean motion is of interest. The most commonly used turbulence models for the prediction of the indoor airflow field are the two-equation eddy-viscosity models: the Standard k-ε and the Re-Normalization Group (RNG) k-ε model.

The Standard k-ε model (Launder and Spalding, 1974) is a two-equation model where the turbulent velocity and length scales are independently determined by computing the turbulence kinetic energy, k, and its dissipation rate, ε. The turbulent viscosity, μ_t, is described by the following relationship:

$$\mu_t = \rho C_\mu \frac{k^2}{\varepsilon} \tag{3.5}$$

where,

μ_t = Turbulent viscosity (kg/m s)

ρ = Density of the fluid (kg/m^3)

C_μ = Constant (0.09)

k = Turbulence kinetic energy (m^2/s^2)

ε = Rate of dissipation of turbulence kinetic energy (m^2/s^3)

The Standard k-ε model was originally developed for fully turbulent high Reynolds Number flows. However, in regions near the wall where the Reynolds Number is low, the Standard k-ε model is known to over-predict the turbulent viscosity, μ_t, thus making it inaccurate for flow prediction in near wall regions. The accuracy of the Standard k-ε model in predicting air pattern and heat transfer largely depends on how well the boundary conditions are imposed. Most researches and commercial codes use Wall Functions in order to predict momentum and heat transfer phenomena very close to the wall. A better prediction can be obtained by using a Low-Reynolds Number k-ε turbulence model, which however could be extremely expensive in computing terms for a 3-D problem especially in a large ventilated enclosure because of the fine grid requirements near the walls (Awbi, 1996).

The Re-Normalization Group (RNG) k-ε model uses a rigorous statistical technique known as the renormalization group theory (Yakhot and Orszag, 1986). The RNG-k-ε model has an additional term that helps to increase the accuracy of rapidly strained flows, while providing analytically derived differential formulae for an enhanced computation of the viscosity effect that does occur in low-Reynolds Number flow regimes. Due to the extra term for the ε equation and the higher degree of non-linearity the computational time of RNG-k-ε model is at least 10-15 % higher than the two-equation Standard k-ε model and is less stable (Airpak Documentation, 2002).

3.2 Numerical Methodology

3.2.1 Flow Domain and the Experimental Setup

For this research, a CFD model for a ventilated enclosure, a typical classroom, equipped with a displacement ventilation system, was constructed and validated using experimental measurements. The experimental measurements were carried out in a Controlled Environmental Chamber (CEC) located at the Center for Building Environment in Sweden (Karimipanah, 2000). The CEC is a 7.2-by-8.4 m classroom (60.48 m^2) with a height of 3 m. A climate chamber was used to simulate the outdoor winter environment behind five tripled-glazed windows on the west wall, each measuring 1.074-by-1.472 m. The classroom was equipped with two displacement ventilation diffusers supplying a total of 233 L/s airflow at the supply temperature of 15.1°C. The diffusers are located at the height of 0.14 m from the floor and are discharging vertically downward. The total internal heat gain in the experimental setup was 2,900 W, corresponding to the presence of twenty-five body simulators and nine overhead lights. The twenty-five body simulators were used in the experimental setup to simulate the presence of twenty-five occupants. Each body simulator has a surface area of 1.69 m^2 and is emitting a total power of 95 W uniformly. The overhead lights (0.3-by-1.65 m) were hung at 51 cm from the ceiling and contributed a total power of 525 W.

Figure 3.1: The actual classroom experimental setup in the controlled environmental chamber (CEC);

3.2.2 Boundary Conditions

The boundary conditions imposed on the related partial differential equations, Equations 3-1 to 3-4, are implemented using a variety of methods as discussed below.

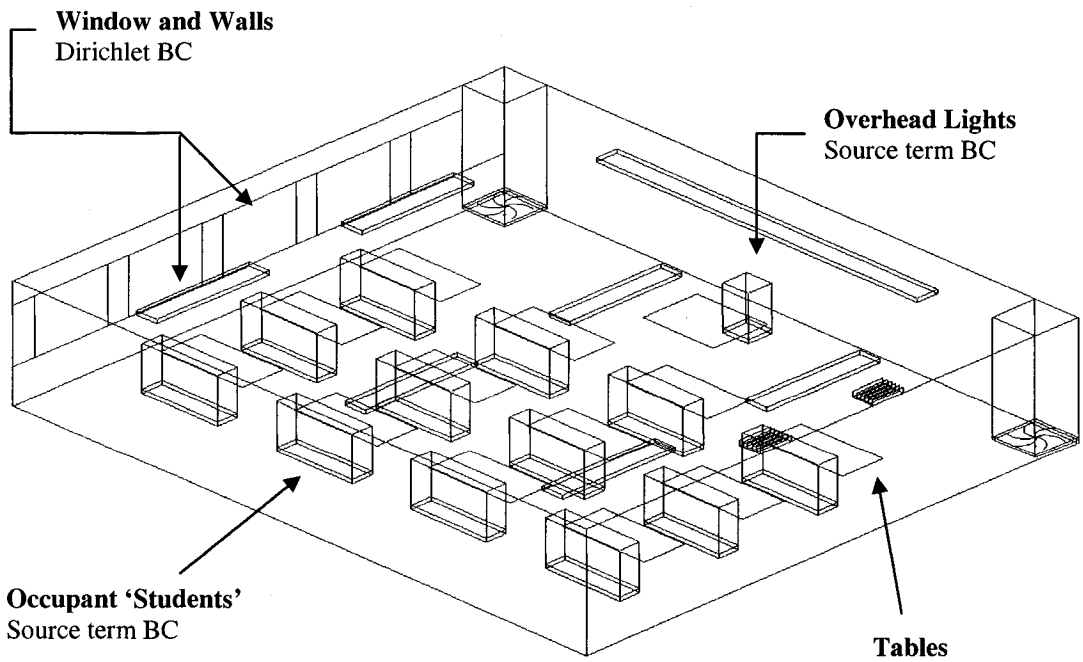

Figure 3.2: Thermal Boundary conditions used for the CFD model

WALLS AND WINDOWS

Heat transfer from walls is modeled using Dirichlet boundary condition where a uniform surface temperature is prescribed on the inner surface of the wall as shown in Table 3.1 and Figure 3.3. Near the wall, the surface friction causes the flow velocity to reduce to zero velocity: the no-slip boundary condition.

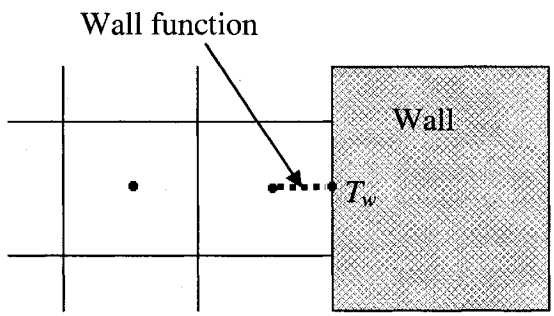

Figure 3.3: Thermal Boundary conditions used for the walls in the CFD model

Dirichlet Boundary Conditions						
Floor	Ceiling	North	East	South	West	Window
21.9 °C	23.4 °C	21.8 °C	22.6 °C	23.2 °C	21.1 °C	14.1 °C

Table 3.1: Walls and windows surface temperature

INTERNAL HEAT SOURCES

Heat transfer from occupants and overhead lights were modeled as sources. All internal heat sources (occupant and lights) are modeled by using 'hollow' blocks with uniform heat flux (q) as the boundary condition, shown in Table 3.2 and Figure 3.4. This method is comparable to using both the inner wall surface temperature, T_w, and convective heat transfer coefficient, h_c, as boundary conditions.

Mixed Boundary Conditions				
Lights	Total Lights	Occupants	Total Occupants	Total Heat Gain
58.33 W	525 W	95 W	2,375 W	2,900 W

Table 3.2: Internal Heat Gain within the classroom and Supply/Boundary conditions

By applying heat flux as boundary conditions, the heat transfer from block surface becomes independent of the grid distribution because the q is directly prescribed into the energy equation as the source term, S_t, shown in Figure 3.4. Nevertheless, the Wall Functions are equally significant because the convective heat transfer coefficient must be computed in order to calculate the block surface temperature, which is needed for radiation heat transfer and the thermal comfort equations.

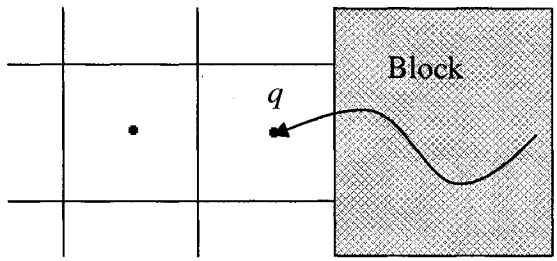

Figure 3.4: Thermal boundary conditions used for the occupant and lights in the CFD model

Near the object surfaces the no-slip boundary condition is applied in order to bring the flow to rest due to viscous effects. In order to reduce computational time, two body simulators located at each table were modeled as one source with a total surface area of 3.38 m^2. All the heated blocks used to model body simulators were located between the heights of 0.1 m to 1.2 m.

DIFFUSERS

Because of the complicated structure of incoming air, the modeling of the diffuser is a challenging task. The detail simulation of flow field induced by diffusers requires rigorous CFD modeling and fine grid distribution, and therefore will be beyond the scope of this work. Nielsen (1992) introduced a simplified approach known as the momentum method for the task of modeling the diffuser. These simplified modeling methods help to greatly reduce the need for large grid refinement near diffusers. The momentum method

assumes that the airflow from a particular diffuser can be predicted by using the isothermal axisymmetric jet formula expressed in Equation 3.6.

$$\frac{u_m}{u_o} = K_1 \left(\frac{\sqrt{A_o}}{x}\right) \tag{3.6}$$

Equation 3.6 takes as input, the centerline jet velocity, u_m, at a distance, x, from the diffuser and the centerline velocity decay constant, K_1. Using these inputs, the initial jet velocity, u_0, and effective area of supply diffuser, A_0, are computed. In the case of the classroom, two displacement ventilation outlets are supplying a total airflow rate of 233 L/s. The simplified diffuser model was based on the criterion that a typical displacement ventilation diffuser discharges air at a low momentum, usually with a velocity of less than 0.3 m/s (Karimipanah et al., 2000). Therefore, the A_{geom} of the diffuser model was calculated based on the constraint for the maximum discharge velocity to be equal or less than 0.3 m/s.

TABLES

All twenty-five tables in the room are modeled as adiabatic partitions where the thermal gradient, $\partial T/\partial x$ was set to zero. All the tables have no-slip boundary conditions imposed on them to bring the flow to rest at the surface.

3.2.3 Modeling Methods

The turbulent nature of the flow can be determined via the Rayleigh Number as shown in Equation 3.6. The Rayleigh Number is used to determine if the flow that is being induced by buoyancy will become unstable and undergo transition to a turbulent condition;

transition occur for values in the range of 10^7 < Ra < 10^9. The Rayleigh Number is computed for this classroom problem using inputs shown in Table 3.3. The large magnitude of the Rayleigh Number indicates that the induced flow due to buoyancy has indeed pass beyond the transition phase and is into the turbulent condition thus justifying the use of a turbulence model.

g	β	ΔT	L	ν	θ	u
m/s^2	K^{-1}	K	m	m^2/s	$W.m^2/J$	m/s
9.8	$3.37x10^{-3}$	6.9	3	$1.58x10^{-5}$	$2.21x10^{-5}$	0.3

Table 3.3: Inputs parameters for the Rayleigh Number.

$$\text{Rayleigh Number} = \frac{g.\beta\ .\Delta T.L^3}{\nu.\theta} = 1.76\times10^{10} \tag{3.7}$$

where,

g = Gravity (m/s^2)

ΔT = Temperature difference (^oC)

L = Reference Length (m)

ν = Kinematics viscosity (m^2/s)

θ = Thermal diffusivity ($W.m^2/J$)

β = Thermal expansion coefficient of air (K^{-1})

The Standard k-ε Model (Launder and Spalding, 1974) was chosen due to its stability and reliability in order to predict the flow pattern. Additionally, in any CFD simulation with numerous heat sources, the effect of radiation is significant. Therefore, the surface-to-surface radiation model was used to take radiation into account.

3.2.4 Numerical Schemes

The coupled, non-linear, partial differential equations for a three-dimensional, turbulent flow field cannot be solved analytically. The commercially available Airpak software from Fluent Inc. is therefore used to compute the flow field numerically. The solver uses the finite volume method to convert the governing equations for conservation of mass, momentum and energy to algebraic equations that can be solved. The First Order Upwind Scheme was used for all parameters except the pressure. For pressure the Body-Force-Weighted Scheme was used, which is recommended for high-Rayleigh-number natural convection flows (Airpak Documentation, 2002).

The pressure-velocity coupling algorithm SIMPLE (Semi-Implicit Method for Pressure-Linked Equations) introduced by Patankar (1980) is used. Given an initial pressure field, the solver computes the momentum equations. The velocity components are then calculated and a correction term is applied to the pressure in order to get a new value for pressure. After the temperature and turbulent quantities are computed, the revised pressure is further taken as the new pressure field until convergence is achieved. Convergence is judged by the steady decrease of the residuals of the discretised conservation equations and by the very small change in the flow field values between two iterations.

Due to high non-linearity of the partial differential equations being solved, the rate of their change is controlled by under-relaxation factors in order to improve the stability of the solution. The under-relaxation factors are generally pre-optimized in order to

accommodate a wide-range of applications. However, for this study the under-relaxation factors for pressure and momentum had to be reconfigured in order to obtain a converged solution. The under-relaxation factor for the pressure was increased from 0.3 to 0.7, and that of momentum was decreased from 0.7 to 0.3. The change in the under-relaxation factor for pressure ensures that the change in pressure value from one iteration to the next will be restricted to 70% of the difference between the initial value and the newly calculated value. While inversely for the momentum, the change in momentum value from one iteration to the next will be restricted to 30% of the difference between the initial and the new one.

Discretization Schemes						
Momentum		Temperature		Turbulent Dissipation	Turbulent Kinetic Energy	
First Order		First Order		First Order	First Order	
Under-Relaxation Factors						
Momentum	Pressure	Temperature	Viscosity	Body Forces	Turbulent Dissipation Rate	Turbulent Kinetic Energy
0.3	0.7	1.0	1.0	0.1	0.5	0.5
Termination Criteria						
Turbulent Kinetic Energy and Dissipation Rate			Flow		Energy	
$1.0x10^{-3}$			$1.0x10^{-3}$		$1.0x10^{-7}$	

Table 3.4: The computational detail for the validation problem

3.2.5 Occupant Thermal Model Configuration

For this study, in order to perform an analysis of the flow field and distribution of temperature in the occupant microclimate, several occupant models of various configurations were constructed. All the constructed configurations were based on a manikin with sixteen segments developed by Tanabe et al. (1994). Using ratios of heat release of a body segment per the entire occupant shown in Table 3.5, the appropriate

heat loss per body segment was computed. Seven distinct occupant thermal models were built from the base-case as shown in Table 3.6.

- Single 'Block' model
- Three-node model (uniform/non-uniform heat distribution)
- Six-node model (uniform/non-uniform heat distribution)
- Eight-node model (uniform/non-uniform heat distribution)

Base Case			
Body Segments	Area m^2	Non-uniform W/m^2	Uniform W/m^2
Head	0.173729	53.8439	56.2130
Chest	0.178555	47.8612	56.2130
Back	0.196893	51.4508	56.2130
Pelvis	0.077213	41.8786	56.2130
Hand (right)	0.048258	70.5954	56.2131
Arm (right)	0.059840	44.8699	56.2130
Shoulder (right)	0.074318	47.8612	56.2130
Hand (left)	0.048258	70.5954	56.2131
Arm (left)	0.059840	44.8699	56.2130
Shoulder (left)	0.074318	47.8612	56.2130
Leg (right)	0.135123	61.0231	56.2130
Thigh (right)	0.154426	58.0317	56.2130
Foot (right)	0.059840	83.7571	56.2130
Leg (left)	0.135123	61.0231	56.2130
Thigh (left)	0.154426	58.0317	56.2130
Foot (left)	0.059840	83.7571	56.2130
Total	**1.69**	**56.213**	**56.2130**

Table 3.5: Occupant configuration based on the experimental work performed by Tanabe et al. (1994) *"Evaluating Thermal Environments by Using a Thermal Manikin with Controlled Skin Surface Temperature", Tanabe, S. et al., ASHRAE Transactions: Research (1994), volume 100, part 1, page 39-48*

Each segment of the multi-node models was created in Airpak as 'hollow blocks'. When two 'hollow blocks' share a surface, there is no heat transfer across that shared surface. All the occupant configurations are located at the height of 0.1 m above the floor since the base-case occupant configuration was located at the distance. There is no heat flux emitting vertically downward from the feet. All the occupant configurations developed in this study have a total heat emitting surface area of 1.69 m^2 and a total heat loss of 95 W:

a value based on the heat emission of the body-simulator used by Karimipanah et al. (2000). The total height of all occupant configurations is 1.2 m. The eight-node configuration further took into account the presence of the chair: the boundary condition at the lower surface area of the 'Body' block was set to zero. Nevertheless, the total heat emitting surface area can be summed to 1.69 m^2. The schematics for various occupant model configurations used in this study are presented in Figures 3.5 and 3.6.

	Area m^2	**Non-uniform** W	**Uniform** W
		Block method	
Block	1.690	95.000	95.000
Total	**1.690**	**95.000**	**95.000**
		Three-node Model	
Head	0.174	9.354	9.766
Lower Body	0.699	44.439	39.280
Body	0.817	41.207	45.954
Total	**1.690**	**95.000**	**95.000**
		Six-node Model	
Head	0.174	9.354	9.766
Arm (Left)	0.182	9.649	10.254
Arm (Right)	0.182	9.649	10.254
Leg	0.390	26.515	21.919
Thigh	0.309	17.923	17.361
Body	0.453	21.910	25.445
Total	**1.690**	**95.000**	**95.000**
		Eight-node Model	
Head	0.174	9.354	9.766
Arm (Left)	0.182	9.649	10.254
Arm (Right)	0.182	9.649	10.254
Leg (Left)	0.195	13.258	10.959
Leg (Right)	0.195	13.258	10.959
Thigh (Left)	0.154	8.962	8.681
Thigh (Right)	0.154	8.962	8.681
Body	0.453	21.910	25.445
Total	**1.690**	**95.000**	**95.000**

Table 3.6: Occupant thermal models developed in this study from Tanabe et al. (1994)

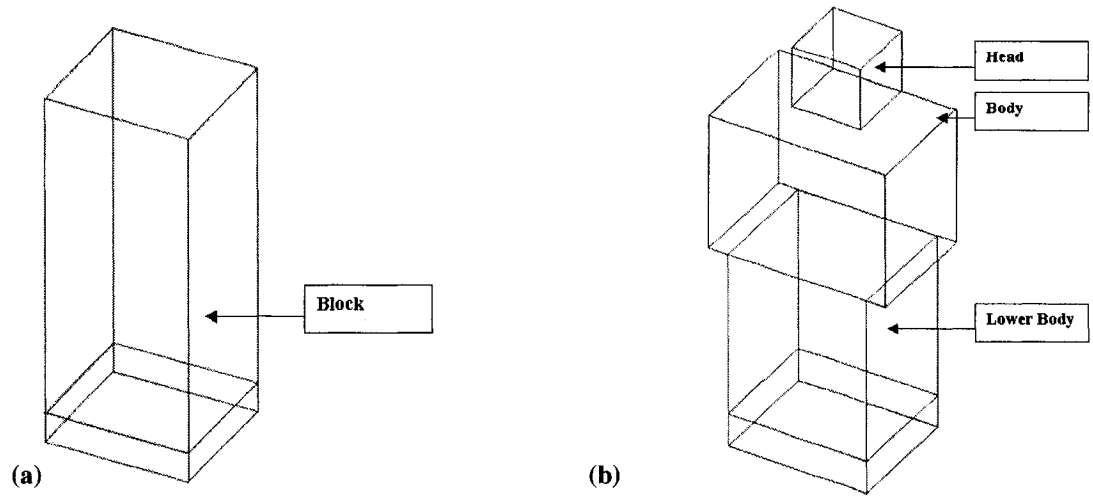

Figure 3.5: Occupant configuration single-node (a) and three-node configurations (b).

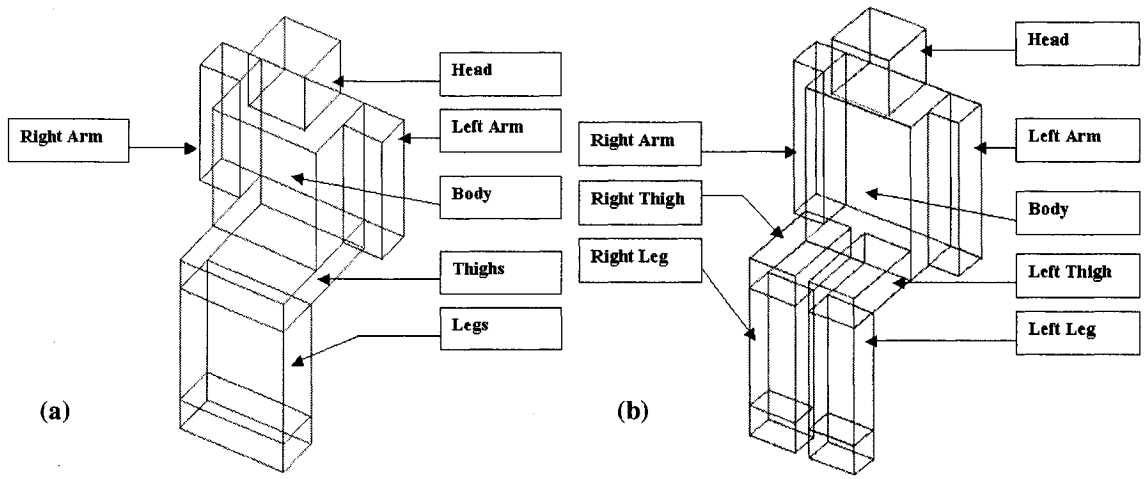

Figure 3.6: Occupant configuration six-node (a) and eight-node configurations (b).

3.2.6 Grid Generation

GRID IN THE CLASSROOM MODEL

A CFD model needs to be meshed into various discrete elements, where the solver calculates the flow and heat equations for each of the element. Two kinds of grid generation techniques are generally used: the structured-hexahedral grid and unstructured-tetrahedral grid for more complicated geometry.

Grid	Volume Element	Location Index	Grid Line Requirement
Structured	Hexahedral	i, j, k, index to locate neighboring element	Continuous between opposite boundaries
Unstructured	Tetrahedral	No location index	No requirements

Table 3.7: Grid topologies

A structured mesh is propagates between opposite boundaries (ex. a heat source between two walls), while an unstructured mesh is typically fine around the object of interest. Therefore, a structured hexahedral mesh continues the fine element distribution outside the area of interest using a larger number of elements. That being said, a hexahedral mesh is a typical approach for simulation of indoor airflow, since the problem setup is straightforward, highly controllable and the solution process normally found to be stable in combination with the Standard k-ε turbulence model (Niu, 1994). On the contrary, an unstructured tetrahedral mesh does require much higher memory and CPU power. Loomans (1992) reported that the use of unstructured tetrahedral mesh is less suited for the generally rectangular shape of an indoor enclosure and is even worse for the cases that are characterized by strong presence of buoyant flow. The grid generation is an iterative procedure where there exists a trade-off between computational cost, mesh quality and accuracy. The quality of the mesh is of outmost importance for a good CFD solution, where the computational cost is directly proportional to the number of elements. Using a coarse mesh may result in large numerical errors, whereas a fine grid may be computationally too expensive for a large enclosure. Therefore, in order to compromise between computational accuracy and computing cost, the mesh should be refined where the gradients are high, near the air inlet/outlet, walls and various heat sources. A typical good quality grid requires: proper resolution, smoothness, low skewness and appropriate number of elements. The mesh quality is quantified by its face alignment, where it is

defined as the following: c_0 and c_1 are the centroids of two adjacent elements and $\vec{f}$ is the normal vector between two elements. A face alignment of 1 indicates an optimal element, whereas a face alignment of less than 0.15 indicates a distorted element (Figure 3.7).

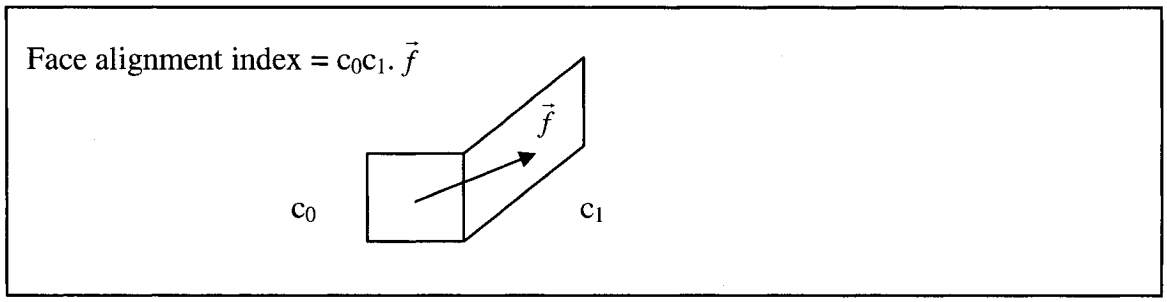

Figure 3.7: Definition of face alignment

A good quality mesh needs to have its number of thin and long elements minimized in order to improve the solution. The aspect ratio for a hexahedral mesh is defined as the ratio of the element's shortest length to its longest length. An aspect ratio of 1 indicates an optimal element, whereas an aspect ratio of less than 0.15 indicates a distorted element (Airpak Documentation, 2002). A bad aspect ratio might create numerical error (Loomans, 1992). The experimental setup of the classroom had mostly circular-coordinate objects: twenty-five body simulators and the two circular-shaped diffuser ducts. As stated previously, the two body simulators at each table were modeled as one block to reduce computational time. The rectangular configuration was chosen for the occupant model in order to improve the mesh quality. Furthermore, it was observed that the modeling of the two circular-shaped diffuser ducts as circular-objects greatly reduced the quality of the mesh at the critical area of the diffuser outlet. Instead, a rectangular geometry was used to model the diffuser duct as illustrated in Figure 3.8. A minimum-count mesh was employed at first and refined globally. Further refinements were made locally near the walls, heat sources and the air inlet/outlets. The first grid at the wall was

positioned at the distance of 10 mm from the wall surface as recommended by Awbi (1998) and Karimipanah (2000). The initial grid, Grid A, had 28 x 51 x 47 nodes along the x, y and z edges, respectively. This resulted in a volume grid of 834,780 hexahedron cells. A second mesh, Grid B, made up of 31 x 51 x 47 nodes along the x, y and z edges, respectively, was used with a total volume grid of 1,323,554 hexahedron cells. A third grid was employed in order to check grid independence by increasing the nodes along the x, y and z edges of the walls as observed in Table 3.8.

Grid	Number of Nodes (x, y and z edges)	Volume Grid	Worse Aspect Ratio	Face Alignment
A	28 x 51 x 47	834,780	0.64678	0.959458
B	31 x 51 x 47	1,323,554	0.86254	0.953364
C	40 x 70 x 60	1,503,734	0.75636	0.971096

Table 3.8: Mesh size and quality for grid dependency

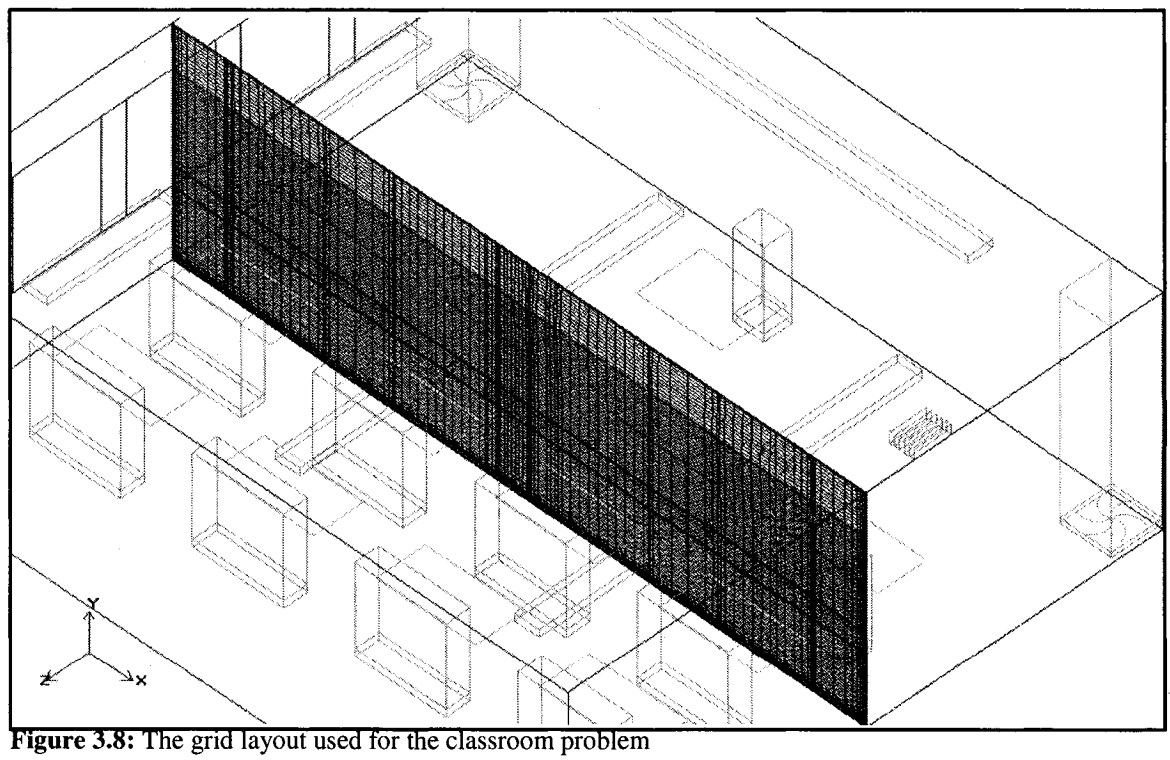

Figure 3.8: The grid layout used for the classroom problem

GRID NEAR THE OCCUPANT

In order to fix the distance of the first grid from the occupant block a local grid independent check was performed. Various cell positions from the surface were tested as shown in Figure 3.10. The results for several flow points show that by putting the first grid at the distance of 10 mm from the block surface the magnitude of air velocity and temperature does not change significantly. Similar conclusions were drawn for other occupant configurations based on tests performed in natural convection and mixed convection dominated flow fields. For all grid layouts a minimum of 60 cells were used in the vertical direction. A typical grid used for the eight-node configuration is illustrated in Figure 3.9.

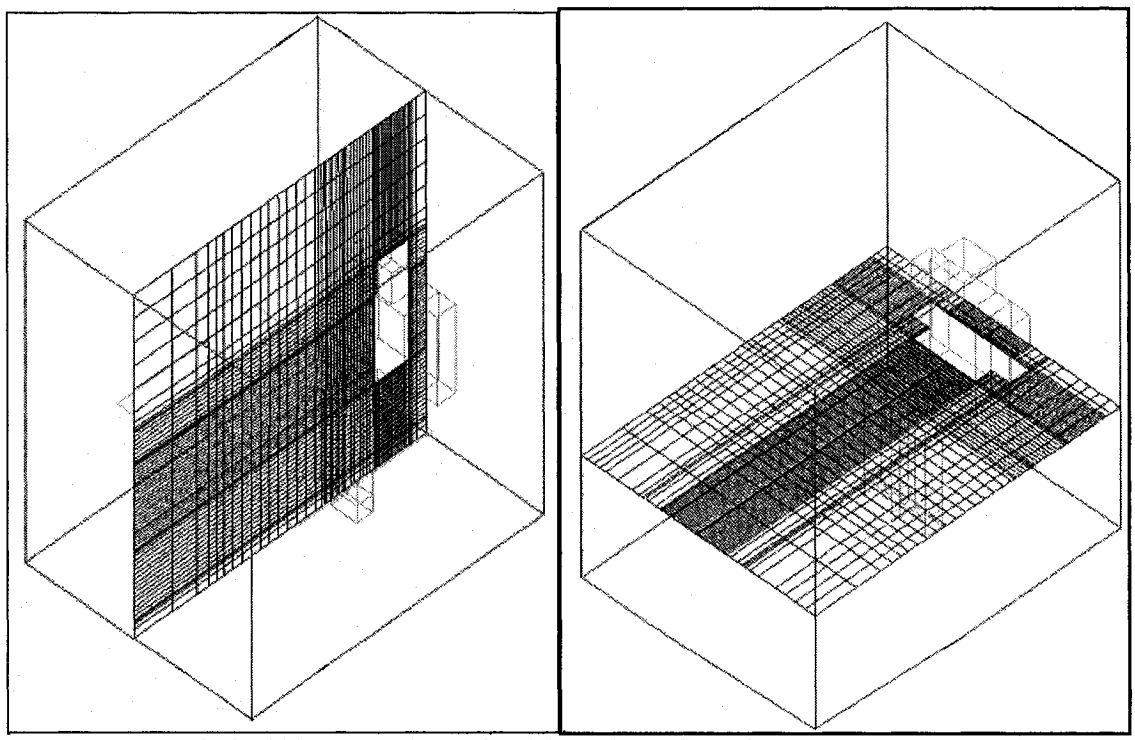

Figure 3.9: A typical grid layout used near the eight-node configuration

For the present study, the dimensionless distance y^+ was computed in order to determine the position of the first node within the boundary layer. By taking the turbulence kinetic energy at the first grid node from the CFD solution file, the y^+ was computed using Equations 3.8 to 3.10. In all cases, the y+ ranges between 47 and 88, with the average y^+ being 71: within the log-law turbulent region. The maximum cell ratio was set to 2, thus making sure that the second computational point falls within the boundary layer.

$$y^+ = \frac{y_p u^*}{\nu} \tag{3.8}$$

$$u^* = \sqrt{\frac{\tau_w}{\rho}} \tag{3.9}$$

$$\tau_w = C_\mu^{1/2} \rho k_p \tag{3.10}$$

where,

y^+ = Dimensionless distance

u^* = Frictional velocity (m/s)

ν = Kinematics viscosity (m^2/s)

y_p = Grid node distance from the surface (m)

τ_w = Wall shear stress (N/m^2)

ρ = Density of the fluid (kg/m^3)

C_μ = Constant (0.09)

k_p = Turbulence kinetic energy at the first grid node (m^2/s^2)

CASE	1	2	3	4	5	6	7	8	9	10	11
grid height (m)	0.05	0.04	0.03	0.02	0.01	0.009	0.008	0.007	0.006	0.005	0.004

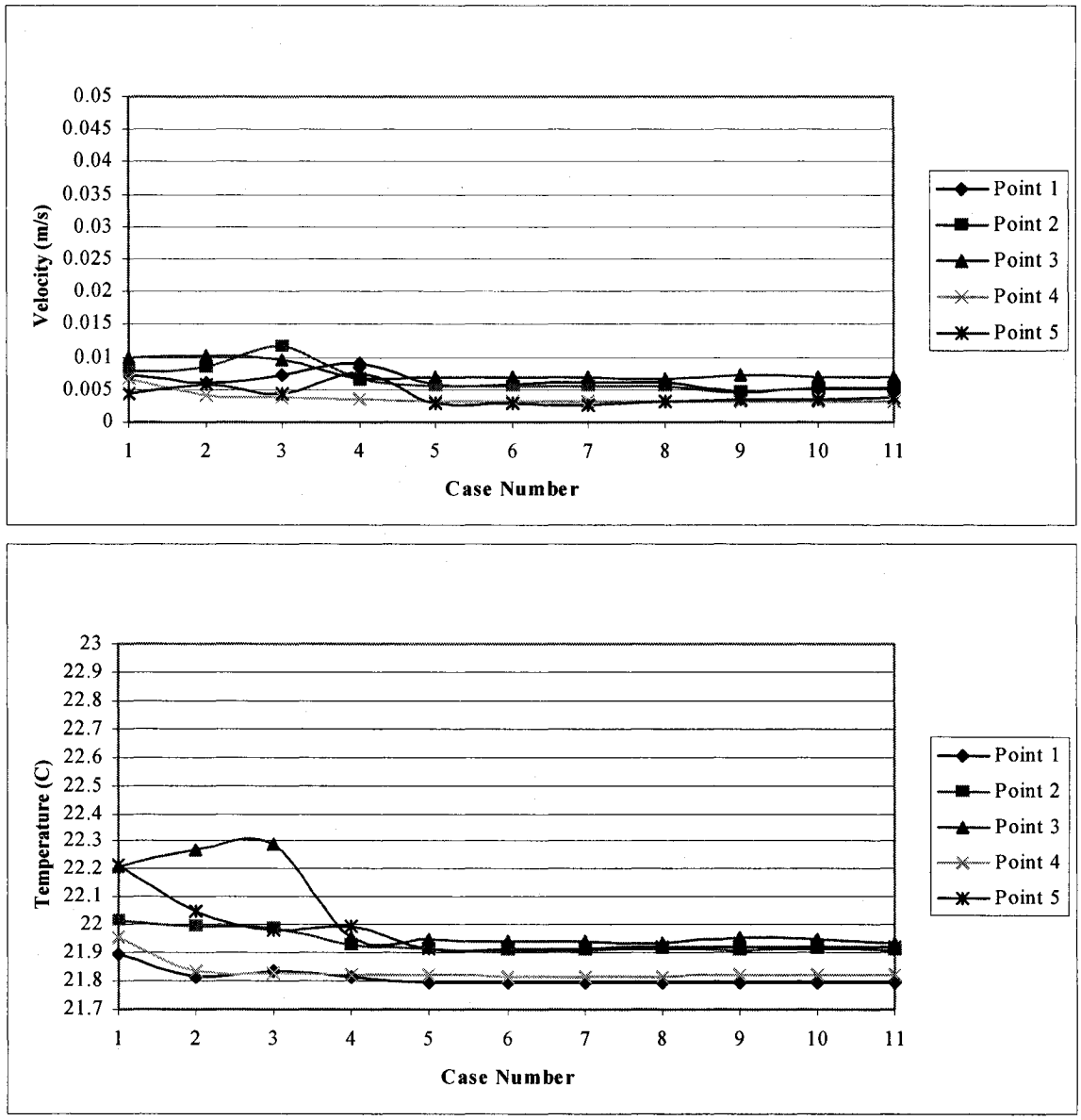

Figure 3.10: The local grid dependent check near the occupant

3.2.7 Thermal Comfort Equations

The performance of a building HVAC system is directly related to three factors: thermal comfort, indoor air quality and energy consumption. Thermal comfort is described as the

condition of mind that expresses satisfaction with the thermal environment (ASHRAE, 1992). The thermal comfort standards are used both as design and diagnostic tools for indoor environments. The thermal comfort study employed by the ASHRAE Standard 55-1992 and ISO Standard 7730 are based on steady-state heat exchange between the occupant and the environment. The influencing physical variables are the air temperature, radiant temperature, relative humidity and air velocity, and the personnel variables are the clothing value and metabolic rate. The energy that is released by metabolism is directly dependant on the level of activity. The metabolic rate for various office workers is typically between 0.9 to 1.2 met, where 'met' is the unit of metabolic rate.

$$1 \text{ met} = 58.2 \text{ W/m}^2 \tag{3.11}$$

Activity		Metabolic Rate (M)
Reclining	45 W/m^2	0.8 met
Seated Relaxed	58 W/m^2	1.0 met
Standing Relaxed	70 W/m^2	1.2 met

Table 3.9: Various activity levels

The heat transfer process through clothing is very complex, accounting for convection through air spaces, conduction through solid material and the radiation between various layers of the clothing. Therefore, a simplification has been adopted in order to combine all these parameters into one overall thermal resistance 'clo'.

$$1 \text{ clo} = 0.155 \text{ m}^2.^{\circ}\text{C/W} \tag{3.12}$$

ASHRAE Thermal Sensation Scale – ASHRAE Standard 55 (1992)						
-3	-2	-1	0	1	2	3
cold	cool	slightly cool	neutral	slightly warm	warm	hot

Figure 3.11: ASHRAE Thermal Sensation Scale
ASHRAE, ANSI/ASHRAE Standard 55-1992, "Thermal Environment Conditions for Human Occupancy", American Society of Heating, Refrigeration, and Air Conditioning Engineers, Inc., Atlanta (1992)

$$PMV = \left(0.303e^{-0.036M} + 0.028\right)\times[M - W - 3.05\times10^{-3}\times(5733 - 6.99(M - W) - P_v)$$
$$-0.42\times(M - W - 58.15) - 1.7\times10^{-5}\times M\times(5867 - P_v) - 0.0014\times M\times(34 - T_a) \quad (3.13)$$
$$-3.96\times10^{-8}\times f_{cl}\times\left((T_{cl}+273)^4 - (T_{mrt}+273)^4\right) - f_{cl}\times h_c\times(T_{cl} - T_a)]$$

where,

$$T_{cl} = 35.7 - 0.028(M - W) - I_{cl}\times$$
$$\left[3.96\times10^{-8}\times f_{cl}\times\left((T_{cl}+273)^4 - (T_{mrt}+273)^4\right) + f_{cl}\times h_c\times\left(T_{cl} - T_a\right)\right] \quad (3.14)$$

$$\begin{cases} h_c = 2.38\times(T_{cl} - T_a)^{0.25} & \text{for } 2.38\times(T_{cl} - T_a)^{0.25} > 12.1\times\sqrt{v_{ar}} \\ h_c = 12.1\times\sqrt{v_{ar}} & \text{for } 2.38\times(T_{cl} - T_a)^{0.25} < 12.1\times\sqrt{v_{ar}} \end{cases} \quad (3.15)$$

$$\begin{cases} f_{cl} = 1.00 + 1.290I_{cl} & \text{for } I_{cl} < 0.078m^2K/W \\ f_{cl} = 1.05 + 0.645I_{cl} & \text{for } I_{cl} > 0.078m^2K/W \\ P_v = \dfrac{P_s\times\phi}{100} \end{cases} \quad (3.16)$$

where,

T_a = Air temperature (°C)

T_{mrt} = Mean radiant temperature (°C)

M = Metabolic rate per unit body surface area (W/m^2)

W = External work (W/m^2), equal to zero for most cases

v_{ar} = Relative air velocity (m/s)

P_v = Partial water vapor pressure in the air (Pa)

I_{cl} = Thermal resistance of the clothing (m^2°C/W)

h_c = Convective heat transfer coefficient (W/m^2 °C)

f_{cl} = Ratio of the surface area of the clothed body to the surface area of the nude body

T_{cl} = Outer surface temperature of clothing (°C)

ϕ = Relative humidity

The PMV takes the six major comfort parameters as inputs and predicts the mean value of the subjective ratings of a group of people in a given environment: – 3 (very cold), 0 (neutral) and +3 (very hot). Therefore, by knowing the metabolic rate and clothing level, the PMV can be computed by using air temperature, radiant temperature, relative humidity and air velocity as the inputs.

The PMV is a prediction method for average thermal sensation of a large group of people with different thermal preferences. Therefore, even if the PMV is computed to be zero, a number of people would be still dissatisfied. Fanger (1970) took this under consideration by developing another index called the Predicted Percentage of Dissatisfied (PPD). The PPD is computed from the PMV and is a quantitative measure of the number of the thermally dissatisfied people in terms of percentage. Even if PMV predicts neutral on the thermal sensation, there will be 5 % dissatisfaction. Realistically, it is impossible to have a 100 % satisfaction while providing for the various thermal preferences of various people.

$$PPD = 100 - 95\, e^{-(0.03353\, PMV^4 + 0.2179\, PMV^2)} \qquad (3.17)$$

The occupant thermal comfort can be quantified using such indices as the Predicted Mean Vote (PMV) and Predicted Percentage of Dissatisfied (PPD). By using these indices, the effect of various occupant configurations could be analyzed further in this study. Figure 3.12 shows the significance of 1°C increase on the whole body thermal comfort: a change in the air temperature from 20°C to 23°C will change the PMV from 0.05 to 0.47!

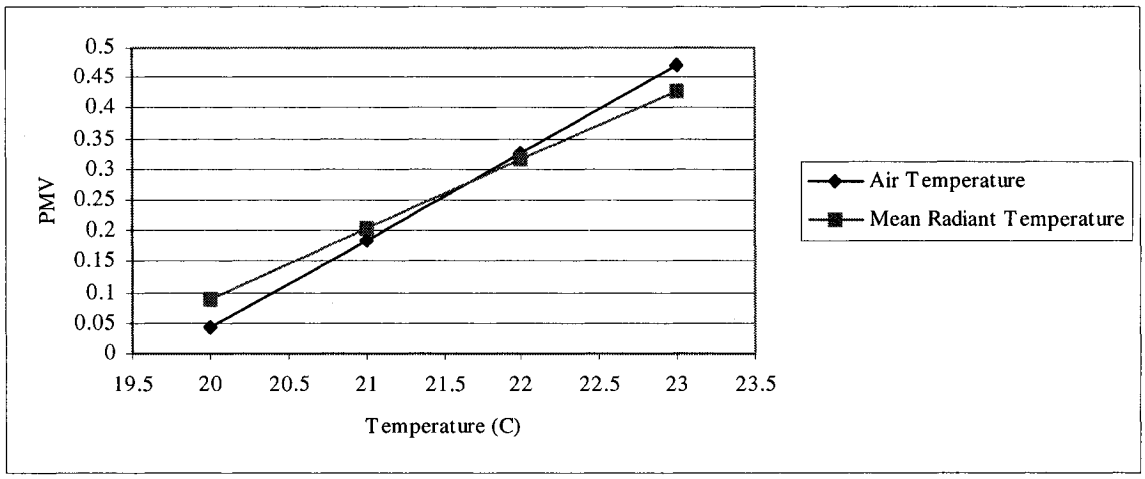

Figure 3.12: The effect of the air temperature and mean radiant temperature on the PMV equations

Figure 3.13 shows that the effect of the air velocity on the whole body thermal comfort is not as significant as that of air temperature: a change in the air velocity from 0.06 m/s to 5 m/s will change the PMV only from – 0.2 to – 1.3 for mixed/forced convection. It should be noted that typical air velocities near occupant are lower than 0.25 m/s. Also for this case, when the air velocities are lower than 0.06 m/s, where there is no mixed/forced convection flow, the convective heat transfer coefficient solely depends upon the temperature gradient between the clothing surface and that of air temperature.

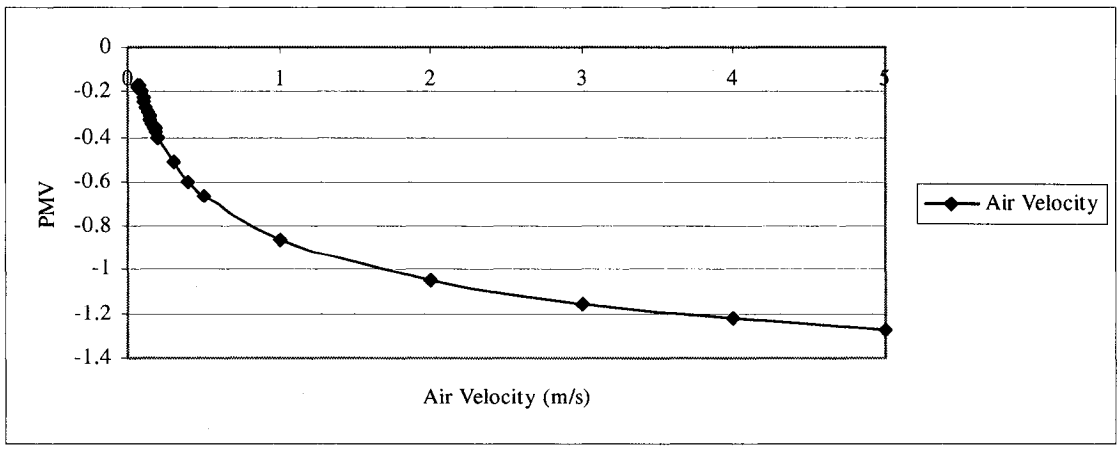

Figure 3.13: The effect of the air velocity on the PMV equations

4.0 RESULTS AND DISCUSSIONS

4.1 Base Case

In order to perform a study on the effect of occupant modeling assumptions within the occupant microclimate in large-scale enclosures, a suitable flow domain was considered. The flow domain was a large classroom, shown in Figure 4.1, on which full-scale measurements were performed by our collaborators from Sweden (Karimipanah et al., 2000). As stated earlier, the experimental setup used twenty-five body simulators, from each heat emitted uniformly. However, the actual distribution of the heat emission from the human body is known to be non-uniform (Huizenga et al. 2004), so in the experimental case the uniform-heat-emitting body simulators were meant to simulate the non-uniform heat distribution characteristics of a real human. For the CFD model, these uniform-heat-emitting body simulators were modeled using blocks with uniform heat distribution. This approach is typical for modeling occupants in a ventilated enclosure. For the validation purposes, various grid resolutions were employed to check the grid independence. The grid was optimized to an 834,871-cell mesh, where refining the grid beyond that point had no significant impact on the results globally. In order to assess the suitability of CFD methods for the current study, experimental data at several points were used to be compared with the numerical results. Karimipanah et al. (2000) conducted measurements for air temperature at twelve points, each at four different heights: 0.1 m, 1.2 m, 1.8 m and 2.25 m. They also conducted measurements for air velocity at the same twelve points, but only at the heights of 0.1 m and 1.2 m.

Figures 4.2 and 4.3 show the comparison between experimental data and those predicted numerically for air temperature and air velocity, respectively, at different heights. Figure 4.2a shows the prediction of the air temperature at the height of 0.1 m. It is observed that the CFD over-predicts the air temperature at all twelve points. The highest difference between the numerical and experimental case is at points 10 and 11 where there is up to 10 % difference. These illustrate that the CFD was not able to predict well the layer of cool air associated with displacement ventilation system at the floor level. This can be explained by the limitations of the Wall Functions employed and the diffuser modeling. Figure 4.3a shows the prediction air velocity at the height of 0.1 m. Good agreement exists between numerical and experimental data except at points 10 and 11. This shows that although the discharged velocity out of the diffuser was properly determined, hence the good agreement at points 9 and 12 that are close to the diffusers, its jet profile was not properly predicted: the incoming air diffuses into room faster and creating a more uniform vertical temperature profile than those seen in the experimental data. Consequently, the amount of stratification in the numerical case is less than those seen in the experimental ones. Figure 4.3a also indicates that the predicted result for the air velocity at all twelve points have a magnitude lower than 0.15 m/s, except for points 9 and 12 which are close to the diffusers. This again shows that in the CFD simulation the incoming air diffuses and mixes with the room air, thus loosing momentum in the process.

Figure 4.2b and Figure 4.3b show the comparison of the predicted air temperature and air velocity, respectively, at the height of 1.2 m to the experimental measurements. It is seen

that very good agreement is reached between the numerical and the experimental results. Figure 4.2c and Figure 4.2d illustrate the comparison between the predicted air temperature and that of air velocity at the height of 1.8 m and 2.25 m, respectively. The numerical results indicate that with increasingly height the difference between the numerical and experimental increases to as high as 5 %. This difference between the numerical and experimental can be explained by the limitations of the Standard k-ε model in modeling the thermal plumes properly. Outside the occupying zone, the thermal plumes become the primary driving force of the flow. However, Karimipanah et al. (2000) reported that the strong buoyant flow cannot be accurately predicted by the Standard k-ε model. Furthermore, it was also pointed out the influence of local buoyant flow, especially in the low velocity region, on the measuring instrument could be another source of discrepancy.

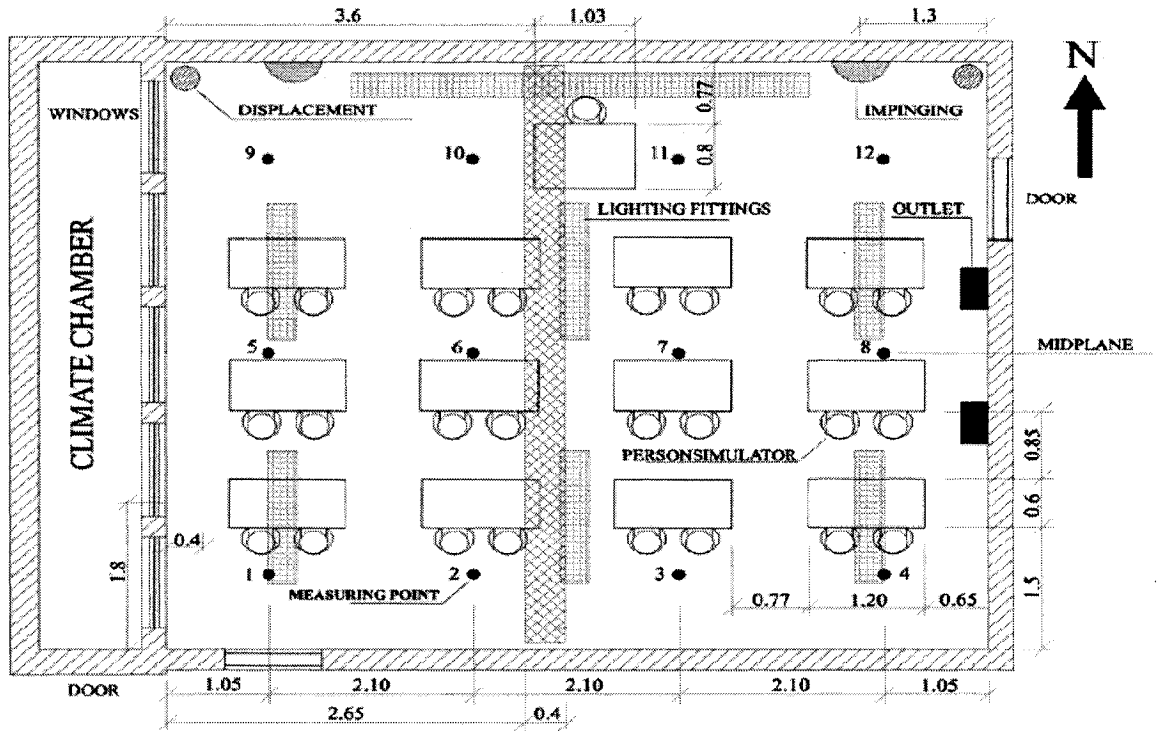

Figure 4.1: The classroom used to validate numerical simulations; (Karimipanah et al., 2000)

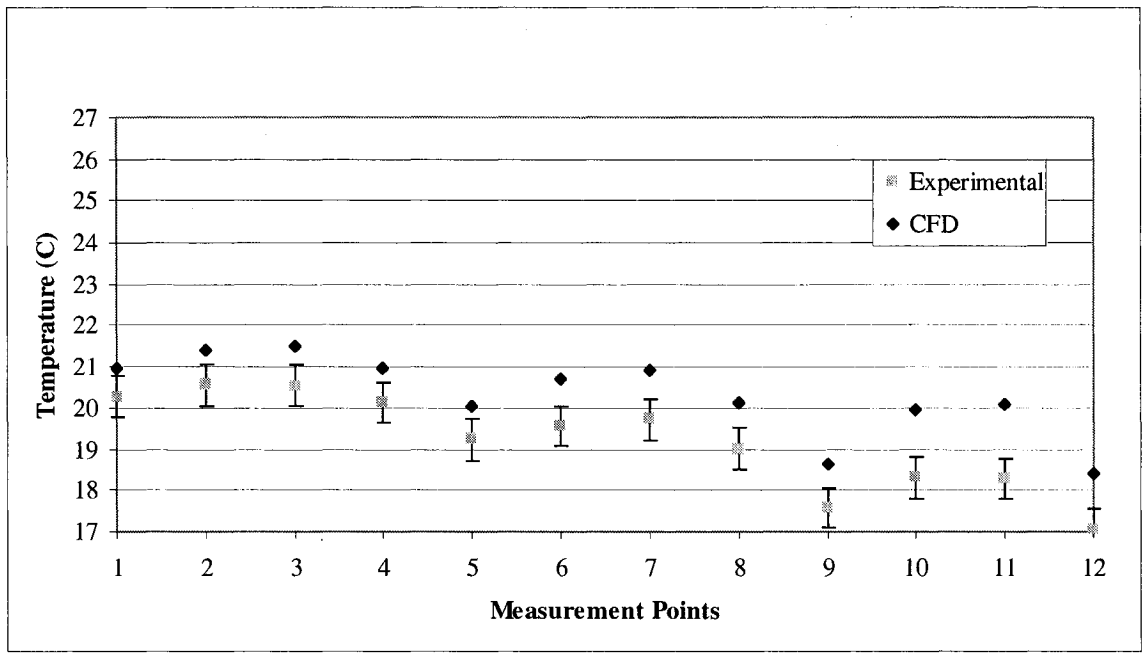

Figure 4.2a: Comparison between experimental measurements of air temperature conducted by Karimipanah et al. (2000) and the numerical results obtained through CFD simulation at the height of 0.1 m

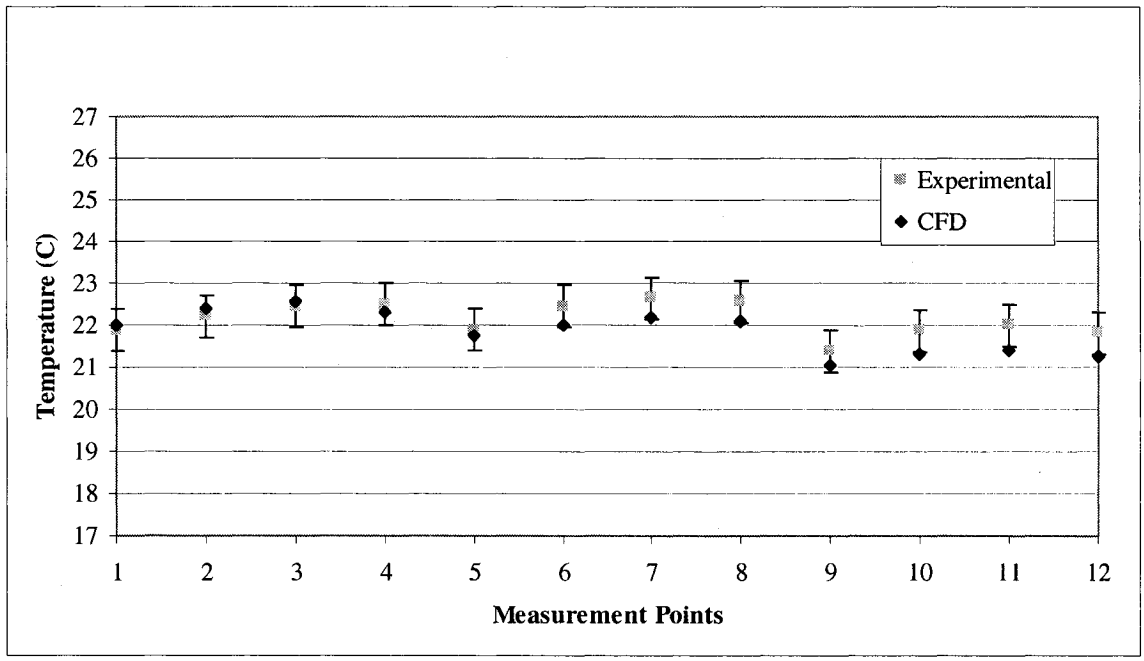

Figure 4.2b: Comparison between experimental measurements of air temperature conducted by Karimipanah et al. (2000) and the numerical results obtained through CFD simulation at the height of 1.2 m

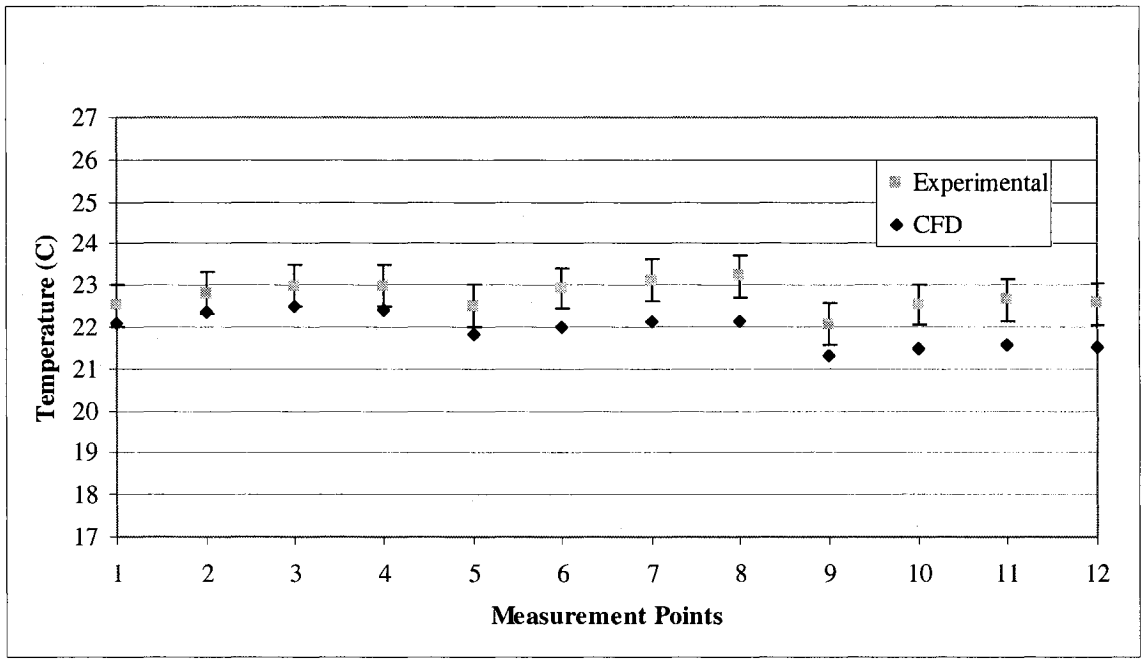

Figure 4.2c: Comparison between experimental measurements of air temperature conducted by Karimipanah et al. (2000) and the numerical results obtained through CFD simulation at the height of 1.8 m

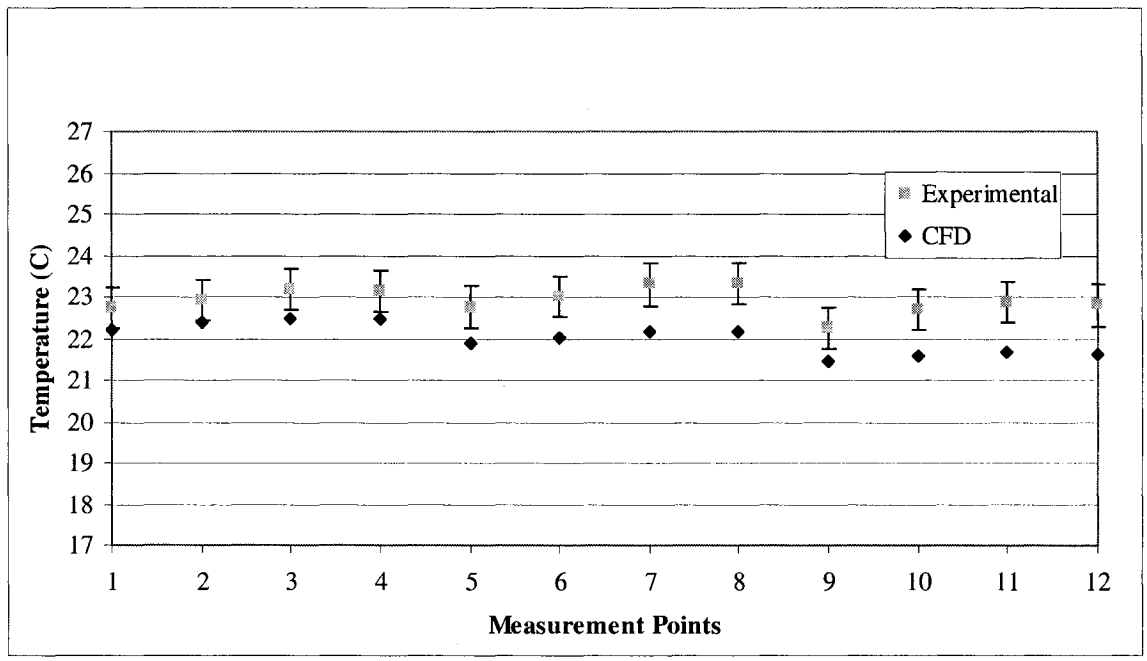

Figure 4.2d: Comparison between experimental measurements of air temperature conducted by Karimipanah et al. (2000) and the numerical results obtained through CFD simulation at the height of 2.25 m

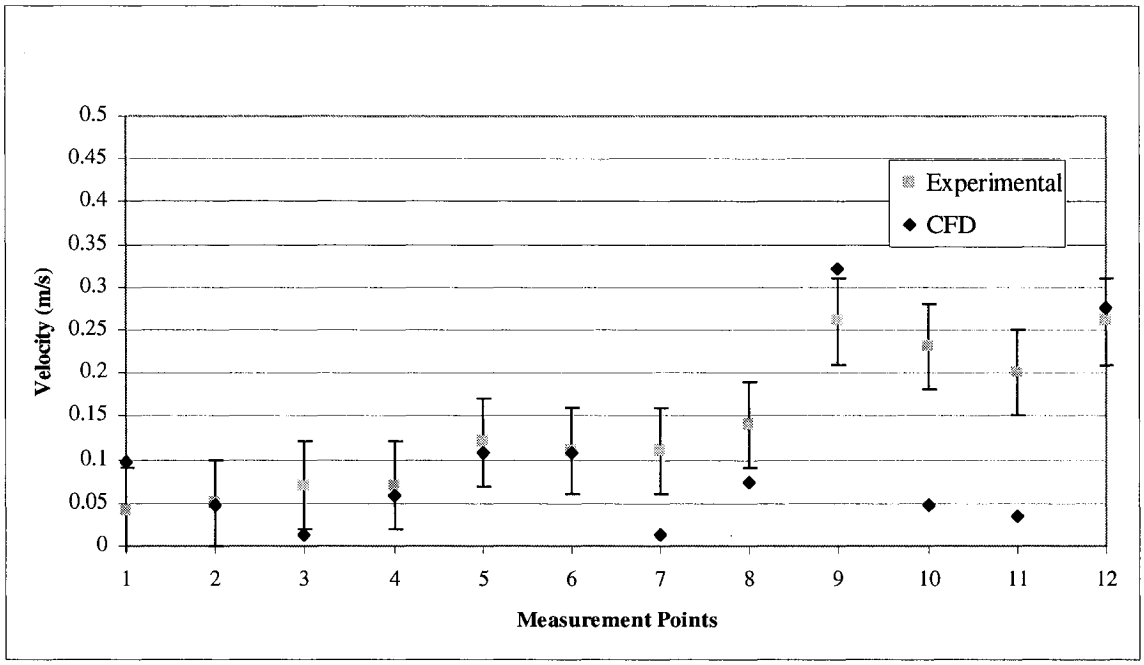

Figure 4.3a: Comparison between experimental measurements of air velocity conducted by Karimipanah et al. (2000) and the numerical results obtained through CFD simulation at the height of 0.1 m

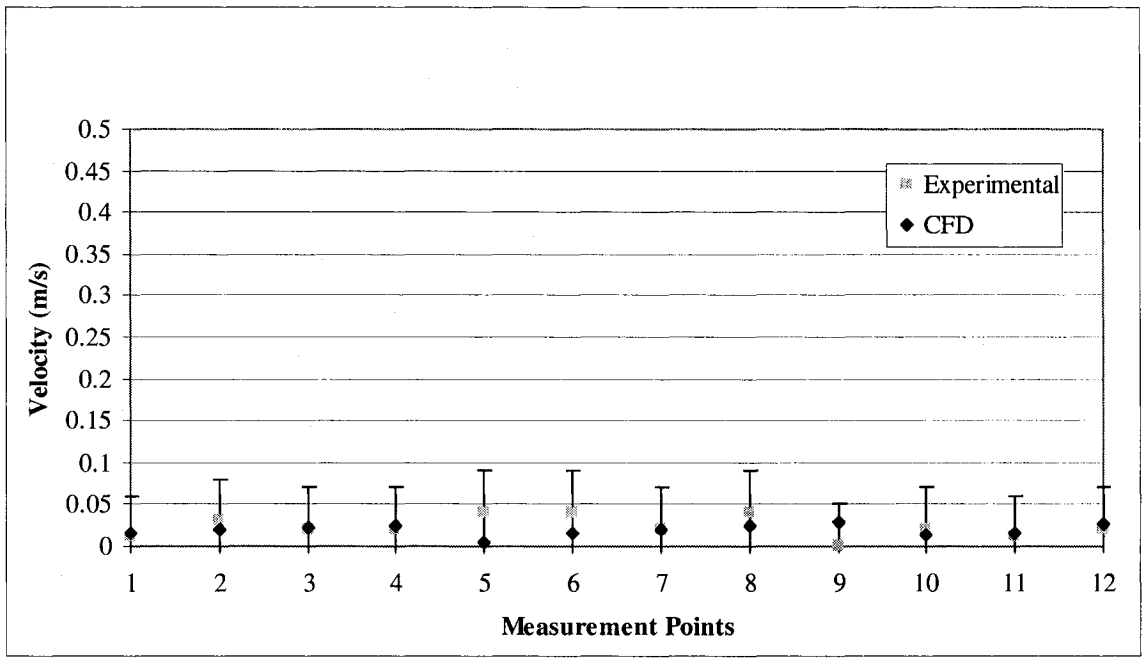

Figure 4.3b: Comparison between experimental measurements of air velocity conducted by Karimipanah et al. (2000) and the numerical results obtained through CFD simulation at the height of 1.2 m

4.2 Occupant Modeling in a Buoyancy-Driven Flow Field

Comparison between numerical results and experimental data proves that a good agreement can be reached via numerical methods. As stated in the previous chapter, six occupant model configurations were constructed: three-node, six-node and eight-node, each with uniform and non-uniform heat distribution. Our objective in this research is to study the effect of various occupant model configurations in a large classroom with various flow fields, i.e. different ventilation systems. Since, the base-case is a classroom fitted with displacement ventilation, it is good opportunity to first study the assumptions of occupant modeling in a buoyancy-driven flow field. For this study, in order to reduce the variances affecting the occupant microclimate, only the microclimate of a single isolated occupant 'teacher' (see Figure 4.4) that is far from other heat sources was studied. Air temperature and velocity are two important parameters affecting thermal comfort, where any significant change on them will have an effect in the overall thermal comfort (Fanger, 1970). Several points close to each body segments (e.g. legs, arms etc.) were used to give an average magnitude for the air temperature and velocity where they are used throughout this study and presented in various charts. The measuring points were located at the distance of 0.1 m from block surface, where the air velocity and temperature were measured at different heights with increments of 0.1 m.

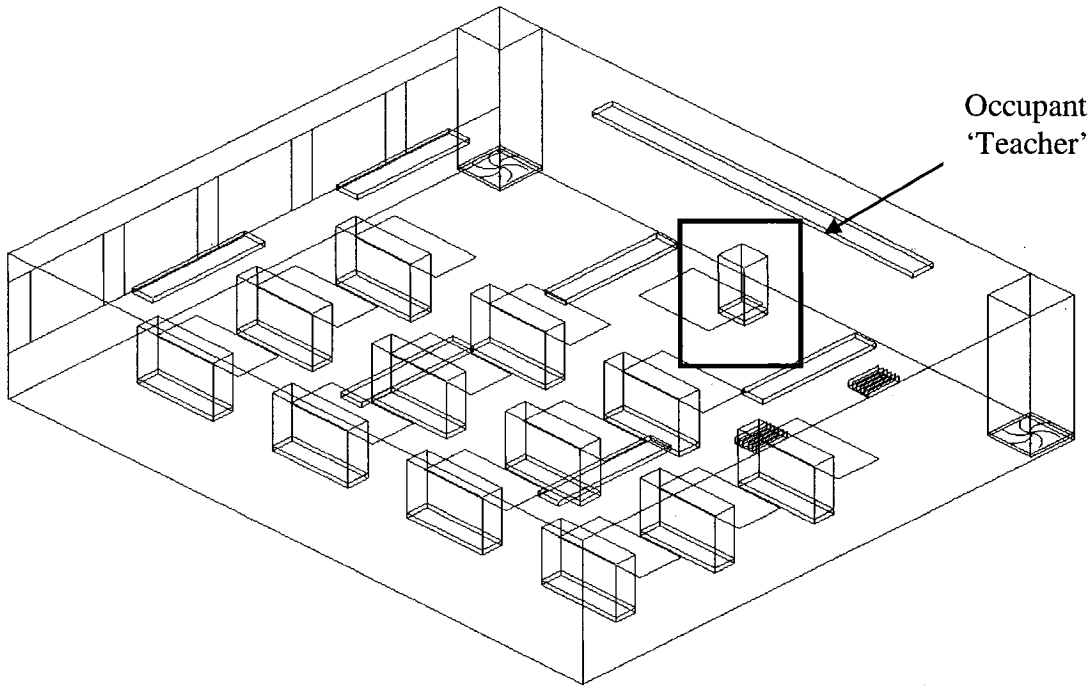

Figure 4.4: The CFD model of the classroom

4.2.1 Study of Occupant Configuration

For the study of occupant model configuration in a buoyancy-driven flow field, four different configurations were used to model the occupant 'teacher': 'Block', three-node, six-node and eight-node configurations as presented in Table 4.1.

Case	Occupant Model Configuration
1	'Block' model
2	Three-node model
3	Six-node model
4	Eight-node model
5	Airpak's Occupant Model

Table 4.1: Various cases considered to study the occupant configuration

As shown in Figure 4.5, the 'Block' configuration underpredicts the air temperature while it over predicts the air velocity. The 'Block' configuration with its uninterrupted vertical

surfaces is more open to its local environment making the heat dissipating faster upward by the buoyant flow. The buoyant flow around the occupant is propelled by natural convection: as the surrounding air absorbs the heat from the occupant, the air expands and its density reduces. Due to the presence of gravity, this change in density induces a change in the body forces, which leads to the movement of the air. Therefore, the uninterrupted 'heated' vertical surfaces of the 'Block' and three-node configurations help to propel the air upward through buoyancy effect, whereas the six-node and the eight-node model configurations do not promote excessive stratification. Furthermore, the three-node, six-node and the eight-node model configurations, have some radiative heat exchange between each of their segments while the 'Block' configuration has radiative heat exchange only with the surrounding walls and objects. That being said the radiative heat exchange is not very significant for the two separate legs of the eight-node configuration. This was previously confirmed by Sørensen et al. (2003) who determined that the pelvic region of the body has the lowest value for the radiative heat transfer coefficient. To conclude, with increasingly detail added to the occupant configuration, the heat emitted from the occupant remains contained more locally. It is also observed in Figure 4.5 that the highest velocities are located behind of the occupant. This is because of the natural convection that is present along the wall that is directly behind the occupant.

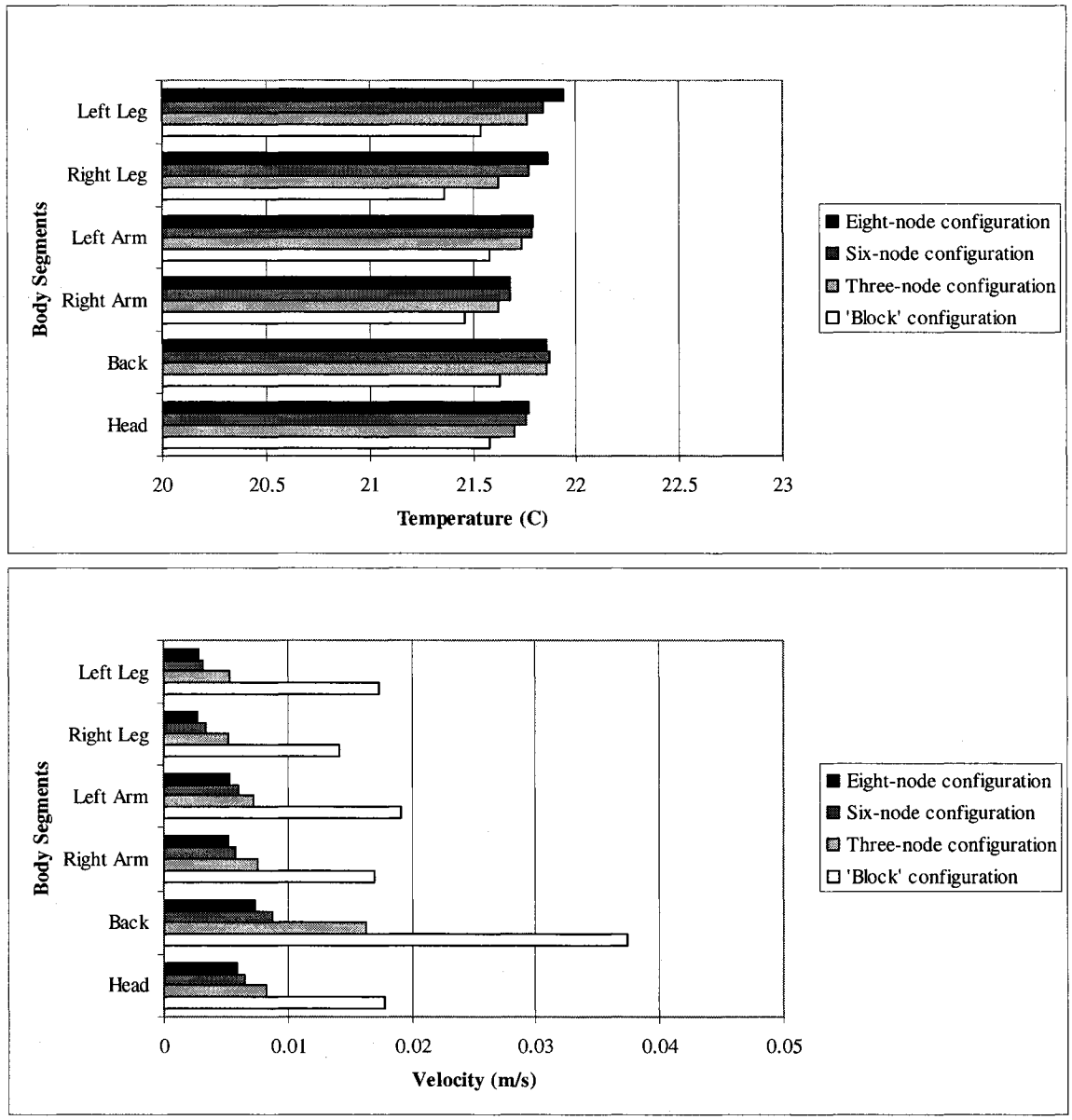

Figure 4.5: The comparison between various occupant configurations (Cases 1 t o 4)

Table 4.2 quantifies the change in the air temperature and velocity for various occupant model configurations. It is observed that the highest difference percent between a 'Block' and a three-node configuration is 1 % and 70 % for the air temperature and velocity, respectively, while, the highest difference percent between a three-node and six-node is less than 1 % and 45 % for the air temperature and velocity, respectively. Finally, the

highest difference percent between a six-node and eight-node is less than 1 % and 23 % for the air temperature and velocity, respectively.

			Flow Variable Change					
	Occupant Configuration		Head	Back	Right Arm	Left Arm	Right Leg	Left Leg
Temperature [C]	Block	Three node	0.12	0.22	0.162	0.157	0.26	0.22
	Three node	Six node	0.06	0.013	0.053	0.0434	0.15	0.08
	Six node	Eight node	0.0118	0.016	0.0014	0.007	0.1	0.1
Velocity [m/s]	Block	Three node	0.009	0.021	0.009	0.011	0.0088	0.012
	Three node	Six node	0.0017	0.0075	0.0017	0.0011	0.0017	0.0021
	Six node	Eight node	0.0005	0.0013	0.0005	0.0006	0.0008	0.0003

Table 4.2: The difference in the magnitude of air temperature and velocity near the occupant

The large difference in the flow field between the simpler models and the six-node is due to the dramatic change in the configuration of the occupant model, whereas the smaller difference for the velocity profile between the six-node and eight-node is due to the smaller change in configuration of the occupant model from six-node to eight-node. It is observed that successive addition of detail to the six-node occupant model does not change the flow field and temperature profile drastically. Figure 4.6 cements this finding further by showing that the airflow patterns near the legs for the six-node and eight-node configurations bear a close resemblance to each other, showing the minimal effect of using separate legs on the airflow pattern for buoyant flows. Therefore, the six-node configuration is recommended since the inclusion of separate legs does not seem to significantly influence the flow field and temperature distribution around the occupant for the present study as presented in Figure 4.6 and Table 4.2.

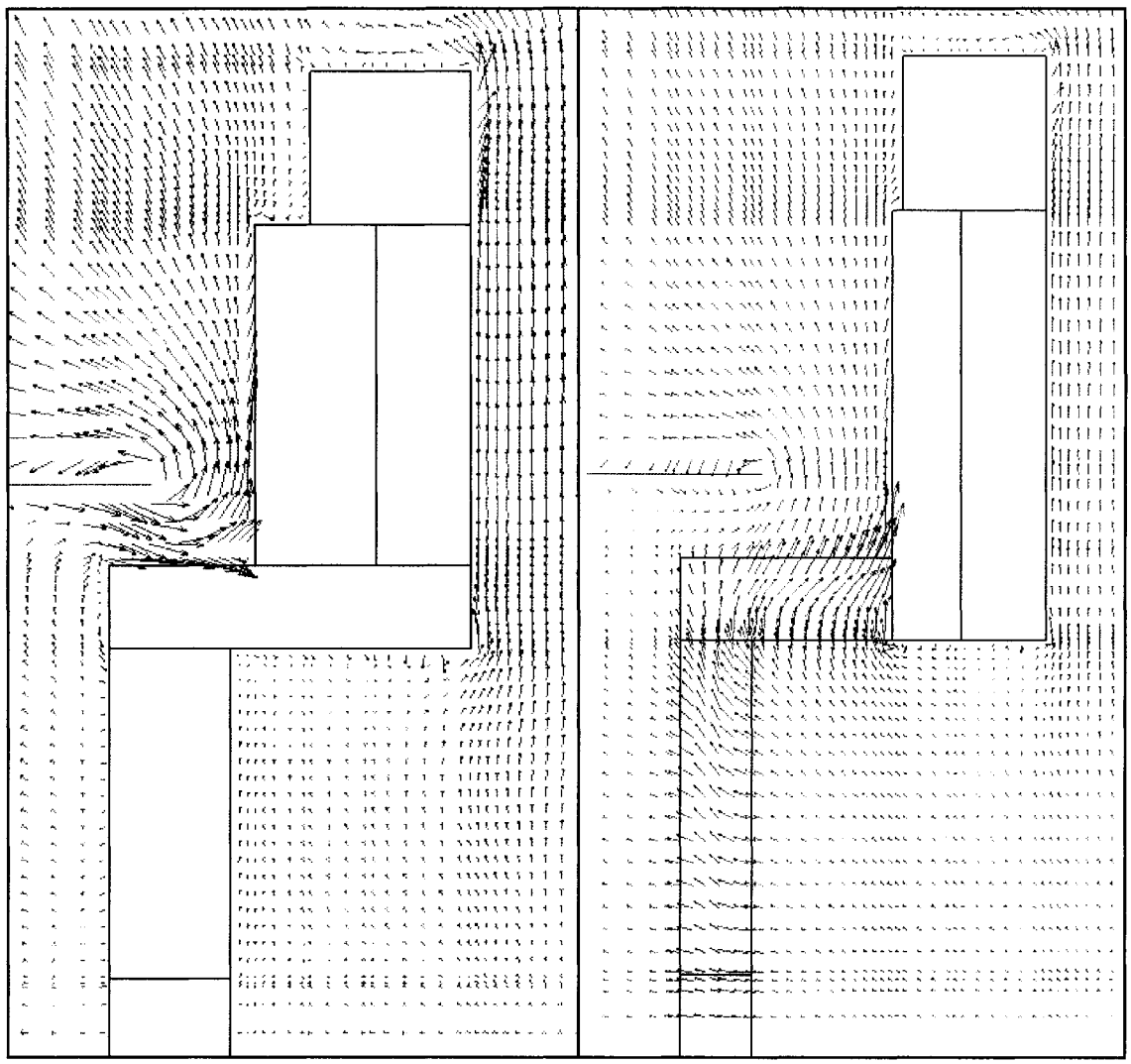

Figure 4.6: The predicted airflow pattern for the six-node (left) and eight-node (right) occupant configurations

Airpak uses an eight-node configuration as its standard occupant model. This gives a good opportunity to compare the flow field around the eight-node configuration developed in this study to that of Airpak's standard occupant model. Figures 4.7 and 4.8 demonstrate very good agreement for air temperature and velocity profiles in various locations around the occupant.

In conclusion, for the 'Block' configuration, since the buoyant flow is rising vertically at each side of the heated block without any obstacles, the velocity profile was higher than the eight-node configuration. The temperature profile of the 'Block' configuration shows a clear rise of temperature with height, i.e. stratification, due to model's simplicity in shape, while the temperature profile of the eight-node configuration was higher due to entrainment of heat at the contained spots, i.e. between the two legs, and to some degree the increase radiative heat transfer between body segments. It should be understood that with increasing the level of detail to occupant model, the grid requirements becomes higher. For example, a 'Block' configuration required a grid size of 834,780 cells in the entire flow domain. Replacing one of the twenty-five occupants with an eight-node configuration augmented the grid size to 1,284,190 cells in the entire flow domain. This study also proved that for some cases the table in front of the occupant had certain impact on the flow field. This indicates the importance of conducting such a study in a realistic ventilated enclosure, where small variances such as the presence of the table add to the realism of the study. Nevertheless, the occupant chosen for this study is relatively isolated from other heat sources and the table is adiabatic and poses only as an obstacle to the flow field.

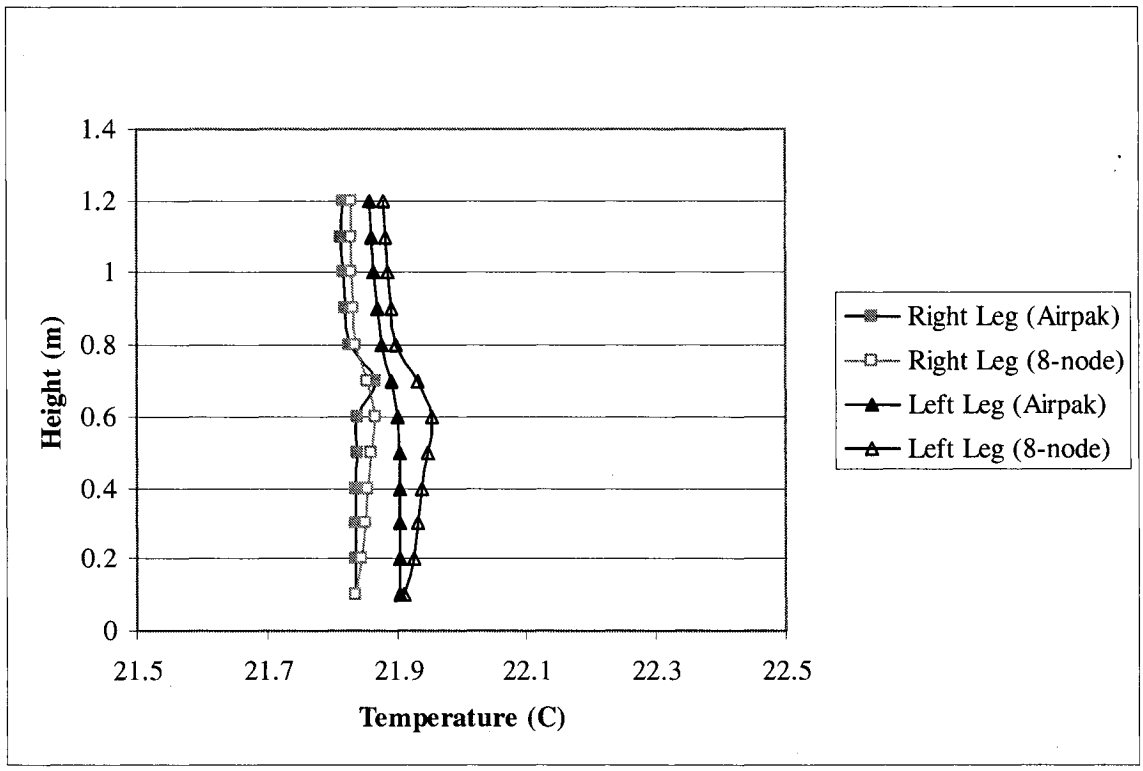

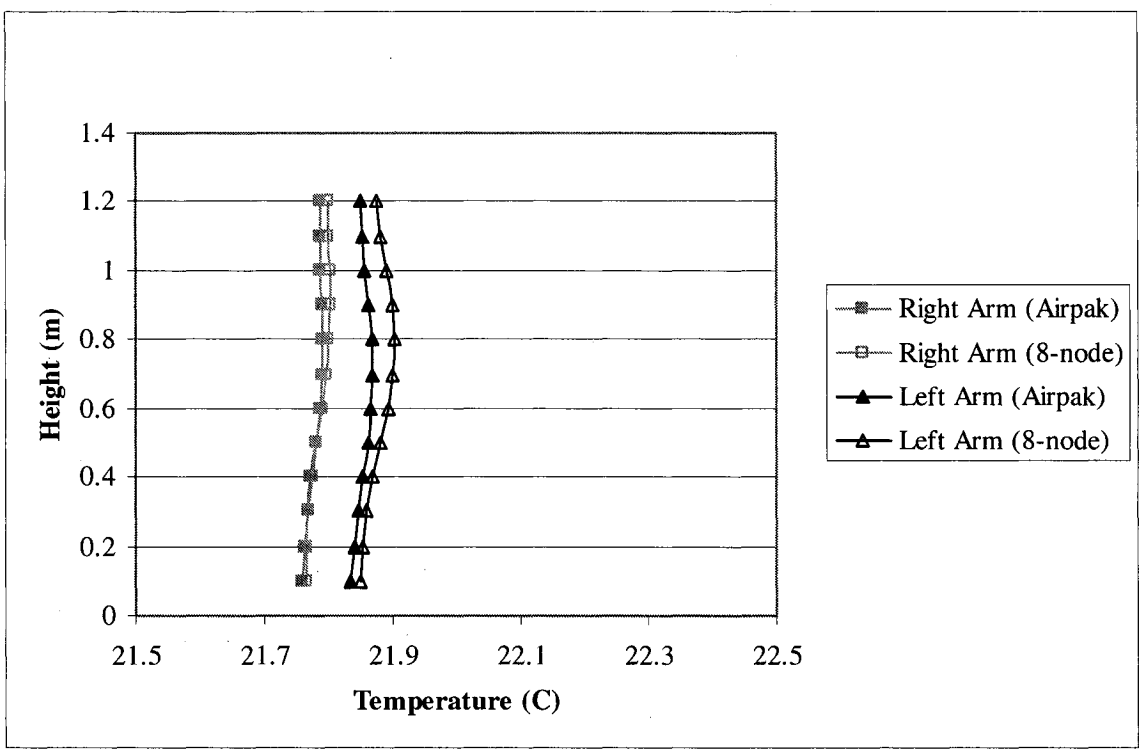

Figure 4.7: The comparison of the eight-node configuration developed in this study with that of Airpak's eight-node configuration for air temperature (Cases 4 and 5)

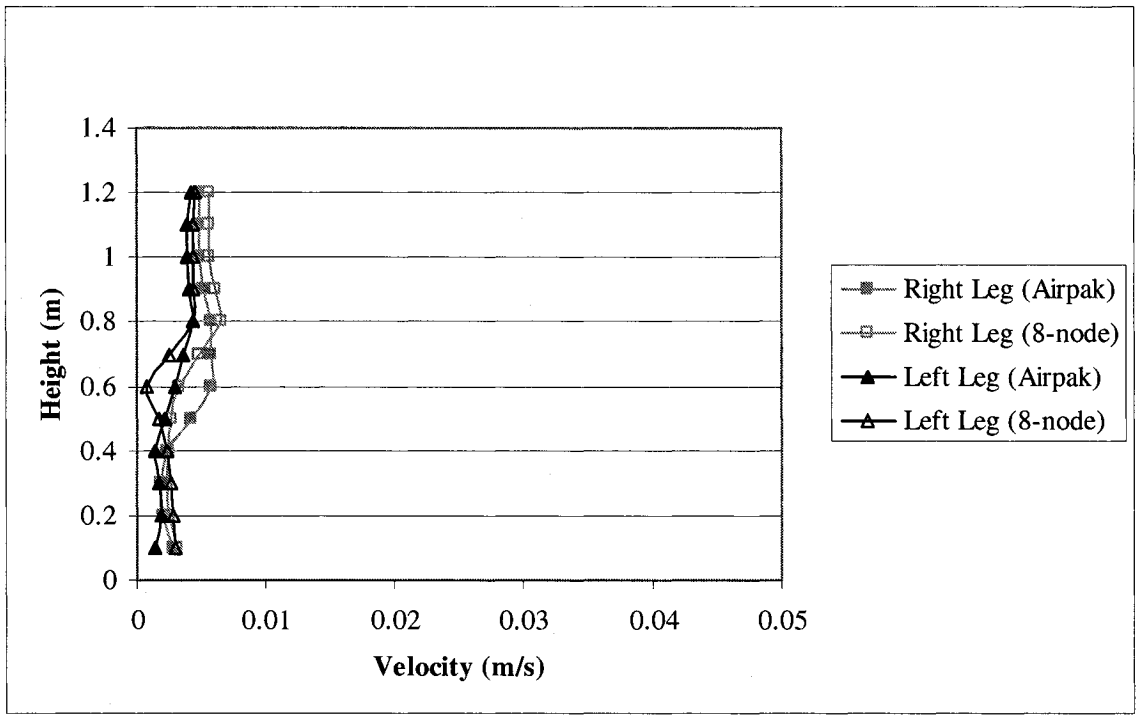

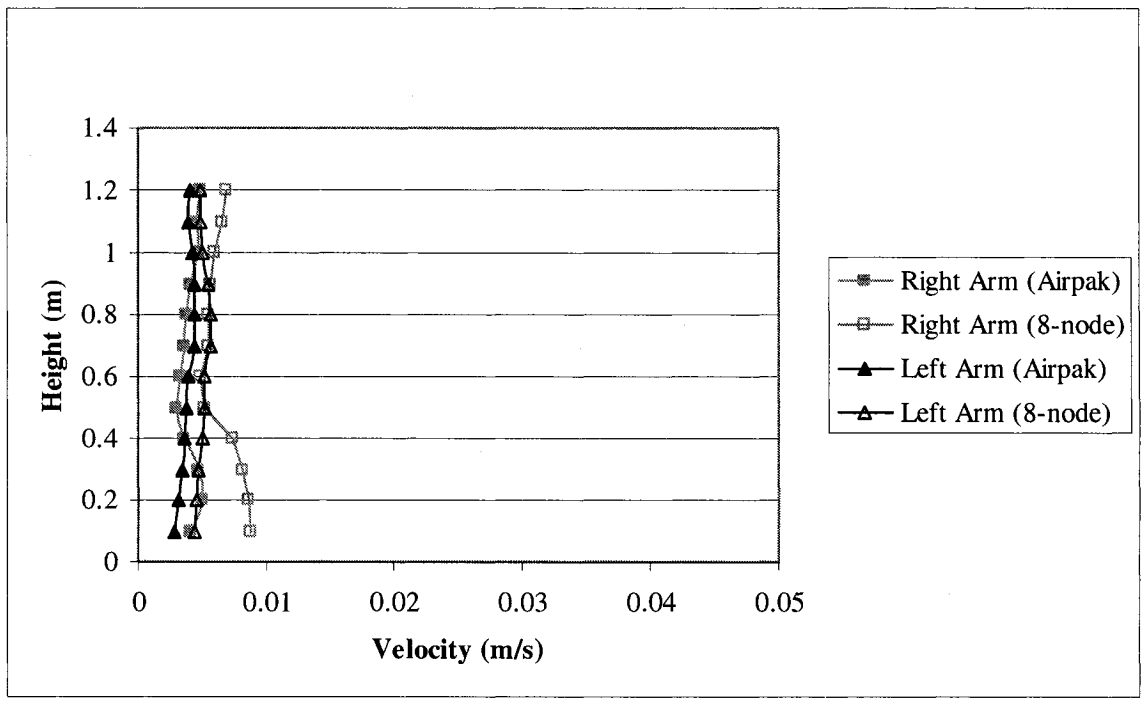

Figure 4.8: The comparison of the eight-node configuration developed in this study with that of Airpak's eight-node configuration for air velocity (Cases 4 and 5)

4.2.2 Verification of Uniform Heat Distribution

As previously stated, the actual distribution of the heat emitted from a human body is known to be non-uniform (Huizenga et al. 2004), i.e. different heat flux per body segment. The experimental case made use of uniform-heat-emitting body simulators to simulate the heat emission from the actual human body. For CFD validation purposes, 'Block' configurations with uniform heat distribution were used in turn to model the body simulators. In the previous section, the impact of different occupant configurations was studied while assuming uniform heat distribution, i.e. uniform heat flux per body segment. For this section, the two identical occupant configurations with different heat distribution methods are compared with each other, as shown in Figure 4.9 and Table 4.3.

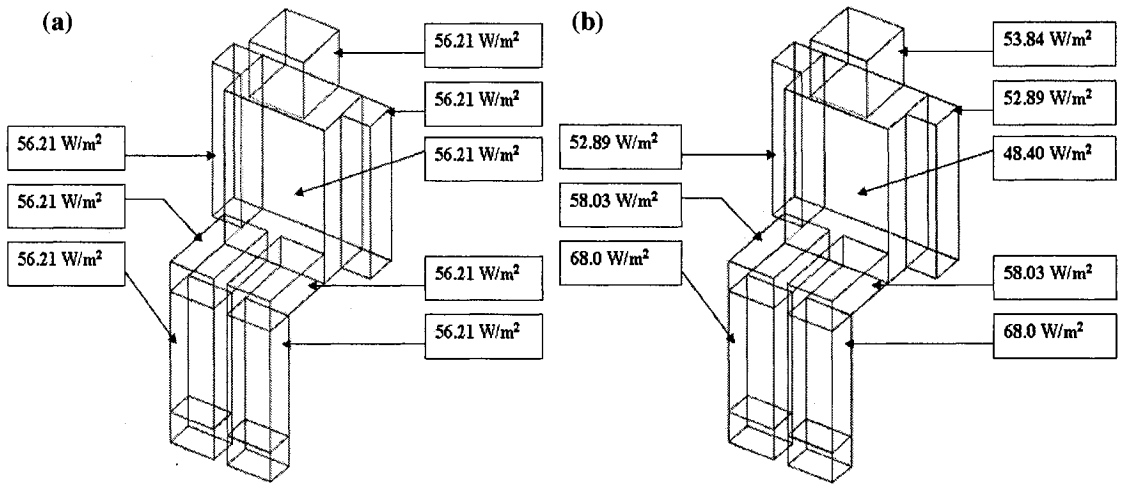

Figure 4.9: Eight-node model with uniform heat distribution (a) and non-uniform heat distribution (b)

Case	Occupant Model Configuration	Thermal Distribution
1	Three-node model	Uniform
2	Three-node model	Non-uniform
3	Six-node model	Uniform
4	Six-node model	Non-uniform
5	Eight-node model	Uniform
6	Eight-node model	Non-uniform

Table 4.3: Various cases considered to study the effect of body heat distribution; Tanabe et al. (1994)

	Percentage Difference (%)						
	Occupant Configuration	Head	Back	Right Arm	Left Arm	Right Leg	Left Leg
Air Temperature	Three node	0.03	0.01	0.04	0.04	0.05	0.05
	Six node	0.03	0.05	0.01	0.01	0.1	0.1
	Eight node	0.03	0.1	0.02	0.02	0.07	0.07
Air Velocity	Three node	0.52	0.1	0.4	0.2	1	1
	Six node	0.6	1.5	0.5	0.3	2.5	2
	Eight node	0.8	1.7	0.8	0.7	2	2

Table 4.4: The percentage difference between the uniform and non-uniform heat distribution cases for the air velocity and temperature profile near the occupant

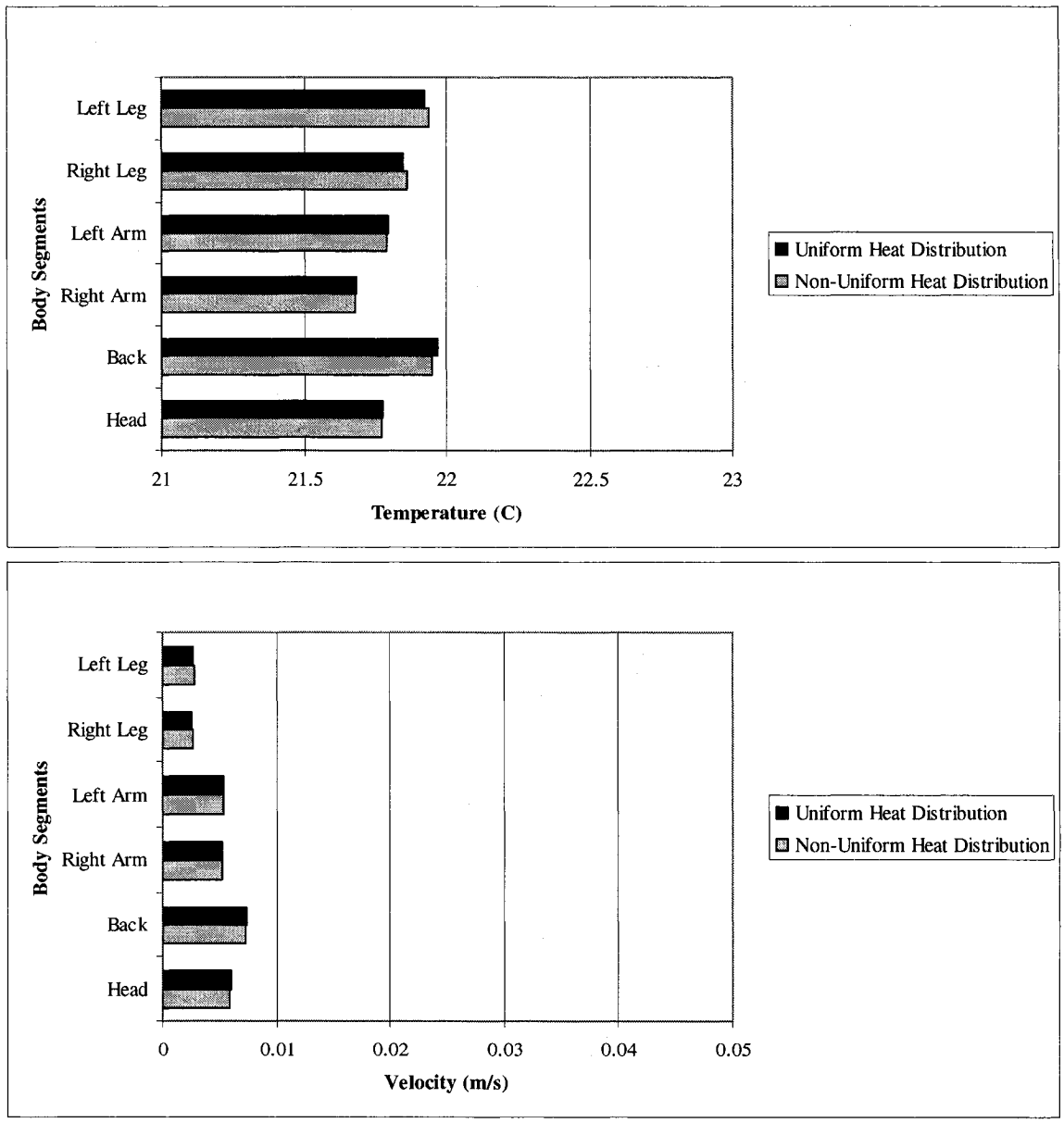

Figure 4.10: The comparison between uniform and non-uniform heat distribution of an eight-node configuration (Cases 6 and 7)

The results were quantified in terms of percentage difference, between non-uniform and uniform heat distributions, for air temperature and velocity as shown in Table 4.4. It was observed that the highest percentage change in air temperature was less than 1 % and the highest percentage change in air velocity was shown to be near 2 % for the case of six-node. Figure 4.10 represents this in more detail for the case of an eight-node configuration, where it was examined that the change in air temperature and air velocity was insignificant, hence showing that the assumption of uniform heat distribution, i.e. same heat flux per body segment, is valid.

4.3 Occupant Modeling in a Inertia-Driven Flow Field

In the past few years, there has been a growing interest in the development and application of localized ventilation systems. One such system is the underfloor air distribution system where the conditioned air is delivered via an underfloor plenum into the close vicinity of the occupant. In contrast, a conventional ceiling air distribution system delivers air via evenly spaced ceiling air diffusers into a room in order to create a uniform thermal environment. The control strategy that is used in conjunction with the ceiling air distribution system provides little opportunity to accommodate various thermal preferences, whereas the underfloor air distribution system provide the potential for individual to have certain amount of control on the microclimate. The international comfort standards, ASHRAE Standard 55-1992 and ISO Standard 7730, define the comfort zone as the region where at least 80 % of the people feel comfortable. There are up to 10 % dissatisfy due to the fact that these comfort standards are based on large-scale

experimental setup, where occupants with various thermal preferences had no control over their environment. The other 10% is added in order to account for any locally non-uniform condition such as excessive thermal stratification, draft and radiant asymmetry (Bauman, 2003). Consequently, the non-uniform and highly asymmetric thermal environment created by such localized ventilation systems requires more investigation of occupant microclimate. Therefore, in order to correctly predict the airflow field and temperature distribution in the microclimate, the occupant should be properly modeled and the effect of occupant modeling assumptions on the inertia-induced flow field should be investigated. To study the effects of various occupant configurations, the CFD model of the classroom was fitted with the underfloor air distribution system. A total airflow rate of 233 L/s for twenty-five occupants gives 9.32 L/s per occupant. This requires four floor diffusers to supply a total of 223.68 L/s for the twenty-four 'students', and a single floor diffuser to supply 9.32 L/s for the 'teacher'. All floor diffusers had a discharge velocity of 2.8 m/s and all wall boundary conditions (walls, windows etc.) were identical to the base case.

4.3.1 Study of Occupant Configuration

It is important to investigate the effect of the occupant configuration for various diffuser setups, since the whole concept of an underfloor air distribution system is that of flexible localized ventilation system where the diffuser could be placed at various distances and set to various supply conditions by the occupant. Therefore, it is not impractical for the occupant to have control over the airflow rate, the distance and orientation of the diffuser from him/herself. However, in this study only one set of supply conditions was studied,

with the airflow rate and supply temperature being kept at 9.32 L/s and 15.1°C, respectively, while other parameters such as distance, location of the diffuser from the occupant and diffuser orientations were varied. The various diffuser layouts used in this study are presented in Table 4.5.

Case	Occupant Model	STUDY OF OCCUPANT CONFIGURATION Distance from Occupant	Airflow Rate	Supply Temperature	Discharge Angle
		Layout Number One			
1	Eight-node model	Front side (0.8 m)	9.32 L/s	15.1 °C	Vertical
2	Six-node model	Front side (0.8 m)	9.32 L/s	15.1 °C	Vertical
3	Block model	Front side (0.8 m)	9.32 L/s	15.1 °C	Vertical
4	Eight-node model	Front side (0.8 m)	9.32 L/s	15.1 °C	Oriented
5	Six-node model	Front side (0.8 m)	9.32 L/s	15.1 °C	Oriented
		Layout Number Two			
6	Eight-node model	Front side (0.5 m)	9.32 L/s	15.1 °C	Vertical
7	Six-node model	Front side (0.5 m)	9.32 L/s	15.1 °C	Vertical
8	Block model	Front side (0.5 m)	9.32 L/s	15.1 °C	Vertical
9	Eight-node model	Front side (0.5 m)	9.32 L/s	15.1 °C	Oriented
10	Six-node model	Front side (0.5 m)	9.32 L/s	15.1 °C	Oriented
11	Block model	Front side (0.5 m)	9.32 L/s	15.1 °C	Oriented
		Layout Number Three			
12	Block model	Right side (0.5 m)	9.32 L/s	15.1 °C	Vertical
13	Eight-node model	Right side (0.5 m)	9.32 L/s	15.1 °C	Vertical

Table 4.5: Various cases for underfloor air distribution case study

Layout Number One (cases 01 to 05) – Matsunawa (1995) experimentally showed that the draft discomfort zone develops within 0.8 m from floor diffusers for a typical floor diffuser. Therefore, for the first layout, a floor diffuser was placed at the distance of 0.8 m from in front of the occupant. The floor diffuser was not exactly on the occupant's central axis in order to represent the realistic scenario. Three occupant model configurations are considered for a case where the diffuser is discharging vertically upward. Figure 4.11 shows the comparison of temperature and velocity for the case of an eight-node, six-node and 'Block' configurations for a diffuser located at a distance of 0.8 m as Cases 01, 02 and 03, respectively.

	Occupant Configuration		Flow Variable Change					
			Head	Back	Right Arm	Left Arm	Right Leg	Left Leg
	Block	Six node	0.0773	0.005	0.059	0.036	0.038	0.02
Temperature [C]	Six node	Eight node	0.0031	0.0042	0.015	0.01	0.03	0.025
	Block	Six node	0.001	0.0016	0.0007	0.0007	0.001	0.001
Velocity [m/s]	Six node	Eight node	0	0.0004	0.0001	0.0001	0.0003	0.0003

Table 4.6: The difference in the magnitude of air temperature and velocity near the occupant

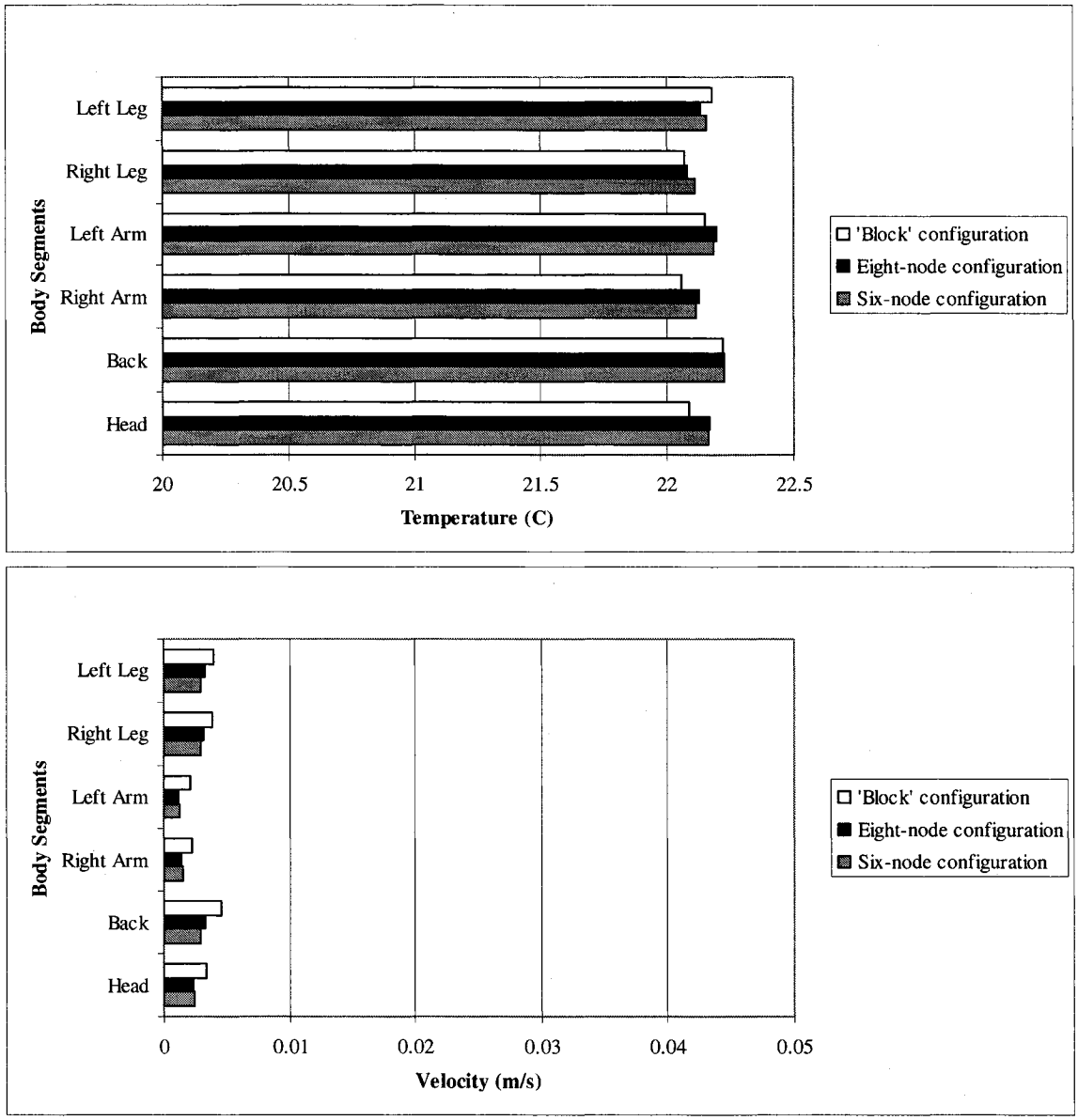

Figure 4.11: The comparison between 'Block', six-node and eight-node configurations for diffuser located at 0.8 m and not oriented toward the occupant (Cases 01, 02 and 03)

The results in Table 4.6 and Figure 4.11 show that the changes in the air temperature and velocity profiles are very small: less than 1 % in air temperature and insignificant change in terms of magnitude of the air velocity. This is expected because the floor diffuser is relatively far from the occupant and is discharging air vertically upward. Therefore, it is concluded that reasonable results could be obtained by using anyone of the presented configurations.

In order to increase the flow gradients due to the diffuser near the occupant and to counter the effect of the 'blockage' by the table, another configuration is considered where the floor diffuser discharges toward the occupant legs still from a distant of 0.8 m. Only the six-node and eight-node configurations are studied here as Cases 04 and 05, respectively. Figure 4.12 shows the comparison of the air temperature and velocity for the Cases 04 and 05. It is observed that the air velocities are much higher on the sides of the occupant lower body for the six-node configuration. This is because the merged legs of six-node configuration obstruct the passage of the incoming air, making the mass of airflow to pass around the legs. That being said, the temperature is seen to be lower behind the eight-node configuration. In summary, it is revealed that as the flow gradients due to the diffuser are increasing near the occupants, the need for a detailed occupant model becomes more important.

	Flow Variable Change							
	Occupant Configuration		Head	Back	Right Arm	Left Arm	Right Leg	Left Leg
Temperature [C]	Six node	Eight node	0.0593	0.0298	0.0404	0.021	0.0908	0.034
Velocity [m/s]	Six node	Eight node	0.0103	0.0364	0.0185	0.0268	0.1092	0.074

Table 4.7: The difference in the magnitude of air temperature and velocity near the occupant

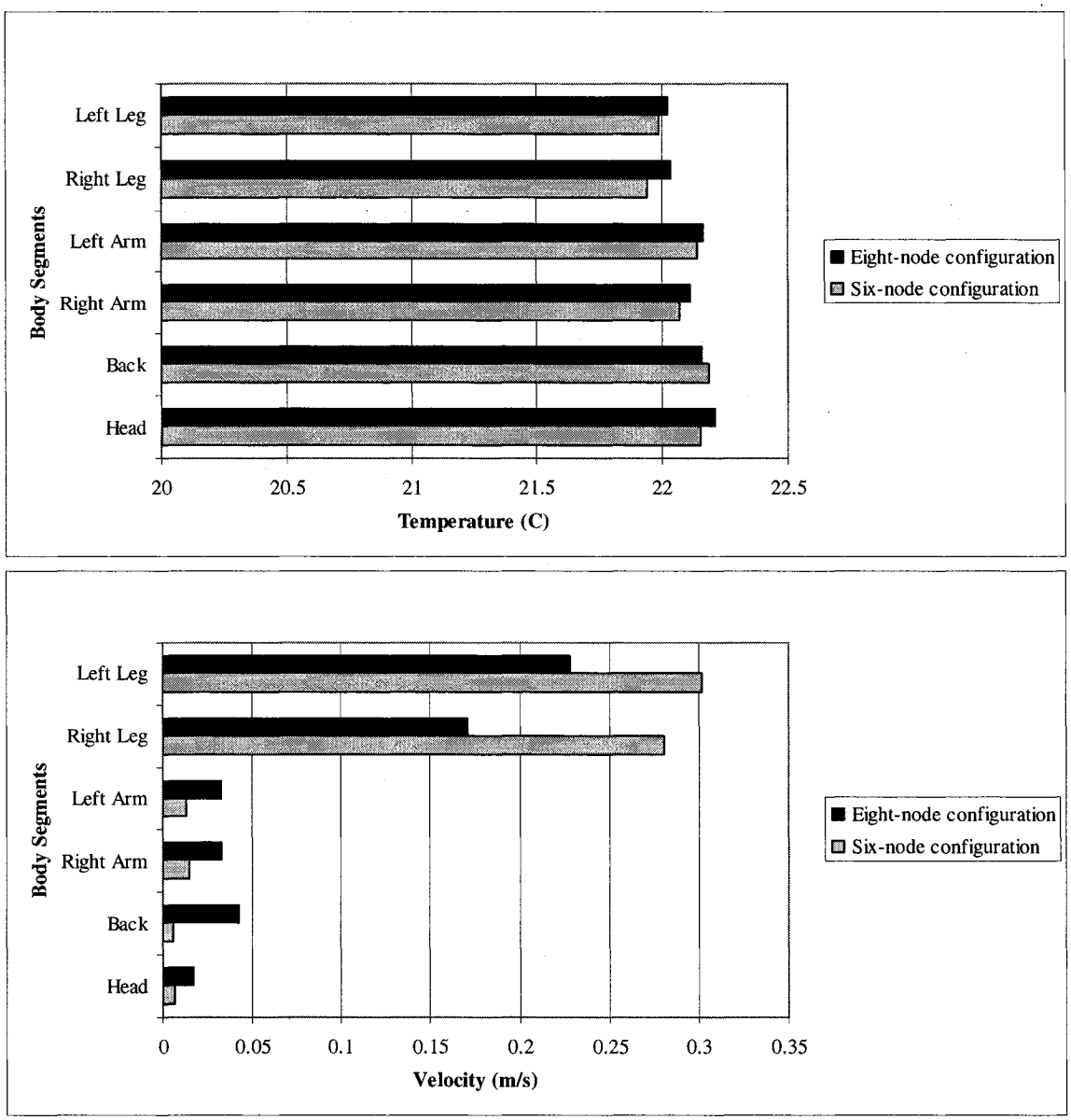

Figure 4.12: The comparison between six-node and eight-node configurations for diffuser located at 0.8 m and oriented toward the occupant (Cases 04 and 05)

Layout Number Two (cases 6 to 11) – As mentioned earlier, the distance of 0.8 m from the occupant was chosen for the diffuser based on a recommendation by Matsunawa et al. (1995). The current comfort Standards treat air velocity in terms of maximum 'allowable velocity' in order to reduce draft risk. The 'allowable velocity' is set by ASHRAE to 0.15 m/s for winter condition and 0.25 m/s for a summer condition. However, if the occupant has control over these velocities the Standard 55-1992 does allow the local air velocities to be higher than the 'allowable velocity' (ASHRAE Standard 55-1992). Therefore, for this problem it is assumed that the occupant 'teacher' has personal control on the floor diffuser. This assumption allows us to examine further the effect of occupant modeling methods in more extreme conditions. Subsequently, three cases are considered where the floor diffuser is placed at a distance of 0.5 m in front of the occupant and discharging air vertically upward: the eight-node, six-node and 'Block' configurations are compared and analyzed as Cases 06, 07 and 08, respectively. Figure 4.13 show that difference between the three occupant configurations used is still not very significant. It is observed that the air velocity for the six-node configuration is higher near the legs. This is because the merged legs configuration tends to re-direct the bulk of the airflow to pass around the legs, as oppose to the separate legs of the eight-node configuration where the bulk of the flow dissipates itself against the two legs. The results in Table 4.8 show that the change in the flow variables. It is seen that the change in air temperature is less than 1 %, whereas the change in air velocity is seen to be more significant. It was previously mentioned that a change in air temperature is more significant to the whole-body thermal comfort than a change in air velocity. However, since the changes in air temperature are low, the PMV equations are not expected to vary much.

			Flow Variable Change					
	Occupant Configuration		Head	Back	Right Arm	Left Arm	Right Leg	Left Leg
	Block	Six node	0.0821	0.0636	0.0718	0.1066	0.0715	0.1368
Temperature [C]	Six node	Eight node	0.1725	0.0937	0.1746	0.1655	0.1507	0.1365
	Block	Six node	0.0004	0.001	0.002	0.002	0.014	0.012
Velocity [m/s]	Six node	Eight node	0.0001	0.0013	0.0015	0.009	0.009	0.013

Table 4.8: The difference in the magnitude of air temperature and velocity near the occupant

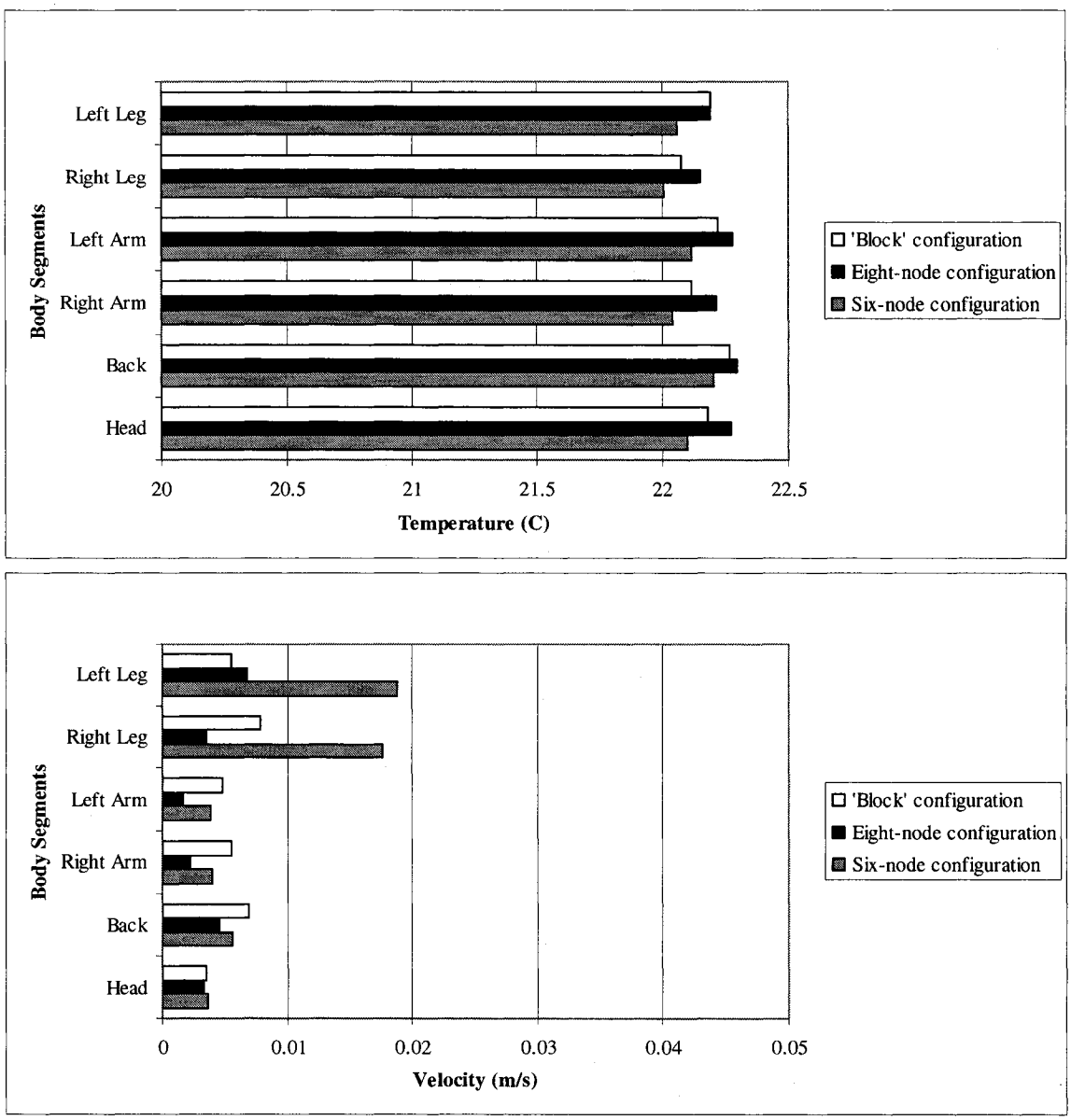

Figure 4.13: The comparison between six-node and eight-node configurations for diffuser located at 0.5 m and not oriented toward the occupant (Cases 06, 07 and 08)

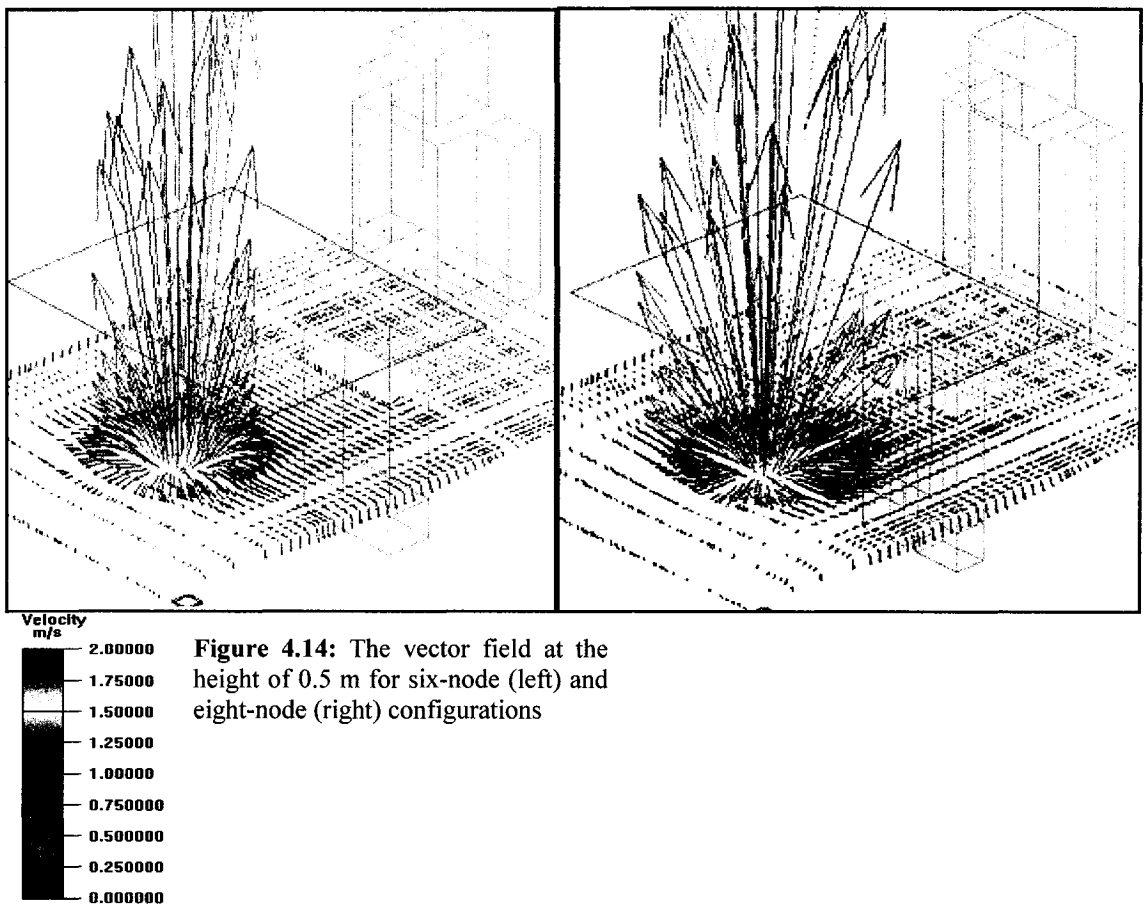

Figure 4.14: The vector field at the height of 0.5 m for six-node (left) and eight-node (right) configurations

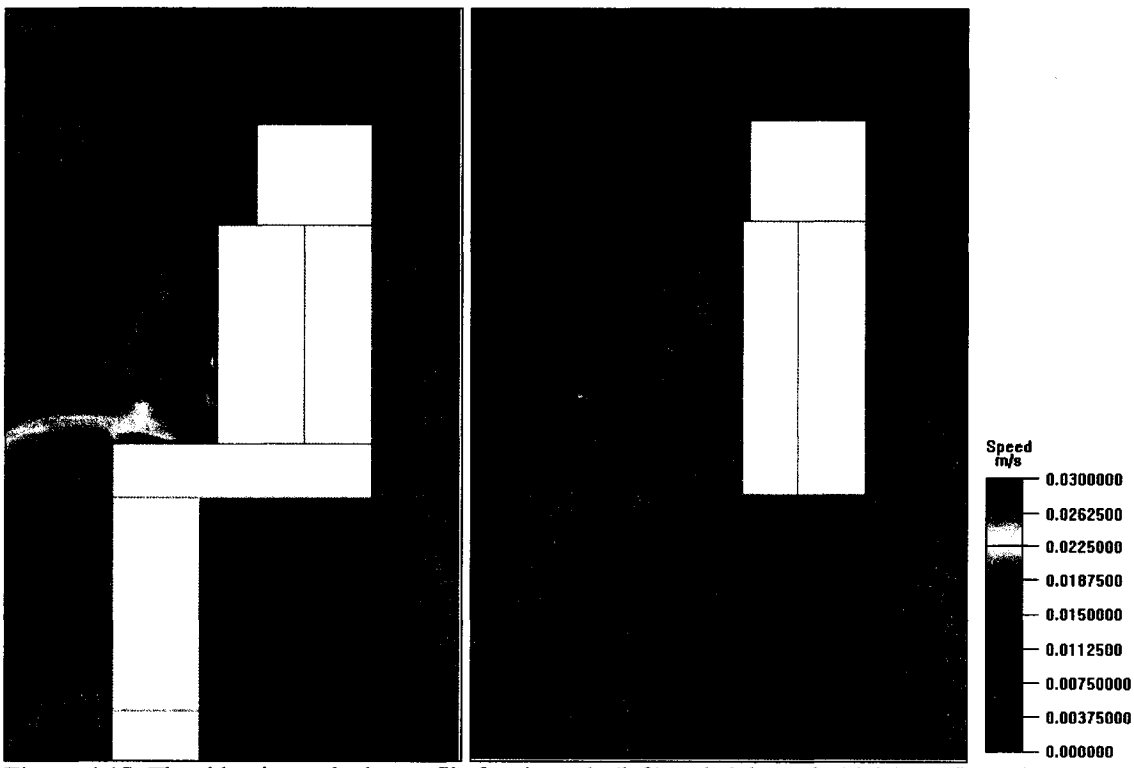

Figure 4.15: The side-view velocity profile for six-node (left) and eight-node (right) configurations

Figures 4.14 and 4.15 show the vector and the velocity profiles near the occupant configurations. It is observed that the six-node configuration keeps the high flow gradients that are due to the diffuser to only to the diffuser-side of the occupant, whereas the eight-node configuration allows the fluid in the back of the occupant to be influenced by the diffuser discharge. That being said the magnitude of the air velocities are still very low and thus do not present any significant change in the thermal comfort level. Calculating the PMV value for six-node and eight-node configurations yields similar results: – 0.148 and – 0.141, respectively.

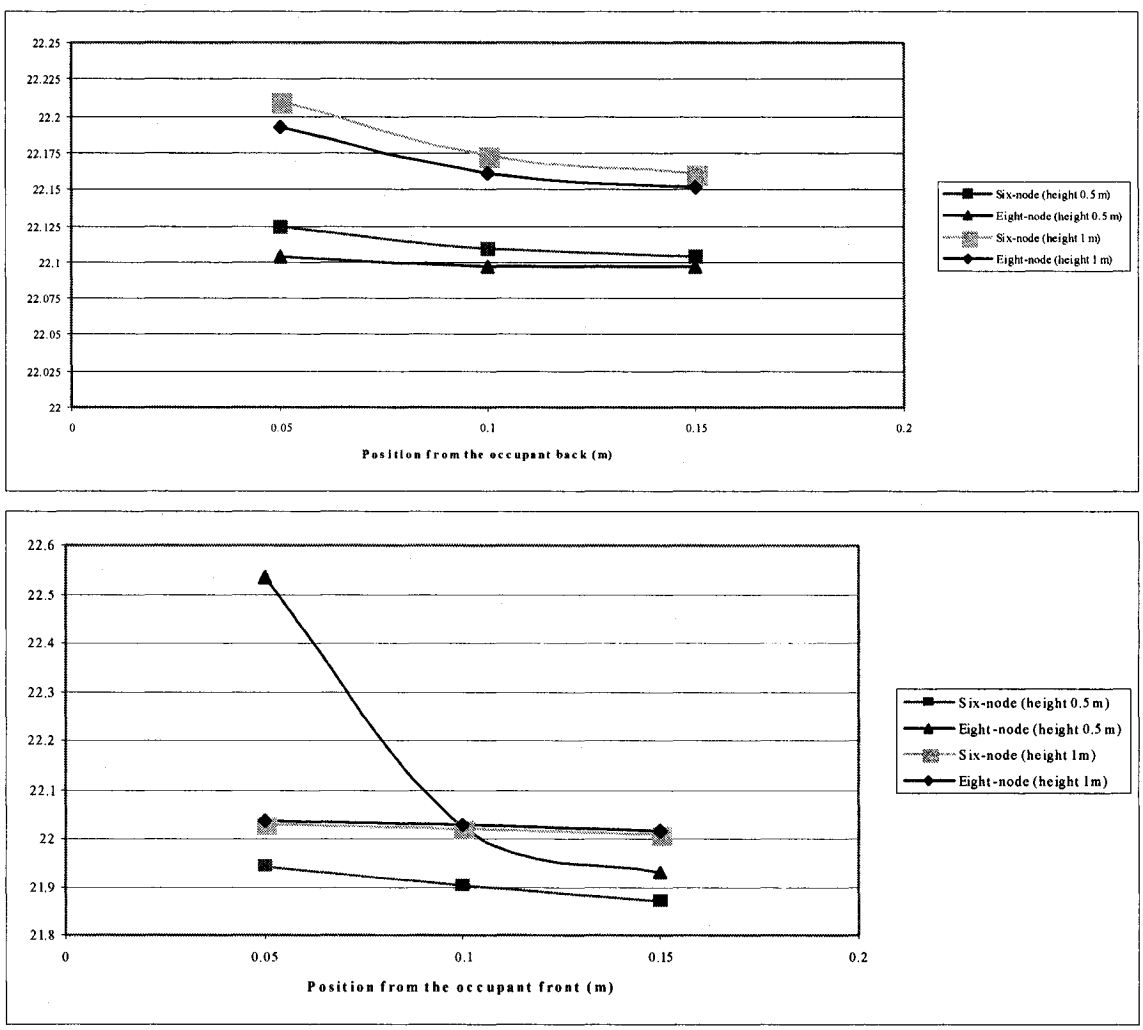

Figure 4.16: The temperature distribution (y-axis) as function of distance (x-axis)

Figure 4.16 shows the temperature profile with respect to distance from the occupant for six-node and eight-node configurations at two different heights. The position '0.05 m' is the closest to the occupant body while inversely the position '0.15 m' is the further from the occupant body. The increment between each position is 0.05 m with the first point being 0.05 m from the body surface. Expectedly, as the measuring points are moved away from the back of the occupant body the measured air temperature decreases with the same rate for both occupant configurations at the two considered heights. As the measuring points are moved away from the front of the occupant body the measured air temperature decreases as well for both occupant configurations but at different rate. At the height of 1 m (above the table) the temperature profiles of the two occupant configurations are very similar. This is expected because the major differences between the two occupant configurations are mainly at the lower part of the body. Therefore, the flow points on the front side of the occupant, above the table, are relatively free of the change in occupant configurations. It is observed that at point '0.05 m' for the eight-node configuration, the measured air temperature is high due to entrainment of heat near the separate legs. Figure 4.17 investigates the same concept but at the right and left sides of the body. It is examined that the air temperature measurements on the right side of the body show lower magnitude due to the global heat loss through the windows. That being said the rate of temperature drop for both cases is similar. Comparing the rate of temperature drop on the sides of the occupant to that of front side at the height of 1 m, it is clearly seen that the presence of the table effectively blocks flow changes that are due to the diffuser in front, while the sides of the occupant are still influenced to a certain degree.

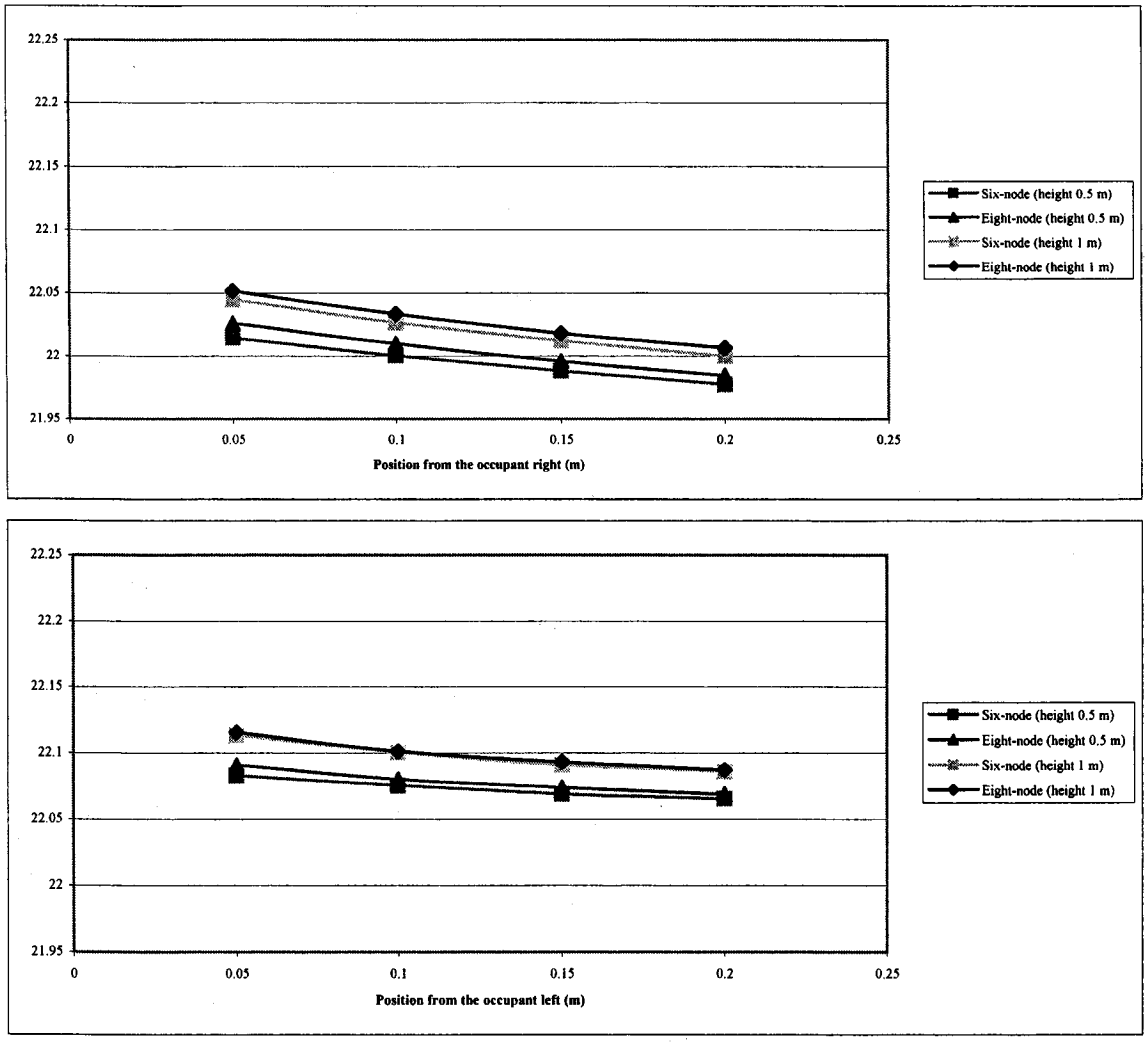

Figure 4.17: The temperature distribution (y-axis) as function of distance (x-axis)

Three other cases are considered for the same layout but the diffuser throw angle is changed from vertical discharge to oriented toward the occupant. The eight-node, six-node and 'Block' configurations are compared and analyzed as Cases 09, 10 and 11, respectively. Figure 4.18 and Table 4.9 shows the change in the air temperature and air velocity for these cases. It is seen that there is significant change in the air velocity. The six-node configuration tends to redirect the incoming airflow to its left and right sides, where it increases the heat dissipation from the legs. Whereas, the eight-node configuration allows the incoming air to pass between the two legs, thus yielding a higher

configuration allows the incoming air to pass between the two legs, thus yielding a higher value for the air velocity for the back of the occupant compared to the six-node configuration.

Figure 4.19 shows the airflow pattern of six-node and eight-node configurations at the height of 1.1 m. It is observed that the airflow pattern for the case of the eight-node configuration is more active in the region behind the occupant because the inertia-induced airflow passes between the two separate legs, while a six-node configuration has a more active airflow pattern in front of the occupant where the inertia-induced airflow collides against the merged legs. By comparing the results for vertical discharge (Cases 06, 07 and 08) and oriented discharge (Cases 09, 10 and 11) it is observed that as the floor diffuser throw angle is changed from vertical discharge to toward the occupant, the flow field in the microclimate becomes more influenced by the configuration of the occupant model. This is expected since as the diffuser becomes more oriented toward occupant and/or as the floor diffuser is moved closer toward the occupant, the flow gradients near the occupant increases. Thus the proper modeling the occupant body becomes more urgent. Calculating the PMV value for the block, six-node and eight-node configurations yields significantly different results: – 0.06, – 0.124 and – 0.131, respectively. The difference in the PMV value between six-node and eight-node configurations is only 5 %, however the difference in the PMV value between Block and eight-node configurations is significantly high (50 %).

	Occupant Configuration		Flow Variable Change Head	Back	Right Arm	Left Arm	Right Leg	Left Leg
	Block	Six node	0.0552	0.0224	0.0465	0.028	0.1139	0.1991
Temperature [C]	Six node	Eight node	0.08817	0.02314	0.07657	0.0462	0.1154	0.1906
	Block	Six node	0.01229	0.03183	0.0234	0.0233	0.059	0.1016
Velocity [m/s]	Six node	Eight node	0.0406	0.019	0.109	0.086	0.0654	0.11231

Table 4.9: The difference in the magnitude of air temperature and velocity near the occupant

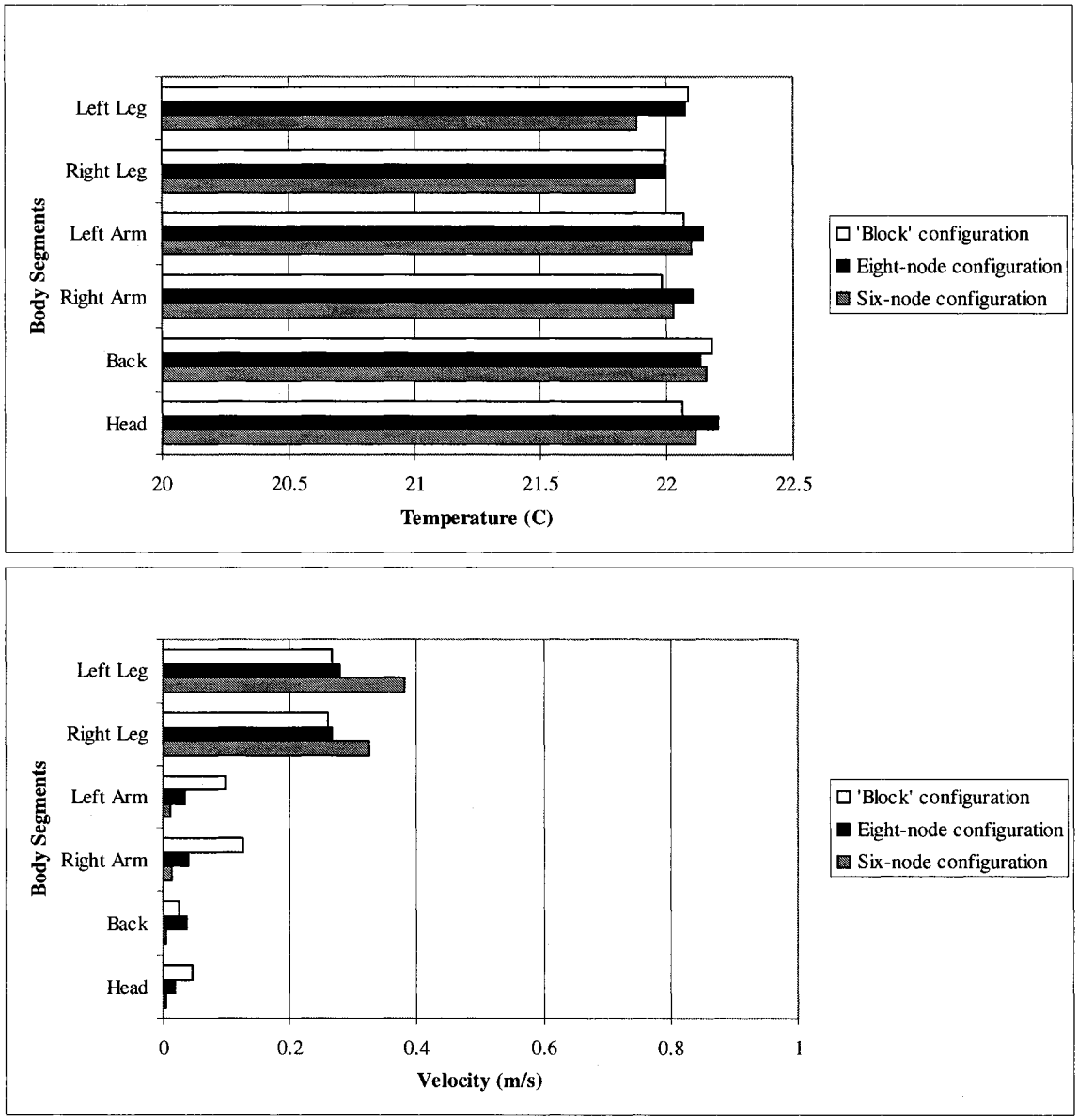

Figure 4.18: The comparison between block, six-node and eight-node configurations for diffuser located at 0.5 m and oriented toward the occupant (Cases 09, 10 and 11)

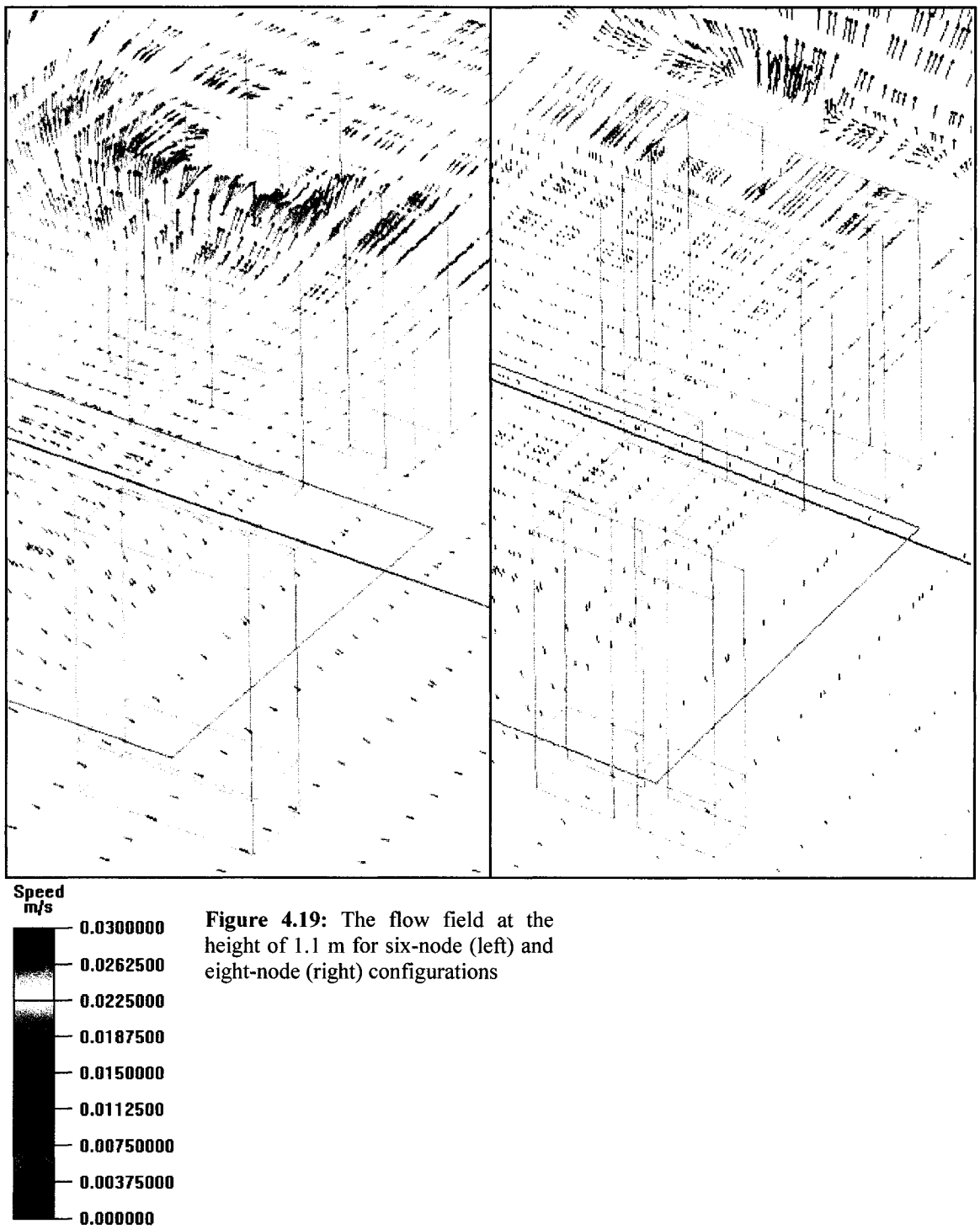

Figure 4.19: The flow field at the height of 1.1 m for six-node (left) and eight-node (right) configurations

Layout Number Three (cases 12 and 13) – Another scenario is conceived where the diffuser is placed at the right side of the occupant model at a distance of 0.5 m. This is another typical scenario associated with underfloor air distribution.

			Flow Variable Change					
	Occupant Configuration		Head	Back	Right Arm	Left Arm	Right Leg	Left Leg
Temperature [C]	Block	Eight node	0.147	0.18	0.088	0.114	0.19	0.107
Velocity [m/s]	Block	Eight node	0.0007	0.0058	0.00094	0.0003	0.013	0.00057

Table 4.10: The difference in the magnitude of air temperature and velocity near the occupant

Table 4.10 shows that air velocity is highly influenced by the configuration of the occupant model. The difference in the air velocity between a 'Block' and an eight-node configuration is as high as 0.013 m/s, though the change in the air temperature is not significant. An occupant model influences the flow field by posing as an obstacle to the flow and by its heat distribution. In this diffuser setup only the air velocity and the airflow pattern was changed considerably but not the air temperature. This confirms that for an inertia-dominated flow field, the proper configuration of the occupant is very important because of the way the configuration is presenting itself as a physical obstacle to the flow field. Calculating the PMV value for the block and eight-node configurations yields significantly different results: – 0.03 and – 0.12, respectively. The difference in the PMV value between Block and eight-node configurations is significantly high (50 %).

4.3.2 Verification of Uniform Heat Distribution

It was previously observed that the configuration of the occupant has influence on the flow field, depending on the diffuser throw angle and diffuser distance from the occupant etc. All the multi-node configurations that were studied in the previous section had uniform heat distribution, i.e. uniform heat flux per body segment. In this section, each two identical occupant configurations with different heat distribution methods are

compared with each other. Establishing various conclusions for a case where the floor diffuser is located at the close distance of 0.5 m will undoubtedly be true for a diffuser located at further distance.

Case	Occupant Model	STUDY OF OCCUPANT CONFIGURATION Distance from Occupant	Airflow Rate	Supply Temperature	Discharge Angle
		Layout Number Three			
14	Eight-node (uniform)	Right side (0.5 m)	9.32 L/s	15.1 °C	Vertical
15	Eight-node (non-uniform)	Right side (0.5 m)	9.32 L/s	15.1 °C	Vertical
		Layout Number Two			
16	Eight-node (uniform)	Front side (0.5 m)	9.32 L/s	15.1 °C	Oriented
17	Eight-node (non-uniform)	Front side (0.5 m)	9.32 L/s	15.1 °C	Oriented
18	Six-node (uniform)	Front side (0.5 m)	9.32 L/s	15.1 °C	Oriented
19	Six-node (non-uniform)	Front side (0.5 m)	9.32 L/s	15.1 °C	Oriented

Table 4.11: Various cases for underfloor air distribution case study

Layout Number Three (cases 14 and 15) – The assumption of uniform heat distribution is verified for the case where the floor diffuser is placed at the right side of the eight-node occupant configuration. As shown in Figure 4.20, the air temperature near the lower body shows a higher value for the case of non-uniform heat distribution. This is expected because for the case of non-uniform heat distribution (Tanabe et al., 1994) the boundary conditions used for the legs of the occupant are higher than those for the case of uniform heat distribution (see Table 3.6). Table 4.12 quantifies the difference between the two cases where the highest percentage difference between the two scenarios is less than 1 % for air temperature and less than 3 % for air velocity. Using non-uniform heat distribution for various body segments is a closer representation of the actual heat loss from a human body; however, its effect on the occupant microclimate is minimal.

		Percentage Difference (%)					
	Occupant Configuration	Head	Back	Righ Arm	Left Arm	Right Leg	Left Leg
Air Temperature	Eight node	0.03	0.09	0.03	0.03	0.06	0.06
Air Velocity	Eight node	0.9	0.8	0.65	1	0.4	2

Table 4.12: The percentage difference between the uniform and non-uniform heat distribution cases for the air velocity and temperature profile near the occupant

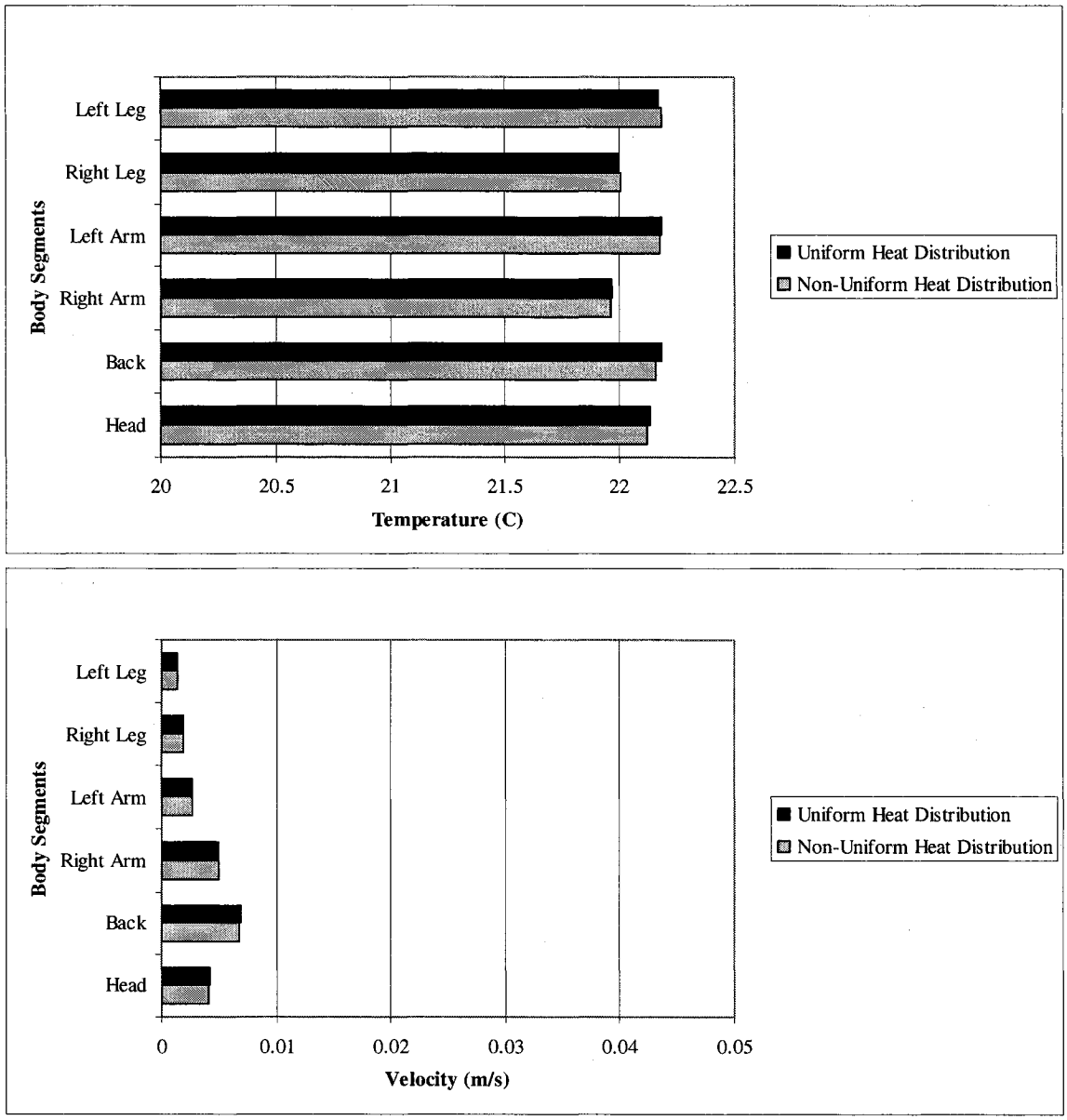

Figure 4.20: The comparison between uniform and non-uniform heat distribution of an eight-node configuration (Cases 14 and 15)

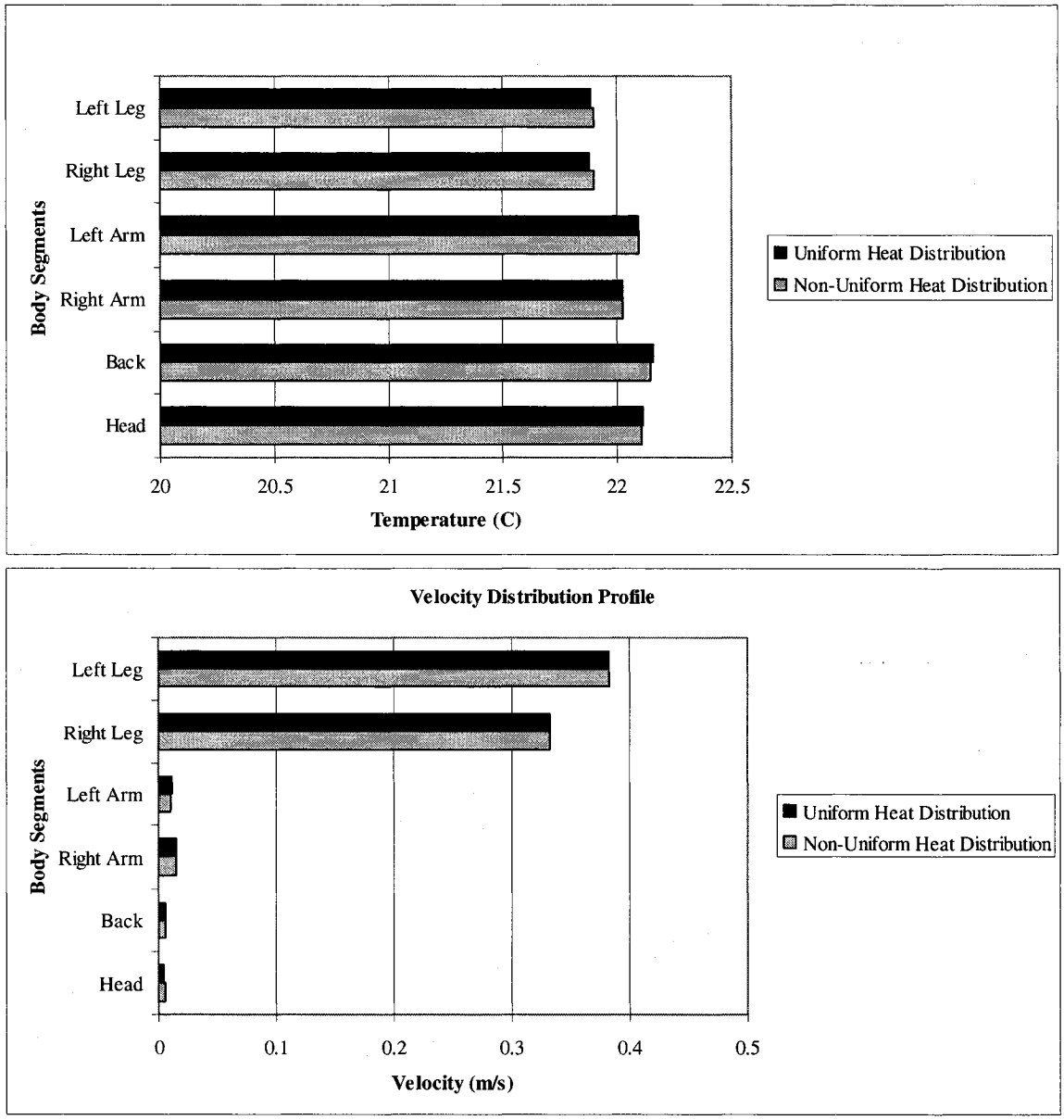

Figure 4.21: The comparison between uniform and non-uniform heat distribution of a six-node configuration (Cases 18 and 19)

Layout Number Two (cases 16 to 19) – The floor diffuser for these four cases was relocated to the front of the occupant at distance of 0.5 m and oriented toward the occupant. The floor diffuser was not installed exactly on the occupant's central axis in order to represent in realistic scenario. The previous diffuser layout was meant to represent a case with highly asymmetric thermal conditions. This diffuser layout that is

investigated here represents a case with high asymmetric thermal conditions as well as high airflow regimes that are directed toward a segment of the body. Figure 4.21 illustrates that the assumption of uniform heat distribution is valid for the modeling of six-node occupant configuration. It is also revealed that the velocities near upper body are much lower than those near lower body due to that fact that the majority of the discharged air is directed toward the legs. Also, it is evident from the air velocities near the legs that the floor diffuser is placed not on the occupant central axis. Similar conclusion over the assumption of uniform heat distribution was obtained for the eight-node configuration.

In order to properly study the microclimate of the occupant in a room that is equipped with underfloor air distribution or other localized ventilation systems, it is recommended to use an eight-node configuration with the inclusion of separate legs. The inclusion of separate legs on the occupant model is extremely important for the prediction of the local airflow pattern, especially on the opposite side of the diffuser discharge. However, the importance of using a detailed occupant configuration becomes trivial as the floor diffuser is moved away from the occupant.

4.4 Occupant Modeling in a Mixing Ventilation Room

The most widely used ventilation system is the full-mixing air distribution system, where the air is discharged through ceiling diffusers at higher velocities than those observed for the displacement ventilation diffusers.

Cases	Occupant Model Configuration	Thermal Distribution
1	'Block' model	Uniform
2	Six-node model	Uniform
3	Eight-node model	Uniform
4	Six-node model	Uniform
5	Six-node model	Non-uniform

Table 4.13: Various cases considered to check the uniformity of heat distribution

The CFD model of the classroom was refitted with a full-mixing ceiling air distribution system. Four ceiling diffusers were placed evenly in the classroom in order to supply a total of 233 L/s, while all wall boundary conditions (walls, windows etc.) were identical to the base case. Three cases were considered using 'Block', six-node and eight-node configurations. Figure 4.22 shows that difference between a six-node and eight-node configuration is negligible. Table 4.14 quantifies the change between the various occupant configurations in terms of percentage. It is observed that reliable prediction of the temperature distribution and velocity field could be obtained by using a 'Block' configuration instead of more computationally expensive occupant configuration.

	Percentage Difference (%)							
	Occupant Configuration		Head	Back	Right Arm	Left Arm	Right Leg	Left Leg
Air Temperature	Block	Six node	0.45	0.5	0.4	0.35	0.5	0.4
	Six node	Eight node	0.15	0.07	0.17	0.15	0.4	0.35
	Uniform	Non-uniform	0.08	0.09	0.07	0.07	0	0
Air Velocity	Block	Six node	30	50	30	>50	60	>50
	Six node	Eight node	12	15	45	50	40	50
	Uniform	Non-uniform	3	1	3	0	5	5

Table 4.14: The percentage difference in air velocity and temperature profile near the occupant

Table 4.14 also shows the percentage change between a six-node configuration with uniform heat distribution and non-uniform heat distribution (Tanabe et al., 1994). It is observed that the assumption of uniform heat distribution is valid.

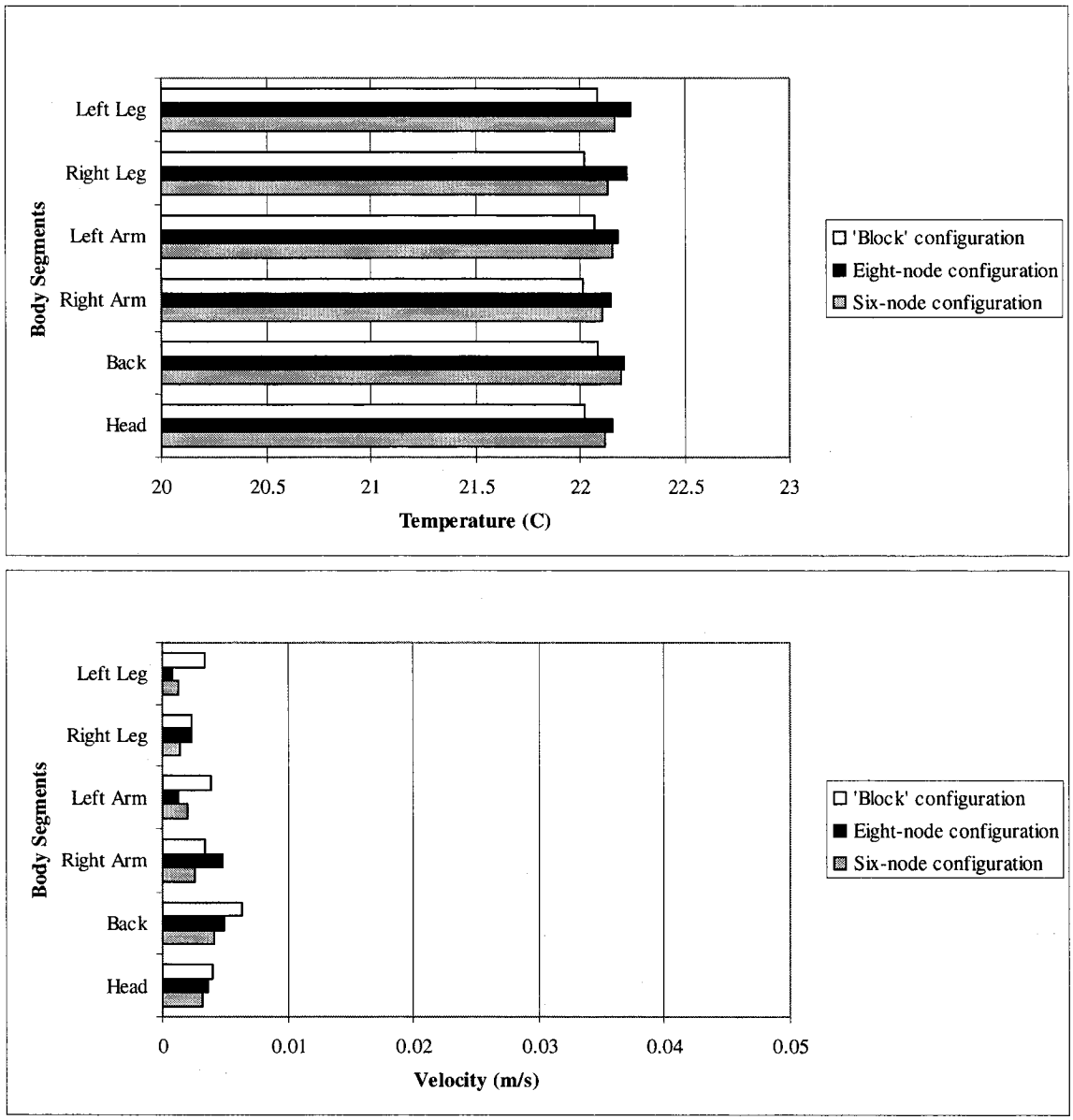

Figure 4.23: The comparison between the 'Block', six-node and eight-node configurations (Cases 1 to 3)

The full-mixing air distribution systems are typically installed on the ceiling outside the occupying zone where the conditioned air is diluted and mixed with the room air creating a uniform profile with lower flow gradients within the occupant microclimate as oppose to the localized ventilation systems. This makes the need of using a highly detailed occupant configuration trivial for these types of flow fields.

5.0 CONCLUSIONS

Today, the most widely used means of ventilation is the full-mixing ceiling air distribution system where the airflow is discharged outside of the occupying zone. In the very near future, the localized ventilation systems are earmarked to replace the aging full-mixing ceiling system as more research are being performed. Modern localized ventilation systems such as underfloor air distribution are being designed and implemented in large quantities. Numerous research studies have been implemented on the subject of the indoor air quality, thermal comfort and ventilation effectiveness of such new systems where the focus of study was on the microclimate of the occupant. Past research work have also established that the Computational Fluid Dynamics (CFD) method is a good alternative for the simulation of indoor airflow. The accuracy of the simulation of local airflow in the microclimate of the occupant is highly dependent on the proper modeling of the occupant model. Previous research works have simplified the occupant model by using blocks with uniform heat distribution as boundary condition. This approach greatly reduces the computational requirement for a large-scale CFD modeling of a ventilated enclosure. To date no guidelines exist for modeling an occupant for a large-scale CFD modeling of a ventilated enclosure.

This study was based on a large ventilated enclosure (8.4 m $\times$ 7.2 m) with large internal heat gain, so that the computational requirement becomes an issue and adds to realism of this study. Seven different occupant models with various configurations were developed for this study in order to fully analyze their effect on the temperature distribution and airflow pattern near the occupants. These Models are:

- 'Block' model
- Three-node model (uniform heat distribution)
- Three-node model (non-uniform heat distribution)
- Six-node model (uniform heat distribution)
- Six-node model (non-uniform heat distribution)
- Eight-node model (uniform heat distribution)
- Eight-node model (non-uniform heat distribution)

It was concluded that the assumption of uniform heat distribution was fairly acceptable for all three ventilation systems. It was observed that the assumption made on the configuration of the occupant model has much more significant effect on the flow field than its thermal distribution.

Ventilation System	Body Heat Distribution	Body Heat Distribution
Ceiling Air Distribution	Uniform heat flux	'Block' configuration
Displacement Ventilation	Uniform heat flux	Six-node configuration
Underfloor Air Distribution	Uniform heat flux	Eight-node configuration

Table 5.1: Recommended occupant model configuration to be used with various ventilation systems

It was viewed that the uniform local environment characterized by the conventional ceiling air distribution system is not significantly affected by the configuration of the occupant model. Therefore, a 'Block' configuration can be used in order to reduce computational time as shown in Table 5.1. The buoyancy-driven flow field of a typical displacement ventilation system justifies the need to use of six-node in order to avoid the simplicity of a 'Block' configuration, which promotes excessive stratification on its

surface. For inertia-driven flow field of localized underfloor air distribution, an eight-node configuration is recommended for the study of the occupant microclimate. It was shown that the inclusion of legs significantly affect the flow field for cases when the diffuser was very close and oriented toward the occupant. It was further concluded that the distance and the orientation of the diffuser plays a key role in determining the importance of considering a detailed occupant model. Therefore, the Airpak standard occupant model can be used for a more reliable prediction of the airflow field within the occupant microclimate for localized ventilation system. All the occupant model configurations developed in this study were designed with the knowledge that the computational resources are an issue. Therefore, they all had simplistic rectangular-coordinate configuration, so that they can be integrated easily with any large-scale CFD modeling of large ventilated enclosures. The following points were concluded:

- Comparison of uniform and non-uniform heat distribution for three distinct occupant models established that the assumption of uniform heat distribution is valid for a wide range of operating conditions.
- Comparison of various occupant models to that of 'Block' model showed that the configuration of the occupant model plays an important role. Therefore, the use of a six-node configuration was recommended for a buoyancy-dominated flow field, in order to avoid the smoothness and simplicity of the 'Block' configuration.
- The inclusion of separate legs on the occupant configuration (eight-node) does not significantly affect the temperature and velocity profiles around of the occupant in a buoyancy-dominated flow field.

- Comparison of uniform and non-uniform heat distribution for an occupant model established that the assumption of uniform heat distribution is valid for a case where the room is equipped with an underfloor air distribution system.
- The distance and the throw angle of the floor diffuser with respect to the occupant play a key role in the investigation of the effect of occupant configuration assumption on the flow field: as the diffuser is approached toward the occupant, the importance of using a detail occupant model becomes more significant. When the throw angle of the floor diffuser is oriented toward the occupant it is seen that the inclusion of separate legs (eight-node) significantly affects the results. These findings were further backed by comparing the whole-body PMV values for different occupant configurations.
- Comparison of uniform and non-uniform heat distribution for a six-node configuration has shown that the assumption of uniform heat distribution is valid for the case of traditional full-mixing ceiling air distribution system.
- It was further observed, on the contrary to the cases with displacement ventilation and underfloor air distribution system, the configuration of the occupant model does not play a significant role for a room equipped with full-mixing ceiling air distribution system.

6.0 FUTURE WORKS

For future work, the effect of various turbulence models, such as Low-Reynolds Number k-ε model, should be analyzed with occupant model configuration of higher detail. The study performed here was not meant to be a detailed analysis of occupant modeling. The idea was to perform the same type of simulation, with the same kinds of restriction and resources such computational power etc., as others CFD studies shown in Table 6.1. Therefore, the immediate effect of using different occupant model configurations on the flow field was studied but other aspects such as very detailed analysis of the flow field was not performed.

Author	Occupant Model	Heat Distribution	Flow Domain	Ventilation System
Karimipanah, T. et al. (2000)	Single Block	Uniform	Large room	DV and impinging
Chiang, H. (2001)	Multi-node	Uniform	Small cavity	Personalized control
Zeng, J. (2001)	Single Block	Uniform	Large room	Linear diffuser
Xing, H. (2001)	Multi-node	Uniform	Small cavity	DV
Awbi, HB. et al. (2001)	Multi-node	Uniform	Small cavity	DV, UFAD and CAD
Karimipanah, T. et al. (2002)	Single Block	Uniform	Large room	DV and impinging
Zhao, B. et al. (2003)	Single Block	Uniform	Large room	DV and mixing
Yang, X. et al. (2004)	Single Block	Uniform	Large room	DV and mixing
Sekhar, SC et al. (2004)	Multi-node	Uniform	Large room	Linear and CAD
Karimipanah, T. et al. (2005)	Single Block	Uniform	Large room	Jet ventilation
Lin, Z. et al. (2005)	Single Block	Uniform	Large room	DV and mixing
Wan, MP. et al. (2005)	Single Block	Uniform	Large room	UFAD
Zhou L. et al. (2005)	Single Block	Uniform	Large room	Nozzle diffusers

Table 6.1: Occupant models used for different application with various level of complexity

There is an increasingly use of localized ventilation system in various indoor locations, e.g. library, workshop etc. Therefore, it could also benefit to expand the same kind of study on other flow domains (see Table 6.1). For example, to study the effect of occupant modeling assumptions in a detailed office workstation that includes not only the occupant but also a computer desktop and task lights. Furthermore, the conclusions drawn in this study for the underfloor air distribution system are based on one set of supply conditions

and are highly dependent upon the diffuser distance from the occupant and diffuser throw angle. Therefore, the effect of the diffuser distance from the occupant and diffuser throw angle in conjunction with various occupant model configurations must be studied for a different set of supply conditions.

Another avenue for the use of detailed model of human body would be that of auto/transportation industry (DeDear et al., 1997). There has been major work in that area for analysis of the passenger thermal comfort in a non-uniform thermal environment inside automobiles using simulation methods as well as manikins (Rugh, 2005; McGuffin, 2001). Similar study of occupant thermal modeling can be performed inside the automobile. Finally, this study can also be used as starting point, for a detail analysis of air distribution system for commercial airplane. In modern commercial aircrafts, the ventilated air are distributed via nozzles and discharged toward the passenger from the ceiling. Thus, it is important to investigate the impact of various occupant modeling methods on this type of localized ventilation system. Furthermore, the interaction between two passengers seating close to each other, using a variety of occupant model configurations, in conjunction with localized ventilation system with different supply conditions must be explored.

Reference:

Airpak Documentation, Version 2.1, Fluent Inc. 2002.

ASHRAE, ANSI/ASHRAE 129-1997, "Measuring Air Change Effectiveness", American Society of Heating, Refrigeration, and Air Conditioning Engineers, Inc., Atlanta (1997)

ASHRAE, ANSI/ASHRAE Standard 55-1992, "Thermal Environment Conditions for Human Occupancy", American Society of Heating, Refrigeration, and Air Conditioning Engineers, Inc., Atlanta (1992)

Awbi, H.B., "Ventilation of Buildings", (1991), E & FN Spon, ISBN 0-419-15690-9

Awbi, H.B., "Thermal Boundary Conditions for Internal Room Surfaces", *ROOMVENT'96* (1996), volume 1, page 243-250

Awbi, H.B., "Calculation of Convective Heat Transfer Coefficients of Rooms Surfaces for Natural Convection", *Energy and Buildings 28* (1998), volume 28, page 219-227

Awbi, H.B. and Karimipanah, T., "A Comparison Between Three Methods of Low-Level Air Supplies", (2002), *The 4th International Conference on Indoor Air Quality, Ventilation and Energy Conservation in Buildings*, University of Reading, United Kingdoms

Bauman, F.S., "Underfloor Air Distribution (UFAD) Design Guide" (2003)

Bauman, F.S., Zhang, H., Arens, E.A. and Benton, C.C., "Localized Comfort Control with a Desktop Task Conditioning System: Laboratory and Field Measurements" *ASHRAE Transactions: Symposia* (1993), page 733-745

Brohus, H. and Nielsen, P., "CFD Models of Persons Evaluated by Full-Scale Wind Channel Experiments", *Proceedings of the 5th International Conference on Air Distribution in Rooms, ROOMVENT'96* (1996), Yokohama, Japan, page 137-144

Brohus, H., "Personal Exposure to Contaminant Sources in Ventilated Rooms", Ph.D. Thesis (1997), Aalborg University, Denmark

Chiang, H., Yen, M.C., Hu, R. and Yang B.C., "Numerical Study of Partition-Type FCU Personal Air-Conditioning System", Air Distribution Techniques 3 (2001)

DeDear, R.J., Arens, E., Zhang Hui and Masayuki Oguro, "Convective and Radiative Heat Transfer Coefficients for Individual Human Body Segments", *Int. J. Biometeorol* (1997), page 141-156

Fanger PO. "Thermal Comfort", New York: McGraw-Hill, (1970).

Gan, G., "Numerical Method for a Full Assessment of Indoor Thermal Comfort", *International Journal of Indoor Air Quality and Climate* (1994), Munksgaard, volume 4, no 3, page 154-168

Heinemeier, K.E., Schiller, G.E. and Benton, C.C., "Task Conditioning for the Workplace: Issues and Challenges", *SL-90-7-3* (1990)

Huizenga C., Zhang H., Arens E. and Wang D., "Skin and Core Temperature Response to Partial- and Whole-body Heating and Cooling", *Journal of Thermal Biology 29* (2004), Munksgaard, volume 29, page 549-558

ISO Standard 7730, "Moderate Thermal Environments-Determination of PMV and PPD Indices and Specification of the Conditions for Thermal Comfort", Geneva: International Standards Organization (1994)

Karimipanah, T. and Awbi, H.B., "A Comparative Study of Different Air Distribution Systems in a Classroom", *5th International Conference, Ventilation for Automotive Industry,* (2000), Stratford upon Avon, United Kingdoms

Karimipanah, T. and Awbi, H.B., "Theoretical and Experimental Investigation of Impinging Jet Ventilation and Comparison with Wall Displacement Ventilation", *Building and Environment 37* (2002), volume 37, page 1330-1342

Karimipanah, T., Awbi, H.B., Blomqvist, C. and Sandberg, M., "Effectiveness of Confluent Jets Ventilation System for Classrooms", *Indoor Air 2005* (2005)

Kato, S., "Numerical Analysis of Contaminant Distribution Around a Human Body", *Proceedings of the 5th International Conference on Air Distribution in Rooms, ROOMVENT'96* (1996), Yokohama, Japan, page 129-136

Launder, B. E. and Spalding, D. B., "The Numerical Computation of Turbulent Flows", *Comp. Meth. Appl. Mech* (1974), volume 3, page 269-289

Lin, Z., Chow, T.T., Fong, K.F., Wang, Q. and Li, Y., "Comparison of Performances of Displacement and Mixing Ventilations. Part I: Thermal Comfort", *International Journal of Refrigeration* (2005)

Lin, Z., Chow, T.T., Tsang, C.F. Fong, K.F., and Wang, Q., "CFD Study of Effect of the Air Supply Location on the Performance of the Displacement Ventilation System", *Building and Environment 40* (2005), volume 40, page 1051-1067

Loomans, M., "The Measurement and Simulation of Indoor Air Flow", Ph.D. Thesis (1992), Technical University of Eindhoven, The Netherlands

Matsunawa, Lizuka and Tanabe, "Development and Application of an Underfloor Air-Conditioning System with Improved Outlets for a 'Smart' Building in Tokyo" *ASHRAE Transactions* (1995), page 887-901

McGuffin, R. and Burke, R., "Modeling of Human Thermal Comfort", *Proceedings of the 5th Vehicle Thermal Management Systems Conference,* SAE, 2001-01-1739, Nashville, TN. 2001

Murakami, S., Kato, S. and Zeng J., "Flow and Temperature Fields Around Human Body with Various Room Air Distribution: CFD Study on Computational Thermal Manikin – Part I" *ASHRAE Transactions* (1997), volume 103, part 1, page 3-15

Murakami, S., Kato, S. and Zeng J., "Numerical Simulation of Contaminant Distribution Around a Modeled Human Body: CFD Study on Computational Thermal Manikin – Part II" *ASHRAE Transactions* (1998), volume 104, part 2, page 226-233

Murakami, S., Kato, S. and Hayashi T., "CFD Analysis of Wind Environment Around a Human Body" *Journal of Wind Engineering and Industrial Aerodynamics* (1999), volume 83, page 393-408

Murakami, S., Kato, S. and Zeng J., "Combined Simulation of Airflow, Radiation and Moisture Transport for Heat Release From a Human Body" *Building and Environment 35* (2000), volume 35, page 489-500

Nielsen, P., "Flow in Air-Conditioned Rooms", Ph.D. Thesis (1974), Danish Technical University, Copenhagen, Denmark

Nielsen, P., "Descriptions of Supply Openings in Numerical Models for Room Air Distribution", *ASHRAE Transactions* (1992), volume 98, part 1, page 963-971

Nielsen, P., Murakami, S., Kato, S., Topp C. and Yang, J.H., "Benchmark Tests for Computer Simulated Person" (2003), *Aalborg University, Indoor Environmental Engineering*

Niu, J., "Modeling of Cooled-Ceiling Air Conditioning Systems", Ph.D. Thesis (1994), Delft University of Technology", The Netherlands

Patankar, S.V., "Numerical Heat Transfer and Fluid Flow", Hemisphere, Washington, D.C., 1980.

Rugh J.P. and Bharathan D., "Predicting Human Thermal Comfort in Automobiles" (2005), *Vehicles Thermal Management Systems Conference,*

Schild, P.G., "Accurate Prediction of Indoor Climate in Glazed Enclosures", Ph.D. Thesis (1997), Norwegian University of Science and Technology (NTNU), Norway

Sideroff, C.N. and Dang, T.Q. "CFD Analysis of the Flow Around a Computer Simulated Person in a Displacement Ventilated Room", *Indoor Air 2005* (2005)

Sideroff, C.N. and Dang, T.Q. "Validation of CFD for the Flow Around a Computer Simulated Person in a Mixing Ventilated Room", (2005)

Sekhar, SC. and Willem, HC, "Impact of Airflow Profile on Indoor Air Quality – a Tropical Study" *Building and Environment 39* (2004), volume 39, page 255-266

Sørensen, DN., "Radiation Between Segments of the Seated Human Body", *ROOMVENT'02* (2002), Copenhagen, Denmark, page 317-320

Sørensen, DN. and Voigt, LK., "Modeling Flow and Heat Transfer Around a Seated Human Body by Computational Fluid Dynamics", *Building and Environment* (2003), Technical University of Denmark, Denmark, page 317-320

Tanabe, S., Arens, E.A., Bauman, F.S., Zhang, H. and Madsen T.L., "Evaluating Thermal Environments by Using a Thermal Manikin with Controlled Skin Surface Temperature", *ASHRAE Transactions: Research* (1994), volume 100, part 1, page 39-48

Topp, C., Nielsen, P.V. and Sørensen D.N., "Application of Computer Simulated Persons I Indoor Environment Modeling", *ASHRAE Transactions* (2002), volume 108, part 2, page 1084-1089

Topp, C., "Influence of Geometry of a Computer Simulated Person on Contaminant Distribution and Personal Exposure", *ROOMVENT'02* (2002), Copenhagen, Denmark, page 265-268

Wyon, D.P. (2004) "The Effect of Indoor Air Quality on Performance and Productivity" *The International Indoor Air*, volume 14, page 92-101.

Xing, H., Hatton, A. and Awbi, H.B., "A Study of the Air Quality in the Breathing Zone in a Room with Displacement Ventilation", *Building and Environment 36* (2001), volume 36, page 809-820

Yakhot, V. and Orszag, S.A., "Renormalization Group Analysis of Turbulence. I. Basic Theory", *Journal of Scientific Computing*, volume 1, No 1, page 3-51

Yigit, A., "The Computer-Based Human Thermal Model", *Int. Comm. Heat Mass Transfer* (1998), volume 25, No 7, page 969-977

Zhao, B., Li, X. and Yan, Q., "A Simplified for Indoor Airflow Simulation", *Building and Environment 38* (2003), volume 38, page 543-552

APPENDICES:

Appendix A

Geometrical configurations of Block Model

Block Occupant Configuration

				Heat Loss	
	x	y	z	Uniform	Area
	m	m	m	W	m^2
Block	0.371	1.100	0.340	95.000	1.690
Underfoot	0.371	0.100	0.340	0.000	
Total				**95.000**	**1.690**

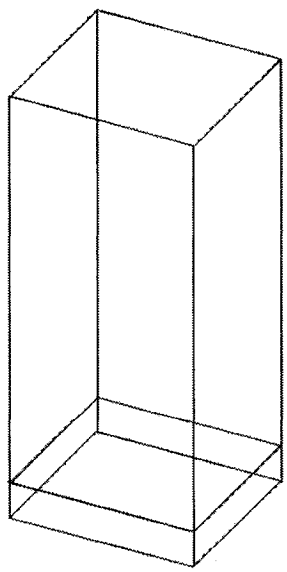

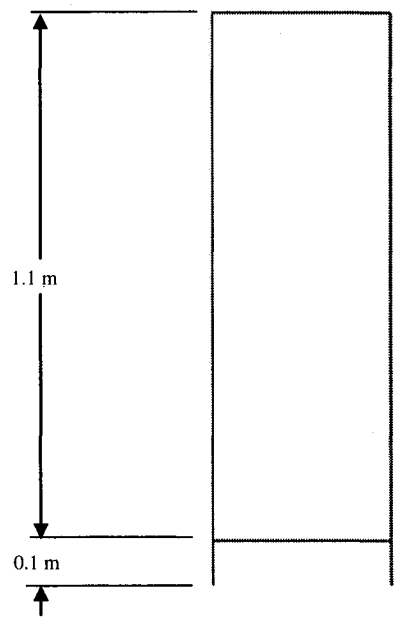

Appendix B

Geometrical configuration of Three-Node Model

Three-Node Occupant Configuration

				Heat Loss		
	x	y	z	Uniform	Non-uniform	Area
	m	m	m	W	W	m^2
Head	0.186	0.186	0.186	9.766	9.354	0.174
Upper Body	0.483	0.414	0.320	39.280	41.207	0.699
Lower Body	0.379	0.500	0.320	45.954	44.439	0.817
Underfoot	0.379	0.100	0.320	0.000	0.000	
Total				**95.000**	**95.000**	**1.690**

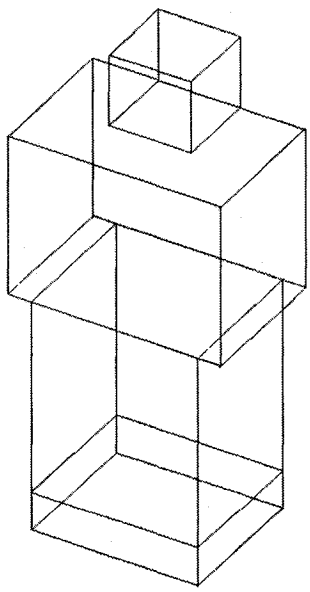

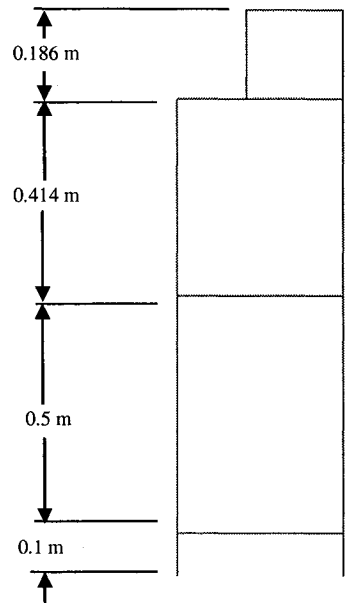

Appendix C

Geometrical configuration of Six-Node Model

Six-Node Occupant Configuration

	x	y	z	Heat Loss Uniform	Heat Loss Non-uniform	Area
	m	m	m	W	W	m^2
Head	0.186	0.186	0.186	9.766	9.354	0.174
Body	0.345	0.414	0.250	25.445	21.910	0.453
Left Arm	0.131	0.414	0.110	10.254	9.649	0.182
Right Arm	0.131	0.414	0.110	10.254	9.649	0.182
Thighs	0.345	0.100	0.422	17.362	17.923	0.309
Legs/Feet	0.345	0.400	0.142	21.919	26.515	0.390
Underfoot	0.345	0.100	0.142	0.000	0.000	0.000
Total				**95.000**	**95.000**	**1.690**

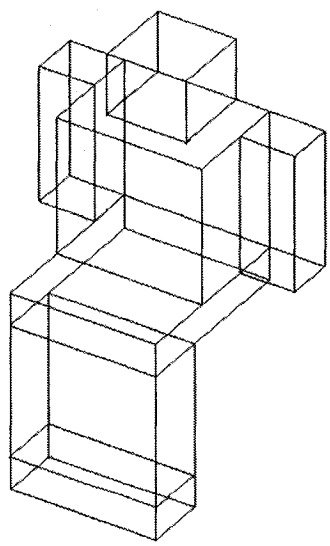

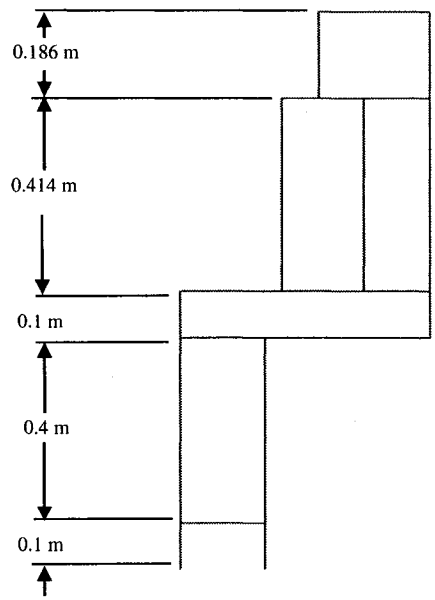

Appendix D

Geometrical configuration of Eight-Node Model

Eight-Node Occupant Configuration

	x	y	z	Heat Loss Uniform	Heat Loss Non-uniform	Area
	m	m	m	W	W	m^2
Head	0.186	0.186	0.186	9.766	9.354	0.174
Body	0.348	0.514	0.200	25.445	21.910	0.453
Right Arm	0.101	0.514	0.110	10.254	9.649	0.182
Left Arm	0.101	0.514	0.110	10.254	9.649	0.182
Right Thigh	0.161	0.100	0.290	8.681	8.962	0.154
Left Thigh	0.161	0.100	0.290	8.681	8.962	0.154
Right Leg/Foot	0.161	0.400	0.082	10.959	13.258	0.195
Left Leg/Foot	0.161	0.400	0.082	10.959	13.258	0.195
Underfoot	0.000	0.100	0.000	0.000	0.000	0.000
Underfoot	0.000	0.100	0.000	0.000	0.000	0.000
Total				**95.000**	**95.000**	**1.690**